Accounting for the speed shear in wind turbine power performance measurement

Wagner, Rozenn; Courtney, Michael

Publication date:
2010

Document Version
Publisher's PDF, also known as Version of record

Accounting for the speed shear in wind turbine power performance measurement

Risø-PhD-Report

Rozenn Wagner
Risø-PhD-58(EN) - Short version
April 2010

Risø DTU
National Laboratory for Sustainable Energy

Author: Rozenn Wagner
Title: Accounting for the speed shear in wind turbine power performance measurement
Division: Wind Energy Division

Risø-PhD-58(EN)
April 2010

Abstract:

The power curve of a wind turbine is the primary characteristic of the machine as it is the basis of the warranty for it power production. The current IEC standard for power performance measurement only requires the measurement of the wind speed at hub height and the air density to characterise the wind field in front of the turbine. However, with the growing size of the turbine rotors during the last years, the effect of the variations of the wind speed within the swept rotor area, and therefore of the power output, cannot be ignored any longer. Primary effects on the power performance are from the vertical wind shear and the turbulence intensity. The work presented in this thesis consists of the description and the investigation of a simple method to account for the wind speed shear in the power performance measurement. Ignoring this effect was shown to result in a power curve dependant on the shear condition, therefore on the season and the site. It was then proposed to use an equivalent wind speed accounting for the whole speed profile in front of the turbine. The method was first tested with aerodynamic simulations of a multi-megawatt wind turbine which demonstrated the decrease of the scatter in the power curve. A power curve defined in terms of this equivalent wind speed would be less dependant on the shear than the standard power curve.
The equivalent wind speed method was then experimentally validated with lidar measurements. Two equivalent wind speed definitions were considered both resulting in the reduction of the scatter in the power curve. As a lidar wind profiler can measure the wind speed at several heights within the rotor span, the wind speed profile is described with more accuracy than with the power law model. The equivalent wind speed derived from measurements, including at least one measurement above hub height, resulted in a smaller scatter in the power curve than the equivalent wind speed derived from profiles extrapolated from measurements at hub height and below only.
It is well established that the turbulence intensity also influences the power performance of a wind turbine. Two ways of accounting for the turbulence were tested with the experimental data: an adaptation of the equivalent wind speed so that it also accounts for the turbulence intensity and the combination of the equivalent wind speed accounting for the wind shear only with the turbulence normalising method for turbulence intensity suggested by Albers. The second method was found to be more suitable for normalising the power curve for the turbulence intensity.
Using the equivalent wind speed accounting for the wind shear in the power performance measurement was shown to result in a more repeatable power curve than the standard power curve and hence, in a better annual energy production estimation. Furthermore, the decrease of the scatter in the power curve corresponds to a decrease of the category A uncertainty in power, resulting in a smaller uncertainty in estimated AEP.

The thesis is submitted to the Danish Technical University in partial fulfilment of the requirements for the PhD degree.

ISBN 978-87-550-3816-5

Contract no.:

Group's own reg. no.:

Sponsorship:
ModObs Network MRTN-CT-2006-019369

Pages:155
References:53

Information Service Department
RisøNational Laboratory for Sustainable Energy
Technical University of Denmark
P.O.Box 49
DK-4000 Roskilde
Denmark
Telephone +45 46774005
bibl@risoe.dtu.dk
Fax +45 46774013
www.risoe.dtu.dk

Contents

Acknowledgements

First of all, I would like to thank a lot my supervisor, Mike Courtney, for his great support and assistance, and the time devoted to constructive "hair-pulling". He was always ready to help me and it was a pleasure to be his student. I also thank all my colleagues from the Test and Measurement group, in particular Uwe Paulsen, Troels Friis Pedersen, Allan Vesth, Petter Lindelöw-Marsden and Julia Gottshall for the very interesting discussions and showing so much interest in my work, which helped to carry on towards results relevant for the wind energy community. Moreover, Per Hansen, Bjarne Sønderskov and Anders R. Vestergaard were very helpful with all the technical and experimental work.

Torben J. Larsen and Helge A. Madsen, from the AED group, are thanked for their very valuable help and support with the aerodynamic simluations.

I am very grateful to my first supervisors, Ioannis Antoniou and Hans Jørgensen, for getting me started at Risø, assisting me at the beginning of the PhD and keeping an eye on my progress during the 3 years.

Many thanks to my friends and various office mates: especially to Alfredo and Ferhat for their scientific inputs and valuable advice, and to the "girl office", Claire, Caroline and Ioanna, for their support and the good atmosphere. A special thank to Eleni for her friendship and for always being game for activities that cut off from work.

Merci à Julien, pour m'avoir accompagnée au Danemark et pour son soutien moral et materiel, en particulier durant la rédaction. Merci à mes parents pour leurs constants encouragements et pour avoir toujours cru en moi.

I acknowledge the PhD funding from the ModObs Network MRTN-CT-2006-019369 and from Vestas Wind Systems A/S. Many thanks to Anna-Maria Sempreviva for initiating and organising the ModObs network.

I thank Siemens Wind Power and Vestas Wind System A/S for permission to use the turbine data. I acknowledge the support from IMPER project financed by the Danish Energy Agency (journal no.: 3302-0106), the EU Upwind project (WP6) and the EU SafeWind project (WP2) in the experimental part of the work.

Chapter 1

Introduction

Power curves are central to the wind industry as they form the basis for the power production warranty of the turbine. Indeed, power curves are frequently presented by turbine manufacturers in their marketing literature. They are of utmost relevance to the wind farm developers in order to chose the turbine best suited to the wind resources of the site and, in conjunction with the wind resource, to predict the energy production of the farm. Once the turbine is installed, the power curve is again of importance since it is necessary to check that the energy production meets that promised by the manufacturer.

The power curve of a wind turbine is a representation of its performance. It shows the power output of the turbine as a function of the wind speed input. Figure 1.1 shows a typical wind turbine power curve. The cut-in wind speed (u_{cut-in}) is the minimum wind speed at which the wind turbine starts to produce power. For wind speeds above the cut-in speed, the power increases with the wind speed until reaching the rated power (P_{rated}), i.e. the maximum power the turbine can produce. The wind speed for which the rated power is first reached is named the rated wind speed (u_{rated}). Between rated wind speed and cut-out wind speed (namely the wind speed for which the wind turbine shuts down, $u_{cut-out}$), the control system of the turbine maintains the power output constant at rated power, by pitching the blades.

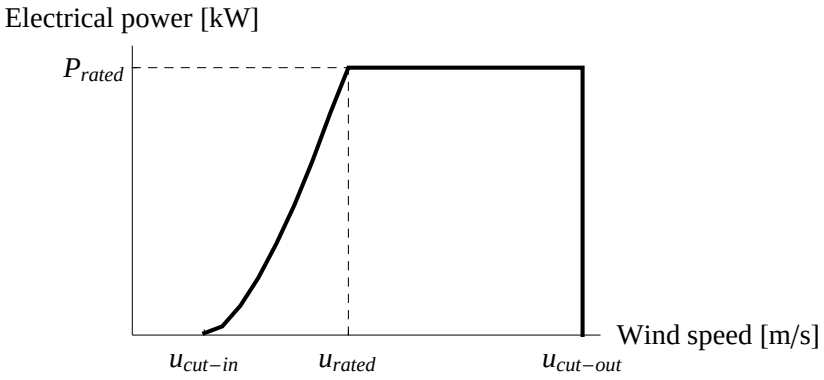

Figure 1.1: *Typical wind turbine power curve*

It is common practice to validate predictions of wind turbine power curves made with computational models by using measured data. Over the past decade, considerable advances have been made in achieving consistency in the measurement of wind turbine power curves. Since the publication in 1998, the IEC 61400-12 (IEC, 1998a) standard is now widely accepted as the contractual guidance for power curve measurement. This standard was withdrawn in 2005 and replaced by the IEC standard 61400-12-1 (IEC, 2005). According to this standard, the power performance of a wind turbine is achieved by measuring the wind speed with a cup anemometer mounted on top of a mast with the same height as the hub of the turbine and located at a distance of 2 to 4 rotor diameters

in front of the turbine (2.5 rotor diameters is recommended). As the air density causes variation in the wind kinetic energy flux through the rotor swept area, the wind speed[1] is normalised to the sea level air density. Simultaneous 10 minute mean wind speed and 10 minute mean power give the power curve scatter plot. These points are averaged in wind speed bins of 0.5 m/s resulting in the mean measured power curve.

The scatter in the power curve scatter plot is due to various factors which affect the wind turbine performance. These factors can be grouped in 3 categories:

1. the turbine operation including the blades conditions and the control algorithm for example;

2. the measurement errors due to the instruments such as the anemometer and the power sensor;

3. the wind conditions including the wind shear, the wind veer and the turbulence.

In this work, the effects on the scatter plot due to the wind conditions were only discussed and investigated.

The IEC 61400-12-1 standard only requires measurements of the wind speed at hub height and the air density (derived from temperature and pressure measurements) to characterise the wind field surrounding the wind turbine. However it has been shown that other wind characteristics such as the variation of the wind speed with altitude, i.e. the vertical wind shear, and the fast variation of wind speed around the 10 minute mean wind speed, which is usually referred to as turbulence, can also influence the power performance of a large turbine. If the power performance testing of a wind turbine was sufficiently long, then a range of conditions typical of the long term would be experienced and there would be no particular bias introduced by ignoring such dependencies. However, performance evaluation uses quite short test durations, too short for an annual range of weather conditions to be experienced. For this reason, power performance tests on one turbine made at different times of the year, or for different wind direction sectors, or tests of two identical turbines located at two different sites can result in different power curves. Such power curves are hardly comparable and repeatable. There is no basis for making confident predictions of turbine performance at commercial sites based on limited type testing that ignores important secondary parameters.

The effect of the wind shear and turbulence on the turbine performance is only briefly mentioned in the IEC 61400-12-1 standard. However they are recognised to possibly increase the uncertainty in power performance measurement. Despite this qualification, no clear recommendation about the manner of accounting for the wind shear and turbulence effects is given in the standard. Other authors have shown that the vertical wind shear has an effect on the power performance. The assumption that the speed profile is constant over the turbine rotor (as is implicit in the IEC standard) leads to inconsistencies. The IEC 64100-12-1 standard is currently under revision and the way of accounting for the wind shear and turbulence are amongst the main points of revision. Within this context, the work presented in this thesis is focused on the effect of the vertical wind shear on the power performance measurement. As the wind shear effect cannot easily be isolated from that of turbulence, turbulence effects were also investigated.

A major obstacle to the investigation of the effect of shear on the power performance of a turbine is the lack of information available to characterise the wind profile over the whole turbine rotor. In particular, there is seldom data available to measure the variation of wind speed above the hub height of the machine. As the size of wind turbines has considerably increased during the last few years, implying higher hubs and larger rotors, such measurements would require very tall, and therefore costly, masts. However, at the same time, remote sensing measurement technology has significantly improved, in particular that of LiDAR (Light Detection And Ranging). Based on fiber

[1] In this work, the wind speed was normalised for air density since modern pitch regulated wind turbines were considered. However, the power should be normalised for stall regulated turbines (IEC, 2005).

optic components available to the communication industry, lidars entered the wind energy field about 5 years ago. Such an instrument is a quite revolutionary tool for power performance measurement as it enables us to obtain speed profile measurements up to the higher tip of a multi-megawatt (multi-MW) wind turbine, relatively easily and with a good accuracy.

The work presented is this thesis had two main aims:

1. to suggest a method that can improve the power performance measurement concerning wind shear influence: that is the use of a wind speed equivalent to the wind speed profile in front of the turbine rotor;

2. to show the possibility of using lidar measurements for power performance measurement and in particular for the application of the method suggested above.

The structure of the thesis is as follows: **Chapter 2** first gives a short review of the main meteorological phenomena that generate various speed profiles. Secondly, the most common ways of characterising the wind shear are presented based on the analysis of long term measurement at the Risø DTU Test Station for Large Wind Turbines where the experimental work was carried out.

Chapter 3 presents the investigation of the effect of shear on the power performance of a wind turbine with aerodynamic simulations. The differences that a sheared inflow makes on the turbine aerodynamic compared to a constant profile were shown with simple simulation cases. The impact of a sheared inflow on the power performance was then shown for various types of wind profile.

In order to focus on the effect of wind shear, only simulations with laminar inflows were considered in chapter 3. However, the effect of turbulence should also be taken into account. Thus, **chapter 4** presents the investigation of the effect of turbulence on the power curve. This investigation was also performed with aerodynamic simulations, but with turbulent inflow. Both cases of turbulence without and with wind shear were discussed.

It is then possible to introduce the method suggested to account for the wind shear in the power performance measurement: the use of an equivalent wind speed representative of the wind speed profile in front of the turbine rotor. Thus, in **chapter 5**, the equivalent wind speed was tested with the results from the simulations described in chapter 3. The equivalent wind speed definitions were discussed. The method was also tested with turbulent inflows (based on the simulations results presented in chapter 4).

The next step was to demonstrate the possibility of applying the equivalent wind speed method with measurements. As this required the measurement of the wind speed profile within the range of heights swept by the turbine rotor, the lidar appeared as a good alternative to a high mast. However, lidar measurements are inherently different from cup anemometer measurements in their way of operation. **Chapter 6** describes the principle of operation of a pulsed lidar system and its imitations. For comparison, the principle of operation of a continuous wave lidar and a SoDAR (Sound Detection And Ranging) are briefly described with an emphasis on their differences with the pulsed lidar.

Chapter 7 describes the first measurement campaign set up with a lidar and a sodar to measure the wind profiles. Sodars have been used for wind energy assessment longer than lidars and can also appear as a good alternative to a mast. This experiment showed the importance of using an accurate remote sensing instrument as the wind sensor for the power curve measurement. It was found that this requirement was met by the lidar but not by the sodar. Furthermore, the equivalent wind speed method could not be validated by this experiment, because the experimental conditions were not optimal for this purpose.

Based on what was learned from this experiment, a second measurement campaign was undertaken. This experiment, described in **chapter 8**, clearly showed the effect of ignoring the speed shear in power performance measurement and the improvement obtained with the equivalent wind speed method. Firstly three definitions of equivalent

wind speed accounting for the wind shear were tested and compared with the experimental results. Secondly, one equivalent wind speed definition was applied with wind speed profiles derived from different number of speed measurements (at 2, 3, 5 or 9 heights) and with profiles extrapolated from measurements below hub height. The last point of this chapter is the combination of the equivalent wind speed method, that "normalises" the power curve for the wind shear effect, with a method normalising the power curve for the turbulence intensity effect.

By defining an equivalent wind speed accounting for the wind shear, a "new" power curve different from the standard power curve was defined. **Chapter 10** addresses the problem of comparing such quantities and the consequences for the Annual Energy Production (AEP).

Finally, **Chapter 11** presents a suggestion for evaluating the uncertainty in the power curve obtained with the equivalent wind speed. This required the definition of the lidar measurement uncertainty. Thus, three kinds of power curve uncertainties were compared: the uncertainty in the power curve measurement obtained with cup anemometer measurements, with lidar measurements at hub height and with the equivalent wind speed (derived from lidar speed profile measurements).

Chapter 12 presents a general discussion about the equivalent wind speed concept, the use of lidar measurements in the power performance context and the limitations of the investigation presented. Finally, **chapter 13** sums up the main conclusions that can be drawn from this work.

During the course of the work, the influence of wind shear on the turbine power performance was first investigated with aerodynamic simulations. The results enabled us to define the equivalent wind speed method. Part of this investigation was published in a journal paper which is given in appendix and is referred to as **Paper I** in chapters 3, 4, and 5. Subsequently, the measurement campaigns where a lidar was used to measure the wind profile in front of a multi-MW wind turbine were performed in order to validate the method. The first results of the second experiment campaign were described in a journal paper that has been submitted for publication. Although the paper is given appendix as **Paper II**, the results are also presented in chapter 8 in order to maintain the consistency of the thesis.

Chapter 2

Wind profiles

The vertical wind shear and wind veer are the variations of the wind speed and direction with altitude, respectively. This study was focused on the vertical variation of the horizontal wind speed; this is what the term "wind shear" or "shear" refers to in the rest of the thesis if no further definition is given. This chapter starts with a short overview of the mechanisms generating the variation of wind speed with altitude in the atmospheric boundary layer (ABL). Then, the test site, where both experiments described in this thesis took place, is briefly described. The wind shear characterisation is then discussed based on observations at this site.

2.1 Effects governing the wind speed profile

The principal effects governing the properties of the boundary-layer wind are the strength of the geostrophic wind, the surface roughness, Coriolis effects due to the Earth's rotation, and thermal effects, i.e. the atmospheric boundary layer stability. On top of this, the wind speed profile can be influenced by local effects.

2.1.1 Geostrophic wind and friction of the surface

The geostrophic wind is the wind arising from pressure differences in the atmosphere. The pressure gradient towards a low-pressure zone causes a mass of air to accelerate along a curve until a state of equilibrium between the pressure gradient and the Coriolis force is reached. Therefore, in areas that are far from high-pressure or low-pressure zones, the geostrophic wind is parallel to the isobars.

On the other hand, friction at the Earth's surface exerts a horizontal force upon the moving air, the effect of which is to retard the flow. The surface roughness is characterized by the density, size, and height of the buildings, trees, vegetation, rocks, etc., on the ground, around and over which the wind must flow; it will be a minimum over ice or open sea without waves and a maximum over urban areas (Dyrbye and Hansen, 1996). A consequence of the equilibrium of forces in the boundary layer is that the wind direction crosses the isobars. The wind direction continues to change down through the boundary layer and the wind speed gradually decreases to zero at the surface.

2.1.2 Static stability of the ABL

Once atmospheric pressure gradients have established the initial wind conditions, additional forcing mechanisms can come into play. Since winds in the turbine layer are of concern here, only the mechanisms that influence the winds in the lowest levels of the atmosphere are addressed. In the surface boundary layer, over flat terrain, the wind profile is primarily influenced by the temperature gradient.

Thermal effects can be classified into three categories (Stull, 1988): stable, unstable and neutral stratification. Conditions are unstable if the potential temperature decreases

significantly up through the atmosphere. As the warm air rises, it expands due to reduced pressure and therefore cools adiabatically. If the cooling is not sufficient to bring the air into thermal equilibrium with the surrounding air, it continues to rise, giving advance to large convection cells. This occurs for instance when the ground is heated by solar radiation, causing warm air near the surface to rise. The result is a thick boundary layer with large-scale turbulent eddies. There is a lot of vertical mixing, resulting in a relatively small change of wind speed with height.

The ABL is stably stratified when the surface is cooler than the air above. If a mass of air moves up in such an atmosphere, the adiabatic cooling effect causes the rising air to become colder than its surroundings and the mass of air moves back to its starting point. It often occurs at night when the ground surface is cold. In this situation, turbulence is limited to that due to the friction with the ground (the mixing thus remaining close to the ground), the wind shear can be large and the flow near laminar.

In the neutral atmosphere, adiabatic cooling of the air as it rises is such that it remains in thermal equilibrium with its surroundings. This is often the case in strong winds, when mechanical turbulence caused by ground roughness causes sufficient mixing of the boundary layer, resulting in a moderate variation in the speed profile.

For power curve purposes, the relevant wind speed range is between cut-in and rated speed as for higher speeds the power remains constant (see chapter 1). Therefore the ABL stability has a significant influence (Sumner and Masson, 2006). Static stability of the lower layer of the ABL varies with season and time of day since it is primarily driven by the magnitude and duration of the solar radiation.

Moreover, as shown by Motta et al. (2005), the diurnal and seasonal variation of the static stability depends on the upwind surface, e.g. offshore or onshore wind. Indeed, the heat capacity of the sea being much larger than that of land, the sea temperature varies much more slowly than the temperature of the land. Consequently, the diurnal variations are much smaller over sea than over land. Moreover, this implies a shift in the seasonal variation of the stability over sea compared to the variation over a nearby land area.

2.1.3 Local effects

Internal boundary layer

The measurement campaigns presented in this thesis were performed at a test site located at the west coast of Denmark (see section 2.2). The parameters influencing the wind speed profiles at sites with upstream roughness changes are therefore of particular interest.

Roughness changes, like those at coastal sites, influence the wind speed profile. As the wind blows onshore from the smooth water surface to the rough land surface, the increased friction decreases the wind speed at the lowest levels. The increased friction and the thermal convection over land increase the turbulence generating an internal boundary layer (IBL), see Figure 2.1. The wind speed profile above the IBL can be considered as the same as the speed profile over the sea, but within the boundary layer, the wind speed profile is much more complex. Indeed, as the surface roughness increases, the lower part of the profiles tends to slow down as it travels further inland. Moreover, Bergström et al. (1988) showed that the decrease in wind speed was larger when the surface layer over land was stably stratified than when the surface layer was unstable. In the unstable surface layer case, the wind speed decrease is smaller because the atmospheric turbulence increases due to enhanced buoyancy production thus compensating for the increased frictional losses.

The wind speed profile at a coastal site is thus influenced by the height of the IBL and it can be relevant to estimate this as a function of the distance from the coast. In the measurements presented by Bergström et al. (1988), the IBL height was determined based on the wind speed profiles at 1500 m inland and it was shown to increase from 40 m for stable stratification to about 80 m during unstable stratification. A wind turbine located at such a site could experience profiles that deviate significantly from the classic forms such as the logarithmic or power law profiles.

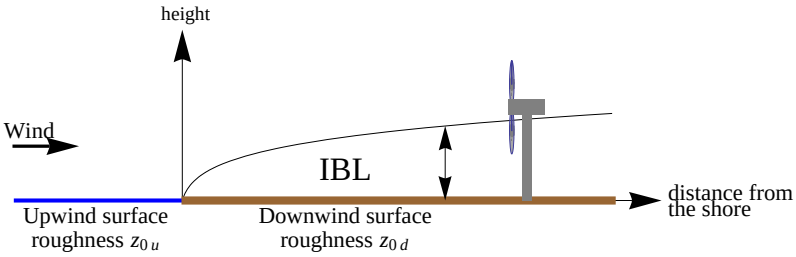

Figure 2.1: *Conceptual model of an internal boundary layer*

Low level jet

A number of mechanisms produce low-level maxima in the wind speed profile. These are generally referred to as low level jets (LLJ). One of the main mechanisms over flat terrain is the decoupling of the flow in very stable conditions. The flow gets decoupled from the surface friction, i.e. the wind is not affected by the surface anymore. The decoupling produces acceleration of the flow above the atmospheric surface layer which is enhanced by the subsequent developed inertial oscillation (Stull, 1988).

LLJs are a regular feature of the night time stable boundary layer and occur very often in plains. This is mentioned here because references to experiments in such sites are made later in the thesis. Banta et al. (2002) studied the characteristics of LLJs over Kansas. Most of the jet maxima they measured occurred below 140m which is within the height range swept by the rotor of a modern multi-MW wind turbine. Moreover, these jets occurred for moderate speed (jet maxima between 7 and 10 m/s), which corresponds to the speed range where a power curve is the most sensitive to shear.

2.2 Wind speed profiles at Høvsøre

2.2.1 Høvsøre test site

Both experiments described in this thesis were performed at Risø DTU's Test Station for Large Wind Turbines. This test station is located at Høvsøre, on the west coast of Denmark. The terrain is flat, surrounded by farmland and is 1.7 km from the coast with the North Sea. This facility comprises a line of 5 multi-MW wind turbines along the North-South direction parallel to the coast, see Figure 2.2. The main wind direction is from West and on the western side of each turbine, at a distance of 250 m (about 2.5 rotor diameters), stands a meteorological mast with a top mounted cup anemometer at the turbine's hub height. These masts are designed and instrumented for power performance measurements in accordance with the IEC 61400-12-1 standard (more information about the test facility in (Jørgensen et al., 2008; Courtney et al., 2008)).

At the southern end of the turbine row stands a meteorological mast (met. mast) intensively instrumented including cup anemometers at several heights between 2 m and 116.5 m. These instruments were used to study the wind speed profiles. A full description of the mast instrumentation is given in the appendix.

2.2.2 Wind shear at Høvsøre

In the absence of orography variations and other local effects, the wind profile is directly affected by the surface layer stability (Businger et al., 1971; VandenBerg, 2008; Swalwell et al., 2008). Figure 2.3 shows the average wind speed difference between 100 and 60 m at the Høvsøre met. mast by hour of the day for each season and for westerly winds (wind direction between 240° and 300°) and easterly winds (wind direction between 60° and 120°). Since both cup anemometers are mounted on south pointing booms with similar geometry, it is assumed that the influence of the mast on both cup anemometers is equal.

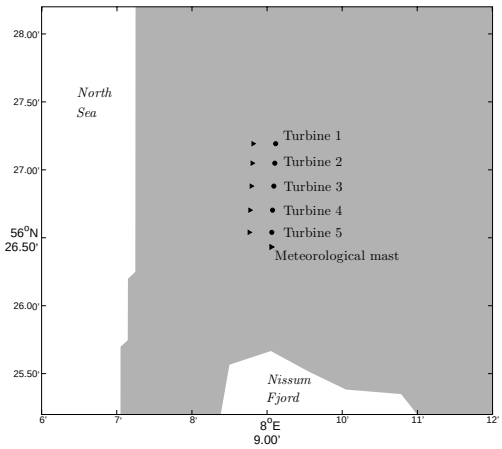

Figure 2.2: *Sketch of the Test Station for Large Wind Turbines, Høvsøre, Denmark.*

The results from the eastern sector exhibit typical variations of wind gradient influenced by the ABL stability, as the wind comes from the land. Clear diurnal variations can be seen in spring and summer, whereas it is more even in winter. The diurnal variations are very much attenuated in winter as the days are shorter, the heating weaker and the temperature differences between day and night are smaller as well as those between air and ground.

For the western sector, where the wind comes from the sea, each histogram in Figure 2.3 is rather even because there is no variation of the wind speed difference with time of the day. The sea temperature changes too slowly to follow the diurnal pattern of the solar radiation because of the large heat capacity of the sea. However, some differences can be seen between the different seasons. The largest speed differences are observed in winter and the smallest in summer. In winter, the wind speeds and the sea roughness are higher and the prevailing conditions are stable, resulting in a larger wind shear than in summer, where there are more unstable conditions.

An example of wind speed time series measured at different levels at the Høvsøre met. mast when the wind was from the East is shown in Figure 2.4. The surface layer stratification, characteristic of stable conditions, appears clearly during the night. This results in a large wind speed shear during the night, whereas the wind speed profile is nearly flat during the day as a consequence of the convective mixing.

An example of wind speed variation for westerly winds is shown in Figure 2.5. The shear remains rather constant all day long.

As the prevailing wind direction at Høvsøre is from the West, the wind speed profiles considered for power curve measurements are influenced by the IBL (see section 2.1.3). Moreover Enevoldsen et al. (2006) showed that peculiarities in the wind from west were observed at Høvsøre, especially in spring, and that the measured power curve was significantly affected by these peculiarities. Furthermore, Nissen (2008) showed that a systematic over-speeding, compared to the traditional logarithmic wind profile, was observed at the top of the surface layer in spring. In order to measure a large range of wind shears in a rather limited period of time, the measurements presented in this thesis were taken in spring (see measurement campaigns described in chapters 7 and 8).

2.3 Wind speed profile characterisation

A categorisation of the wind shear is necessary to investigate its effect on the wind turbine power performance. Various methods of categorisation are generally used for wind resource assessment. This section presents a review of these methods with a discussion of their use in the power performance measurement context.

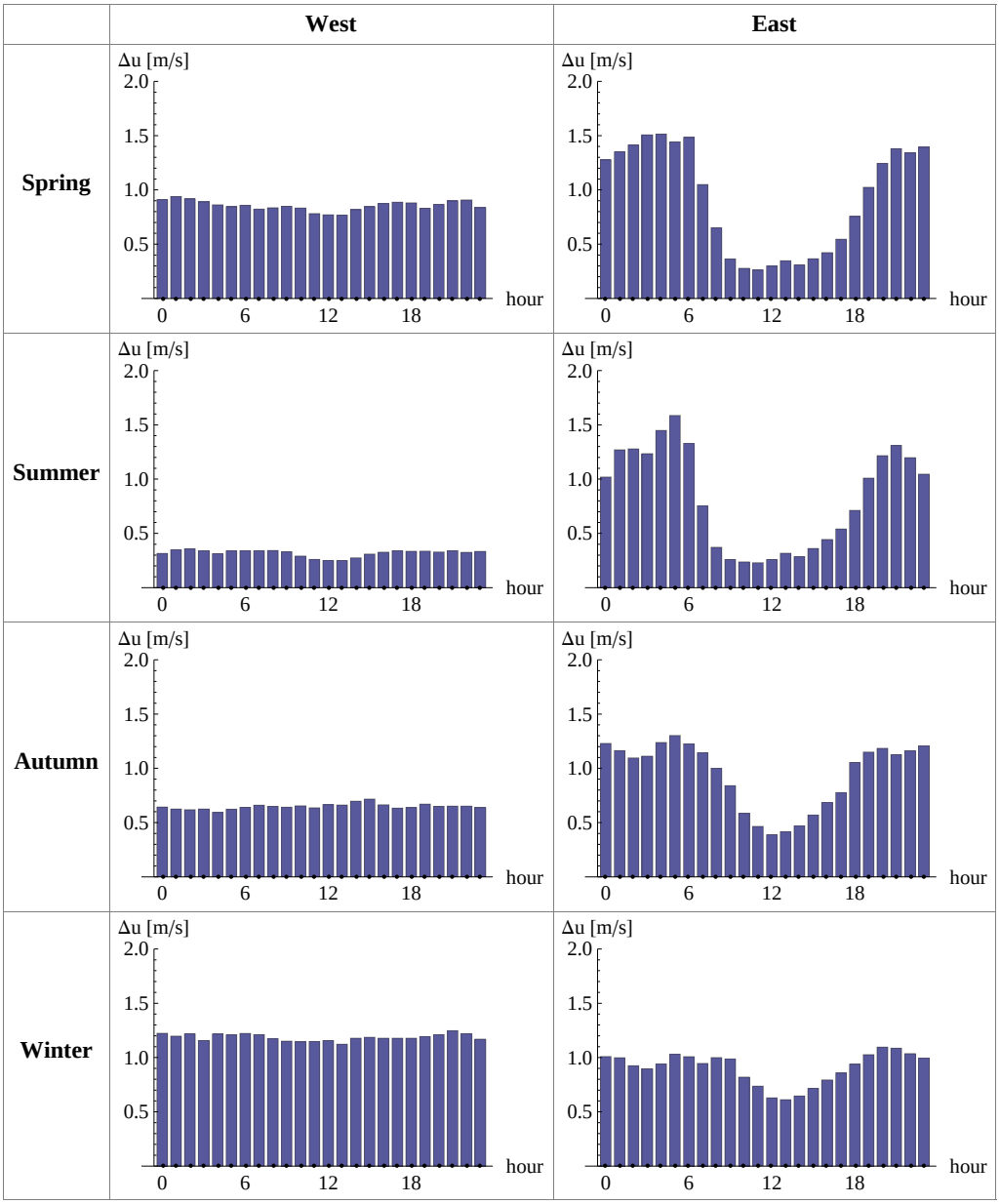

Figure 2.3: *Diurnal variations of the mean wind speed difference, Δu, between 100 and 60 m for the western and eastern wind sectors at Høvsøre and for each season. Average over 5 years of cup anemometer measurements (2005–2009)*

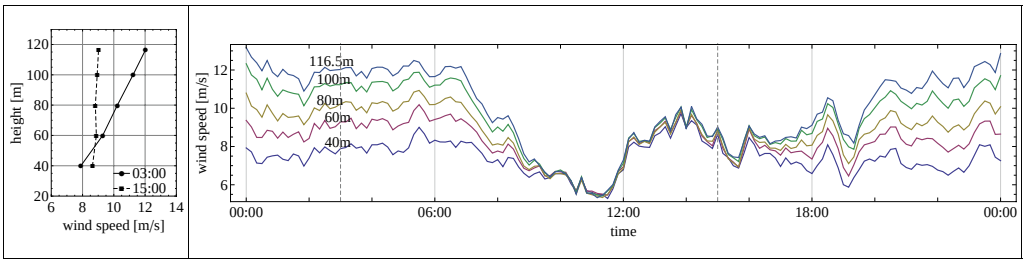

Figure 2.4: *Time series of the wind speed at 5 heights and example of night time and day time profiles from East at Høvsøre on the 25/03/2007*

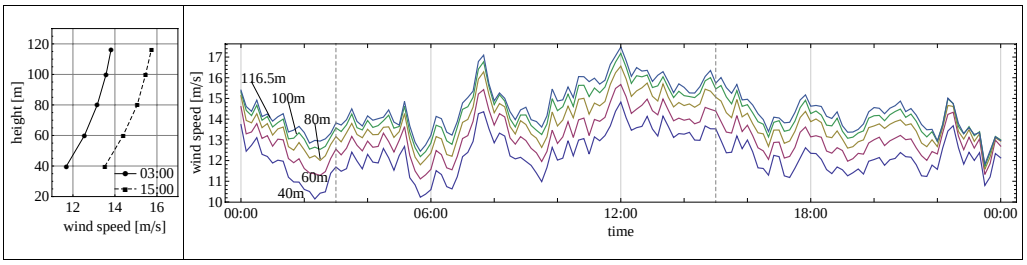

Figure 2.5: *Time series of the wind speed at 5 heights and example of night time and day time profiles from West at Høvsøre on the 05/04/2007*

2.3.1 Stability

As shown previously, the ABL stability has a significant impact on the speed shear. Figure 2.6 shows the distribution of the relative wind speed difference between 100 and 60 m by season for each sector considered in section 2.2.2.

As shown in Figure 2.3, the mean wind speed gradient is larger in winter than in summer. The distribution in spring shows the transition between summer and winter with both a peak at low gradients and some very large shear.

Moreover, in each case are also shown the distribution of stable, neutral and unstable conditions. The stability was quantified with the Obukhov length, L, giving a measure of the degree of dominance of buoyancy over mechanical effects:

$$L = -\frac{u_*^3\, T}{\kappa g \langle w'\theta_v' \rangle} \tag{2.1}$$

where u_* is the friction velocity, κ is the von Kármán constant, taken here to be 0.4, g the gravitational acceleration, T the mean air layer temperature and $\langle w'\theta_v' \rangle$ the kinematic virtual heat flux. Three stability classes were defined as follows:

- unstable: $-500 < L < 0$;
- neutral: $L < -500$ or $500 < L$;
- stable: $0 < L < 500$.

Figure 2.6 illustrates that, for the eastern sector, high shear coincides with stable conditions and low shear with unstable conditions. This is consistent with the fact that, for easterly winds, the shear is mainly governed by the ABL stability. On the contrary, for westerly winds, the correlation between the wind shear and the ABL stability is much weaker because the wind speed profiles for this sector are influenced by the local effects due to the proximity of the coast. As the western sector is the sector of interest for the power curve measurement at Høvsøre, the ABL stability was not chosen as the criterion to categorise the shear.

2.3.2 The logarithmic wind profile

The logarithmic wind profile relates the surface wind stress (here represented by u_*) to the wind shear in the surface layer over homogeneous terrain in neutral conditions as:

$$u(z) = \frac{u_*}{\kappa} \ln\left(\frac{z}{z_0}\right) \tag{2.2}$$

where $u(z)$ is the mean wind speed at the height z and z_0 is the roughness length. z_0 is the height where the downward extrapolated logarithmic velocity profile reaches zero velocity. In the formulation here, variation due to stability and any displacement height is ignored. However, in presence of high surface heat fluxes, such an approach tends to underestimate the high-level wind speeds under stable conditions and to overestimate

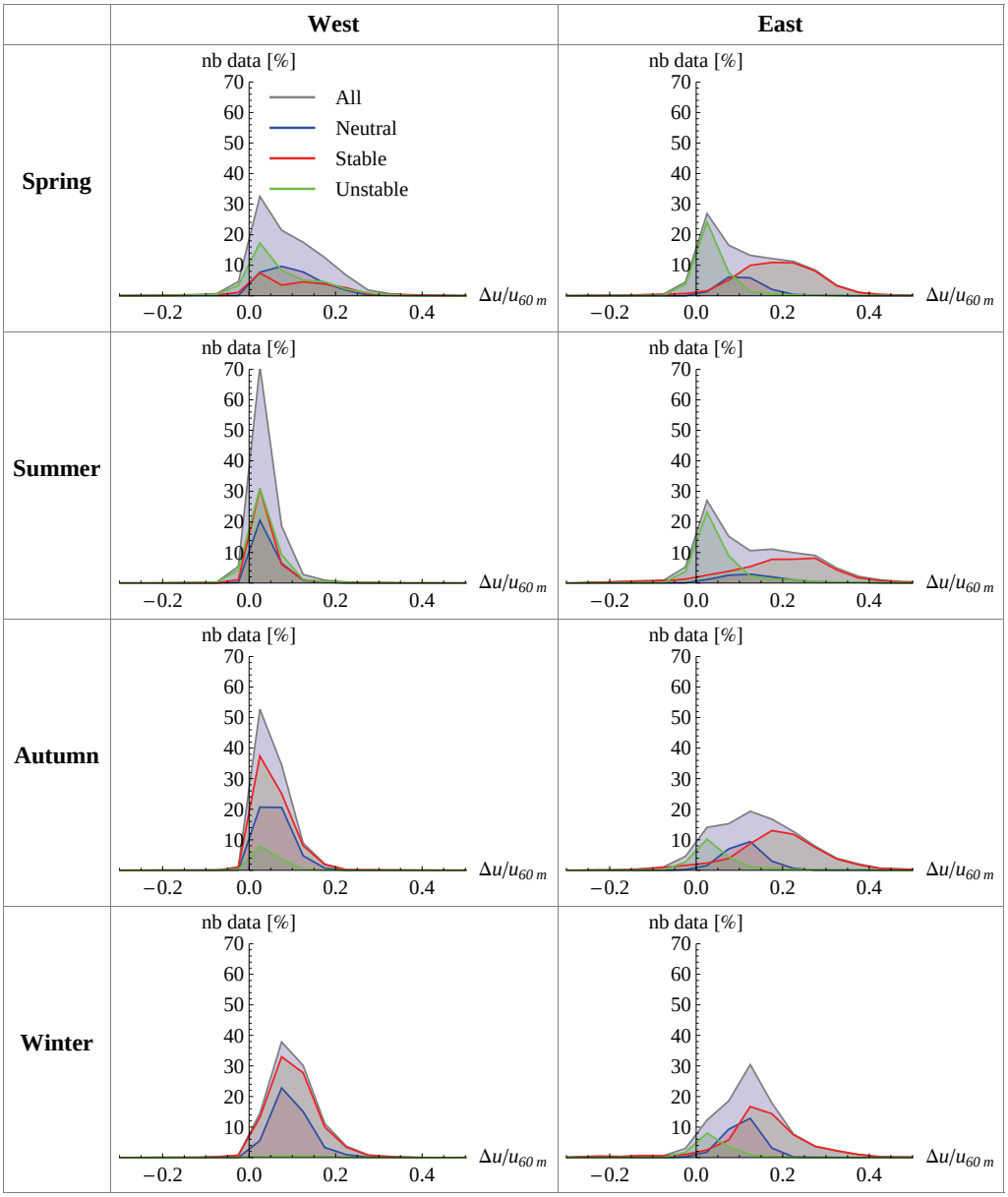

Figure 2.6: *Distribution of the wind speed difference between 100 and 60 m, Δu, normalised with the wind speed at 60 m, $u_{60\,m}$, for all data and each stability class, for the western and eastern sectors at Høvsøre and for each season. The results are given as percentage of the number of data (nb data). Results obtained for 5 years of cup anemometer measurements (2005–2009).*

them under unstable conditions. According to the Monin-Obukhov similarity theory (MOST), the wind speed gradient is a function of the stability parameter z/L (Monin and Obukhov, 1954). For unstable and stable conditions, the wind speed profile is given by:

$$u(z) = \frac{u_*}{\kappa}\left[\ln\left(\frac{z}{z_0}\right) - \psi_m\left(\frac{z}{L}\right)\right] \tag{2.3}$$

where ψ_m is the correction function of the logarithmic profile for stability and its form depends on the sign of L. However MOST is applicable only in homogeneous surface layers which might differ at coastal sites, for example. This is illustrated in Figure 2.7 which shows, for each sector separately, the dimensionless shear (ϕ_m) at 40 m as a function of the stability parameter z/L at $z = 20\,m$. The wind speed gradient, $\partial u/\partial z$,

was derived from cup anemometer measurements at 6 heights, 10–116.5 m, from the Høvsøre met. mast. These measurements were fitted to a second-order polynomial in $\ln(z)$:

$$U = U_0 + A\ln(z) + B\ln(z)^2 \tag{2.4}$$

where U_0, A and B are fitted parameters determined by a least-squares method. The dimensionless wind shear was then obtained by differentiation and normalisation of eq. (2.4):

$$\phi_m = \frac{\kappa z}{u_*}\frac{\partial u}{\partial z} = \frac{\kappa}{u_*}(A + 2B\ln(z)) \tag{2.5}$$

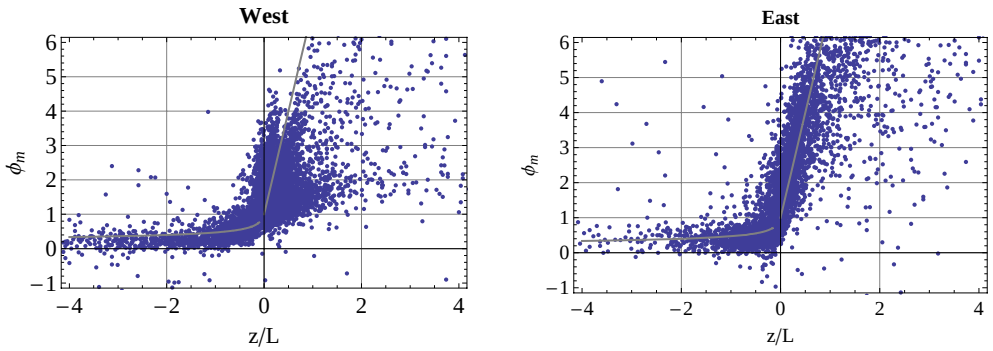

Figure 2.7: *Dimensionless wind shear ϕ_m as function of the stability parameter z/L. The blue dots represent the measurements at Høvsøre. The gray solid line corresponds to a theoretical suggestion from (Högström, 1971).*

Figure 2.7 shows that measurements from the eastern sector follow better MOST than those from the western sector. For the eastern sector, the upstream terrain is mainly characterised by flat farm land and the surface layer is rather homogeneous. For the western sector, the horizontal homogeneity criterion is violated by the presence of an upstream coast. For this sector, the shear is lower than the prediction in unstable conditions, whereas it is higher in the neutral region. Under stable conditions, ϕ_m is broadly distributed and seems to split in different branches, which are probably due to seasonal variations.

2.3.3 Vertical wind gradient

Another approach is to characterise each profile with its gradient at a given height. Based on the approach of section 2.3.2, the wind gradient, $\partial u/\partial z$, at 40 m was derived from differentiation of eq. (2.4). As it is based on a fit to a polynomial, the accuracy of this approach depends on the number of measurement points available. This issue is illustrated in Figure 2.8 (a) showing an example of a measured profile together with the different curves obtained by fitting different measurement points. Figure 2.8 (b) shows that the distributions of the wind gradient strongly depend on the number of points, demonstrating that this result is quite general.

Consistent comparison of the wind shear at different sites with this method requires measurements at the same heights at all sites (same number and same altitudes).

2.3.4 The power law profile

For structural purposes, the power law profile has been used most widely because of its simplicity:

$$u(z) = u(z_{ref})\left(\frac{z}{z_{ref}}\right)^{\alpha} \tag{2.6}$$

where $u(z_{ref})$ is the wind speed at a reference height z_{ref} and α is the shear exponent. It was first introduced by Davenport (1960) to represent the wind speed profile in the

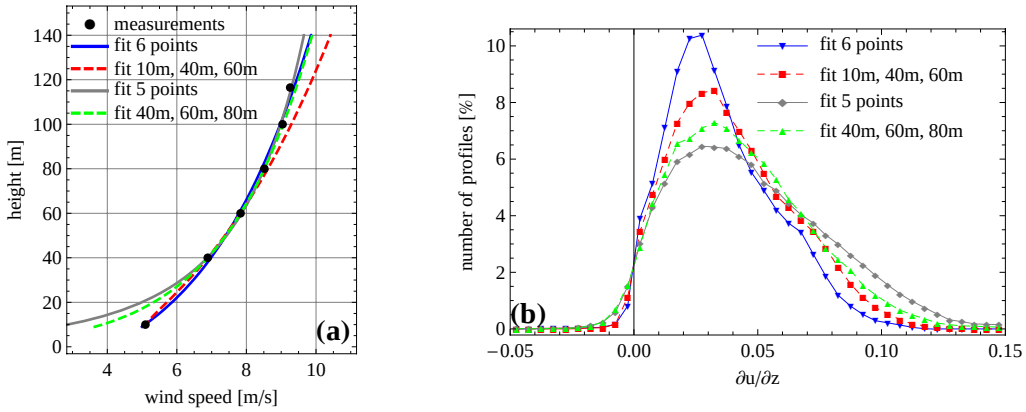

Figure 2.8: *(a) Example of a wind profile measured by the met. mast at Høvsøre and the different curves obtained by fitting the measurements at 6 points (10–116.5 m), at the 3 lowest points (10, 40, 60 m), at 5 points (40–116.5 m), at 3 points (40, 60, 80 m); (b) Distributions of the wind gradient at 40 m obtained by differentiation of the different curves listed previously (Høvsøre, West sector, 2005–2009)*

boundary layer as a function of the gradient wind speed. The power law has been broadly accepted in engineering applications and α is commonly estimated from measurements at two heights on a met. mast:

$$\alpha = \log\left(\frac{u(z_2)}{u(z_1)}\right) / \log\left(\frac{z_2}{z_1}\right) \tag{2.7}$$

where $u(z_1)$ and $u(z_2)$ are the wind speeds measured at the heights z_1 and z_2, respectively. The exponent increases with the roughness of the terrain, and decreases with increasing geometric mean height (Tielmann, 2008). By suitable choice of α, the power law profile closely corresponds to a considerable range of wind profiles compared to the other less empirical forms, and it was found to provide a reasonable fit to the observed wind speed profiles over a wide range of surface roughness and stability conditions (Perez et al., 2005). Based on measurements, Davenport (1960) suggested typical shear exponent values of 1/7,1/3.5 and 1/2.5 for three roughness classes: grassland, forest and city, respectively. The IEC 61400-1 standard for wind turbine design specifies a normal wind shear with $\alpha = 0.2$ (IEC, 1998b). However, numerous sites present shear exponent much larger than 0.2 (Swalwell et al., 2008).

The derivation of the shear exponent from measurements at two heights can be criticized as it depends on the measurement heights. Figure 2.9 (a) shows an example of a measured wind profile and the different power law profiles obtained by deriving the shear exponent from different pairs of measurement heights. Figure 2.9 (b) displays the distribution of the shear exponents obtained with different couples of measurement heights. The higher the measurement points, the smaller the shear exponent. This method fixes the number of measurements points to 2, but a comparison of α for different sites is only meaningful when using identical measurement altitudes.

Furthermore the derivation of the whole wind profile from measurements at only two heights can lead to an ambiguity as shown in Figure 2.10. This figure shows two different measured profiles with very similar wind speed at 40 and 80 m, and the power law profiles derived from the wind speed measurements at those two heights. The power law profile is a poor representation of either of the two measured profiles and it is not possible to distinguish the two profiles from each other with this shear exponent.

A fit to three measurements may be more robust. However, if none of the measurement heights is above hub height, the shear exponent might not be representative of the shear above hub height especially in case of influence of an IBL or for a LLJ. Moreover, the same problem as in section 2.3.3, related to the number and heights of the measurements used to make the fit, is encountered.

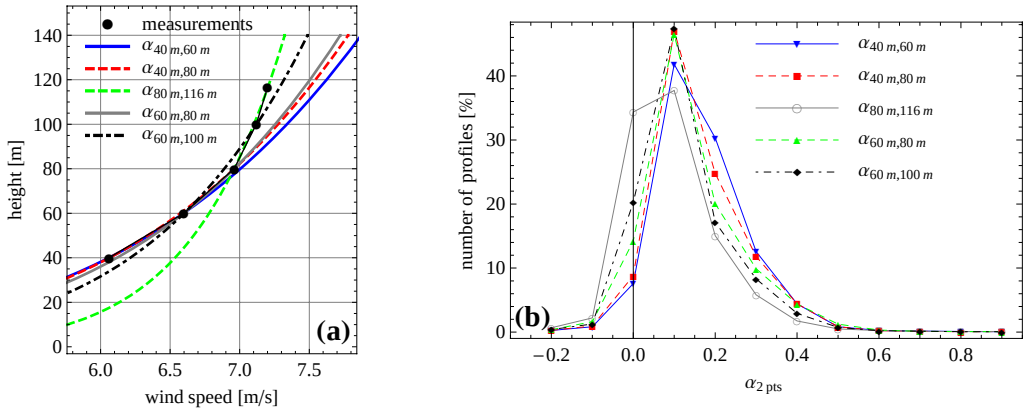

Figure 2.9: *(a) Example of a wind profile measured with the met. mast at Høvsøre and the curves from the power law for the different shear exponents considering measurements at 40-60 m, 40-80 m, 60-80 m, 80-116.5 m, 60-100 m; (b) Distributions of the shear exponents obtained with eq. (2.7) applied to the pairs of measurement heights listed previously (Høvsøre, West sector, 2005–2009)*

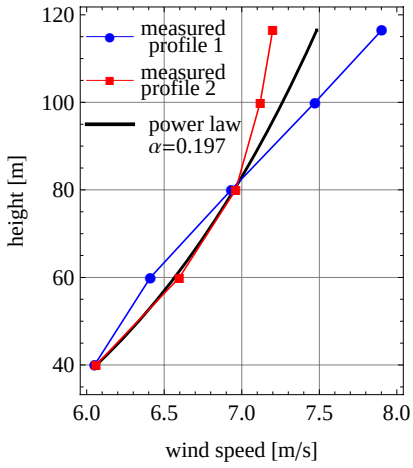

Figure 2.10: *Example of two different observed wind profiles that are represented by the same shear exponent if it is derived from eq. (2.7) at 40 and 80 m*

Although the power law can represent a large range of wind speed profiles, it is limited to wind shear increasing with altitude and wind speed. The only shear exponent cannot accurately represent every 10 minute mean wind profile encountered during a power curve measurement.

2.3.5 Comparison of methods

The different methods used to characterise the wind shear, reviewed in this section, are suitable to obtain the general tendency for the behavior of the wind speed profile at a site or for a wind sector, based on a long measurement periods (a year, for example). However, power performance measurements need to be performed in shorter time period. The IEC 61400-12-1 standard requires a minimum of 180 hours of measurements, which can typically be achieved in a few weeks.

The goodness of fit for various of the methods presented in this chapter was estimated. The goodness of fit was quantified by the residual sum of squares, RSS, derived from

measurements at different heights:

$$RSS = \sum_{i=1}^{N} (u_{fit}(z_i) - u_i)^2 \tag{2.8}$$

where u_{fit} is the fit function (polynomial or power law), u_i is the wind speed measurement at the height z_i, and N is the number of points where the residual is calculated ($N = 5$ here).

The methods compared were:

- polynomial profile obtained by fitting of the speed measurements at 3 heights (40–80m) to eq. (2.4);
- power law profile obtained by fitting of the speed measurements at 3 heights (40–80m) to eq. (2.6);
- power law profile with a shear exponent calculated according to eq. (2.7) using the speed measurements at 40 and 80 m;
- power law profile obtained by fitting of the speed measurements at 5 heights (40–116.5 m) to eq. (2.6).

The RSS distribution for the 4 methods are shown in Figure 2.11. Although all distributions have their maximum at about $RSS = 0.3$, the best representation is obtained with the fit to the power law using 5 measurement points. Indeed, 90% of the $RSSs$ obtained with this method are below 0.7, whereas, for the other methods using 2 or 3 points, at least 21% of the $RSSs$ are above 0.7. The best profile characterisation requires a reasonable number of measurement points that include observations above hub height. Moreover, the RSS distributions for the power law profile derived from 2 and 3 measurement heights are very similar. The polynomial approach is the poorest profile representation, contrary to what one could expect given its extra degrees of freedom in comparison to the power law.

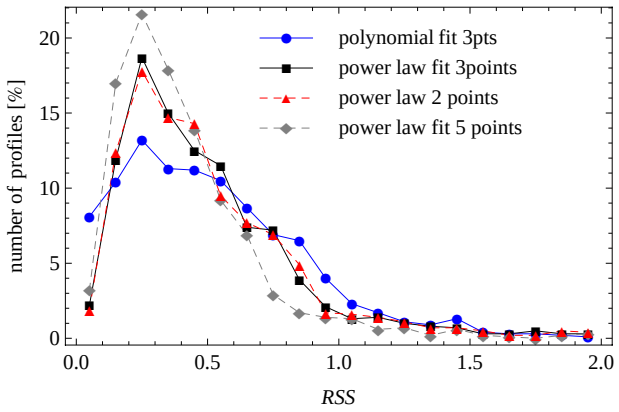

Figure 2.11: *Distribution of RSS (eq. (2.8)) for 4 methods used to represent the wind profile*

Chapter 3

Effect of speed shear on the power performance

The previous chapter showed how variable the wind speed profile can be depending on many parameters such as the geographical location, the wind direction, the season and the time of the day. Seasonal effects on the power output of a turbine have been shown in flat terrain and it was demonstrated that they were due to the seasonal variations of the wind characteristics such as shear and turbulence. The relation between turbine power output variations and shear variations was shown in previous investigations. A review of the main investigations is given as the first part of this chapter. Then, a preliminary study, based on aerodynamic simulations, shows how the shear is related to the power output variations by simulating the response of the turbine in a sheared inflow. This short study also shows the consequence of these variations on the power curve which is the main theme of this thesis.

3.1 Literature review

The effect of the wind shear on the power performance of a wind turbine was the subject of a few earlier investigations. The analysis of the influence of the wind shear on the power performance of a wind turbine is not easy because of the lack of the necessary measurements. Indeed, when shear measurements are available (generally at tests sites dedicated to research), power data are not available, whereas, when power data are available (for instance where a power performance verification is performed), shear measurements are often lacking.

Sumner and Masson (2006) investigated the effect of atmospheric stability on wind turbine power performance. Missing speed profile measurements, the authors used their model, based on the Monin-Obukhov similarity theory, to derive the wind speed profiles from speed and temperature measurements at hub height. They found that the variation in wind speed over the rotor swept area had some effect on the power performance and that characterising the energy with the wind speed at hub height generally overestimate the resource. For the site considered, the difference in annual energy production (AEP) calculated using hub height and disk average wind speed was on the order of 5%. These results were generated for a wind park located in very simple terrain. Larger differences could be expected for higher roughness. However, it was shown in chapter 2 that numerous parameters other than the ABL stability could influence the speed profiles. The profile model used in (Sumner and Masson, 2006) would probably shows some limitations at coastal sites or in places experiencing low level jets. For example, Antoniou et al. (2009) found two different power curves by considering day time and night time measurements separately, in the US Midwest, resulting in an increase in AEP of 3% during the nigh time. No shear measurements were available at the turbine site, but previous studies had shown that low level jets occurred frequently at night in that region. The

authors used an aerodynamic model to simulate the power output of their turbine in case of such a LLJ. They found an increase in power comparable to that they measured during night. These two investigations showed that the power variations coincide with the shear variations. However, assumptions on the speed profiles had to be made.

Other investigations included both speed profile and power measurements. VanLuvanee et al. (2009), for example, categorised measured profiles in two groups: the profiles presenting a low level jet on the one hand, and the profile following a power law on the other hand. Combined with power measurements, these two groups of data resulted in two different power curves. The low level jets gave more power than the power law profiles. Elliott and Cadogan (1990) obtained different power curves for different turbulence intensities, however the difference between the power curves was larger than what could be expected from differences in turbulence intensity. Further investigations showed that the large differences were due to speed shear. During low turbulence conditions, they observed strong shear in the lower half of the rotor and weak or negative in the upper half. The authors concluded that a significant error in power curve measurement could result if the effect of shear was ignored and that with increasing rotor diameter, the hub height wind speed generally became less representative of the disk average wind speed. This investigation also pointed out that it is important to distinguish the effects of the different parameters such as turbulence and shear, which is not always easy to do with measurements as these parameters are often correlated. For example, a stably stratified surface layer generally implies low turbulence and high shear. At the other extreme, under unstable conditions, the turbulence intensity is generally high and the speed profile nearly constant because of the thermal mixing (see chapter 2). This was also shown by Albers et al. (2007) who investigated the power curve measurements of three multi-megawatt wind turbines in flat terrain. The wind shear was characterised by a gradient derived from wind speed measurements at two heights (hub height and below). The data were binned according to the vertical speed gradient but also to the turbulence intensity in order to isolate the shear effect from the turbulence effects. High shear resulted in lower power output than low shear for the turbine with the lowest hub height (therefore experiencing the highest speed gradient), whereas no clear effect of the shear was observed for the two other turbines.

All these investigations showed that speed shear had an influence on the power output of a wind turbine which leads to variations in the power curve. They also showed that investigating the effects of wind shear and turbulence on the turbine power output is not straightforward since these parameters are correlated. Because of this correlation, it is difficult to investigate the influence on the power output of shear independently of turbulence. Numerical models of wind turbine aerodynamics make possible the investigation of the effect of various parameters independently of each other. Walter (2007) performed an advanced analysis of the variations of shear in Texas. Lacking power measurements, he used a blade element momentum (BEM) model to simulate the power output of a large wind turbine subjected to various inflows characterised by different shear exponents. His results showed a decrease in power compared to the power obtained with uniform inflow.

3.2 Aerodynamic simulations set up

The influence of a non-uniform flow on the mechanical power output of a horizontal axis wind turbine is complicated since each section of the rotor blade is subjected to spatially and temporally varying wind during rotation. The use of aerodynamic simulations is a good tool in order to get a better understanding of what difference a sheared inflow makes for a turbine compared to an uniform inflow. It was therefore chosen to make a preliminary investigation with such a tool.

3.2.1 Aerodynamic model

The turbine modeled was a 3.6 MW Siemens, with a rotor diameter of 107 m, hub height of 90 m and a variable-speed, variable-(collective) pitch control strategy. The aerody-

namics of the turbine were simulated with HAWC2Aero (Larsen, 2008). This model simulates, in the time domain, the response of a rigid rotor subjected to aerodynamic forces. The code is a simplified version of the full aeroelastic code HAWC2 (Larsen, 2007) with a different (rigid) structural model. The aerodynamic part of the code is based on the BEM theory, but extended from the classic approach to handle dynamic inflow, dynamic stall, skew inflow and shear effects on the induction (Larsen and Hansen, 2006). Apart from a simplified structural formulation, all other substructures of the code in HAWC2 and HAWC2Aero are identical. In HAWC2Aero the rotor is assumed rigid which leaves only one degree of freedom namely the rotor rotation, whereas the HAWC2 code is based on a multibody formulation with very few limitations on the structural layout. The controller would change the pitch angle though, but only for wind speeds above rated power (which are not of interest in this study). The main benefit of the HAWC2Aero code is the simulation speed (approximately 10 times faster than real time on a standard pc) and the reduced complexity of the input parameters compared to the full HAWC2 code.

In order to check if the rigid structure simplification was acceptable, simulations with the full HAWC2 model were run for a typical multi-MW wind turbine[1], for both cases of elastic and rigid structures. For each type of structure, various wind speed at hub height were considered, and, for each wind speed, two kinds of profiles: a uniform profile (same wind speed at all heights) and a power law profile with a shear exponent of 0.5. The difference in power output obtained for those two kinds of profiles is shown in Figure 3.1 for an elastic structure on one hand and for a stiff structure on the other hand.

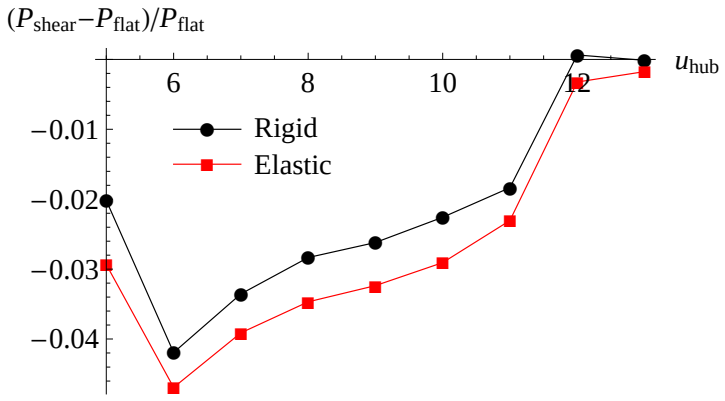

Figure 3.1: *Wind shear effect on the power output for a rigid structure and an elastic structure. Relative power output obtained with simulations carried out with full HAWC2 model for a fictive 5MW wind turbine with a uniform inflow and a sheared inflow (power law with shear exponent of 0.5).*

Figure 3.1 shows that, for the elastic structure, the shear effect on the power output is slightly larger than with the stiff model. However, the difference between the two models is rather small (less than 1% on average). It was therefore assumed for the rest of the investigation that the results obtained with a rigid structural model were representative of the effect of shear on the power performance. Moreover, the fictive wind turbine was modelled with parameter values typical for a modern multi-MW wind turbine. These results are therefore expected to be comparable for the simulations of any multi-MW turbines, similar in concept.

3.2.2 Model limitations

The BEM model is based on a number of assumptions for the flow properties in order to derive simple relations for the axial and tangential induction. One of these assumptions is to ignore the pressure term from the rotation of the wake. Madsen et al. (2007) showed

[1]the 5MW reference wind turbine defined by Jonkman et al. (2009)

that it resulted in an overestimation of the induction in the inner part of the rotor. Moreover, the BEM model does not account for the wake expansion which results in an underestimation of the induction at the tip region.

Furthermore, complicated aerodynamics occur when a horizontal axis wind turbine operates in shear inflow. The existence of wind shear in the free stream can create substantial asymmetries and non periodicities in the structure of the wake behind the rotor (Sezer-Uzol and Uzol, 2009). Zahle and Sørensen (2008) showed that the wind shear resulted in tilting the wake and that the wake expands asymmetrically. This causes a non-uniform induced flow over the rotor which varies with the azimuth position of the blade. However, the classical BEM model assumes a constant induction factor for a given radius as the equations are solved for each annulus independently from the adjacent annuli.

For this reason, the BEM model used in HAWC2 was modified so that the induced velocity varies with azimuth angle. "The characteristic of this implementation of BEM with respect to wind shear is that the local thrust coefficient is based on the local loads of the blade at this specific point but normalized with the free stream velocity averaged over the whole rotor disc. The final induced velocity will thus vary along the blade as a function of azimuth position of the blade" (Bak, 2006).

This code was compared to a classic BEM code, Flex5, and two more advanced models, the Actuator Line model and the CFD based EllipSys3D code, in (Madsen, 2008) and (Madsen et al., 2010). In these investigations, the more advanced models showed the variations of axial induction with azimuth position. A serious concern for the investigation made in this chapter is the fact that some models showed that a sheared inflow resulted in a decrease of the power output whereas others show an increase (see Table 3.1). There is therefore a high uncertainty regarding the influence of wind shear on the turbine rotor, probably because the induction was implemented in different ways in the various models. Even the more advanced models did not demonstrate any convergence, thus not allowing any conclusions as to the correct method.

	El. Power [kW] no shear	El. Power [kW] shear
HAWC2	1928	1870
EllipSys3D	1937	2036
FLEX5	1958	1958
AC-Line	1958	1942

Table 3.1: *Comparison of electrical power at 8 m/s for uniform inflow and shear inflow (power law with exponent of 0.5), from (Madsen et al., 2010).*

The results from the investigation presented here are therefore restricted to HAWC2Aero and the underlying modeling assumptions and uncertainties must be remembered. Despite the high uncertainty of the results, HAWC2Aero was a good compromise as it is based on an improved BEM model that is believed to model the underlying physics in a convincing manner, and yet has a low computational time.

The turbine modeled was a 3.6 MW Siemens, with a rotor diameter of 107m, hub height of 90 m and a variable-speed, variable-(collective) pitch control strategy. The rotation speed was limited to a maximum of 1.963 rad/s for noise reduction. Once this maximum is reached for a given wind speed (about 5m/s), the rotation speed remains constant for higher wind speeds.

In order to restrict the variations in power to the variations due to the speed shear (and not to any other effect), each case is assumed as idealised as possible. The lower part of the boundary layer (corresponding to the "turbine layer" where the turbine rotor stands) is assumed horizontally homogeneous. The wind speed can vary vertically, but is uniform in horizontal planes at each height: $\mathbf{u}(x, y, z) = \mathbf{u}(z) = (u_x(z), u_y(z), u_z(z))$. This assumption is fair to model the surface layer over flat terrain. Moreover, the tower shadow effect is turned off. The tower shadow induces a 3p oscillations of the loads on the

rotor with a larger amplitude than that due to shear (Dolan and Lehn, 2006) but it does not significantly influence the difference in power output between constant and sheared inflows. Finally, the shaft tilt angle was set to 0°, in order to be able to observe the azimuth dependent variations of the angle of attack and the relative speed experienced by the blade due to the wind shear. The tilt angle results in oscillations of the loads with a different phase and larger amplitude than that due to the shear alone. It may therefore reduce the effect of the wind shear on the power performance but it was neglected here in order to focus on the effect of the wind shear.

3.3 Effect of the wind speed shear on the aerodynamics of the turbine

This section aims at showing the differences a sheared inflow makes in the aerodynamics of the turbine compared to a uniform inflow. In order to focus on the vertical variation of the horizontal wind speed on the power output of the turbine, the results presented in this section were all obtained with laminar inflow (no turbulence).

3.3.1 Free wind speed

The simulations results obtained with a sheared inflow, defined by a power law (see eq. (2.6)) with a shear exponent of 0.5, are compared to the results obtained with a constant inflow. Both speed profiles have the same wind speed at hub height: 8 m/s; they are shown in Figure 3.2.

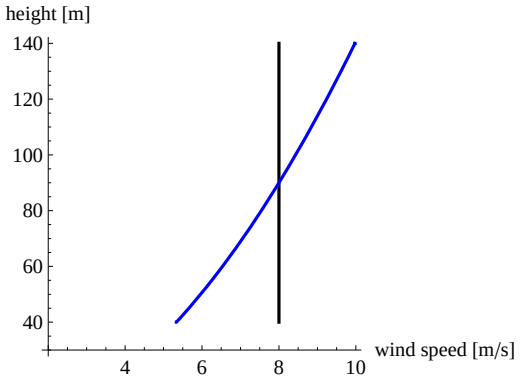

Figure 3.2: *Profiles used as input. Black: constant profile (i.e. no shear); Blue: power law profile with a shear exponent of 0.5. Both profiles have the same wind speed at hub height.*

Figure 3.3 shows the free wind speed (i.e. wind speed as if there were no turbine) seen by a point at a radius of 30m from the rotor centre and rotating at the same speed as the rotor as a function of time. Whereas in a uniform inflow the point is subjected to a constant wind speed, in a sheared flow, the point is exposed to large variations of wind speed (even though the inflow is laminar). The variation of the wind speed seen by this point in time is only due to the fact that it is rotating within a non uniform flow (speed varying with altitude).

Figure 3.4 shows the variations of the free wind speed seen by the same rotating point as previously but as a function of the azimuth position (0° corresponds to the downwards position). The point experiences the hub height wind speed at ±90°, lower wind speed when it is downward (0°) and higher wind speed when it is upward (180°). As the wind speed increases with height in the case of the power law profile, the amplitude of the variations of the free wind speed seen by a rotating point increases with the radius (not shown here), whereas for a uniform flow, the free wind speed is the same whatever the position on the swept rotor disc (any radius, any azimuth).

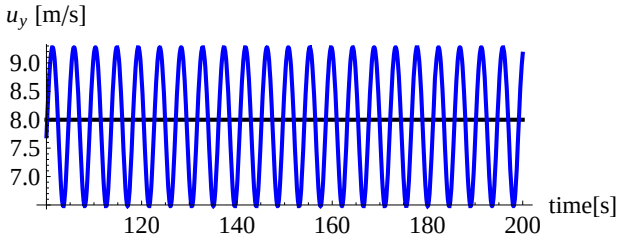

Figure 3.3: *Time series of free wind speed seen from a rotating point, positioned at a radius of 30m, rotating at rotor speed. Black: no shear; Blue: power law profile with shear exponent of 0.5.*

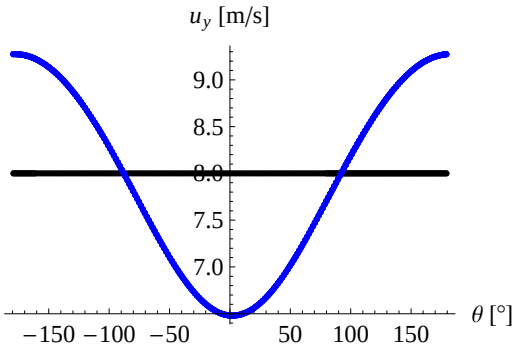

Figure 3.4: *Free wind speed seen from a rotating point, positioned at a radius of 30m, as a function of the azimuth angle. Black: no shear; Blue: power law profile with shear exponent of 0.5.(0° corresponds to downwards)*

3.3.2 Relative speed and angle of attack

A rotating blade does not experience the free wind speed because of the induction due to the drag of the rotor. The forces acting on the rotating blade are directly related to the relative speed - i.e. the speed of the wind passing over the airfoil relative to the rotating blade - and the angle of attack - i.e. the angle between the blade chord line and the relative wind speed - which depends on the induced speed, see Figure 3.5.

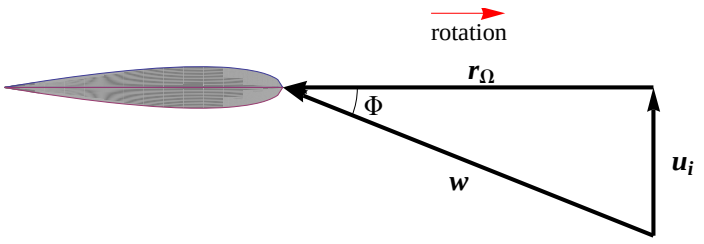

Figure 3.5: *Speed triangle for a blade element.* $\mathbf{u_i}$ *is the induced wind speed,* $\mathbf{r_\Omega}$ *the opposite of blade speed at this radius,* $\mathbf{w}$ *the relative speed and* $\mathbf{\Phi}$ *the angle between the rotor plane and* $\mathbf{w}$ *corresponding to the sum of the pitch angle, the twist angle and the angle of attack.*

The variations of the relative speed and the angle of attack as a function of the blade azimuth angle are shown in Figure 3.6. These two parameters vary with the azimuth angle in a sheared inflow whereas they remain constant in a uniform inflow.

The relative speed and the angle of attack are derived from the rotor speed and the induced velocity, therefore they depend on the way the induction is modeled. It appears that it is difficult to evaluate their variations due to a non uniform flow in a simple way. However, some basic considerations, ignoring the induction, can give a basic insight to the variation of the relative speed and the angle of attack as the blade rotates in a sheared

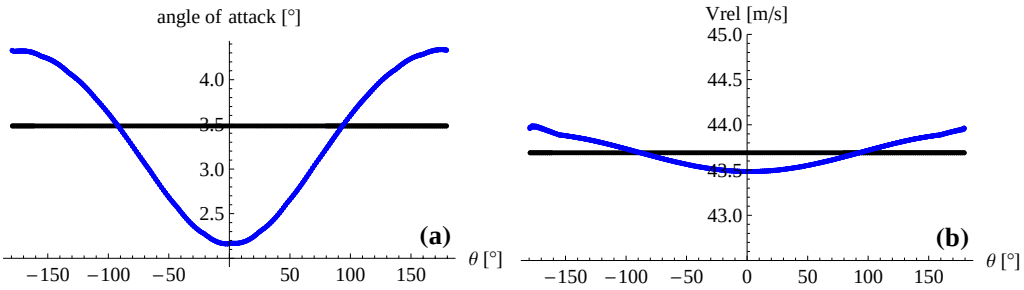

Figure 3.6: *(a): Angle of attack and (b): relative speed as a function of the azimuth angle, seen from a point at radius r=30m on a rotating blade. Black: no shear; Blue: power law profile with shear exponent of 0.5.*

inflow. When the blade points upward, the free wind speed increases compared to the wind speed at hub height (or uniform inflow case), and so does the relative speed and the angle of attack, see Figure 3.7 (right). Inversely, when the blade points downward, they decrease, see Figure 3.7 (left).

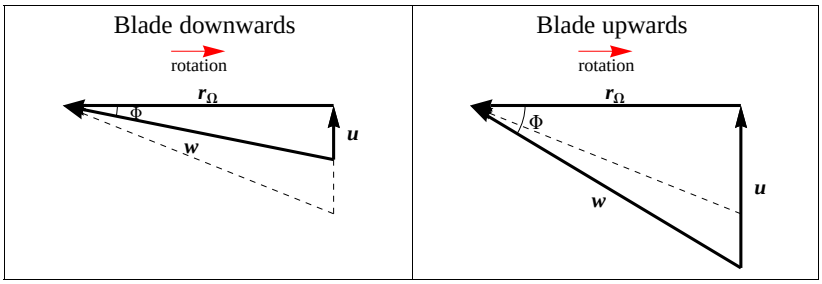

Figure 3.7: *Simplified speed triangles for an upward and downward blade showing the effect of wind speed shear. The speed triangle for a horizontal blade is shown with dashed arrows. As the twist angle is constant for a given position on the blade and the pitch angle is* 0° *for wind speed below rated speed, the variations of* Φ *represents the variation of the angle of attack.*

3.3.3 Tangential force and Torque

The angle of attack and relative speed variations result in a variation of the local lift and drag as the blade rotates, which in turn results in the variation of the local tangential force, see Figure 3.8. The angle Φ, the local lift (dF_L) and the local drag(dF_D) were obtained as output of the model and the local tangential force (dF_T) is given by:

$$dF_T = dF_L Cos(\Phi) - dF_D Sin(\Phi) \tag{3.1}$$

The torque depends on the integral of the tangential force over the whole rotor, hence it does not only depend on the wind speed at hub height but also on the distribution of the speed over the rotor. As shown in Figure 3.9, the torque obtained with a sheared inflow has a small 3p oscillation and the mean torque is lower that the torque obtained for uniform inflow.

3.4 Consequences on the power production

In order to look at the effect of speed shear on the power output of the turbine, simulations were run for various shear exponents between -0.1 and +0.5 and for a range of wind speeds at hub height from 5 to 10 m/s.

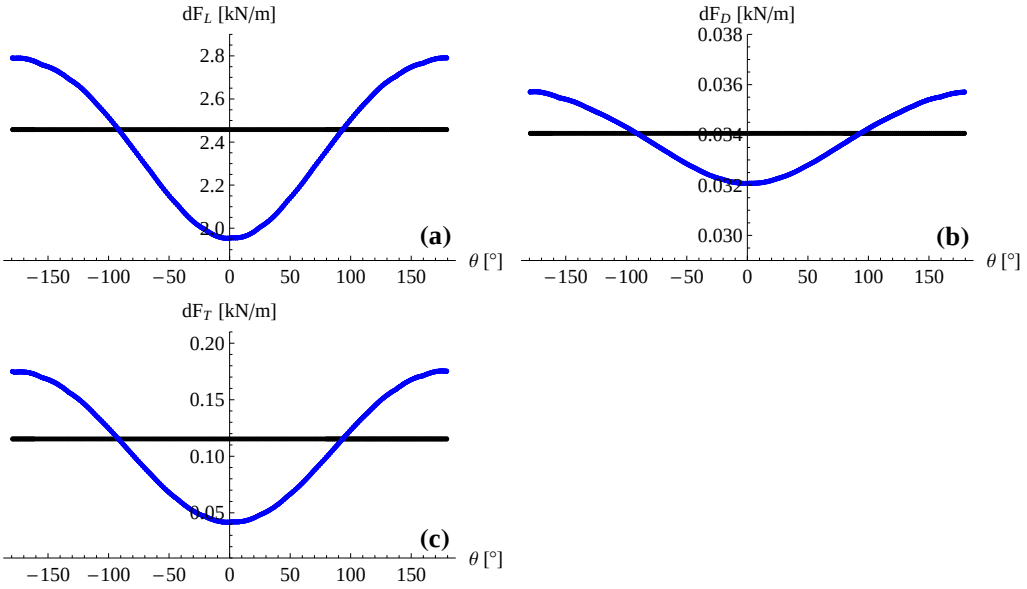

Figure 3.8: *(a): Local lift , (b): local drag , (c): local tangential force seen from a point at radius r=30m on a rotating blade as a function of its azimuth position. Black: no shear; Blue: power law profile with shear exponent of 0.5.*

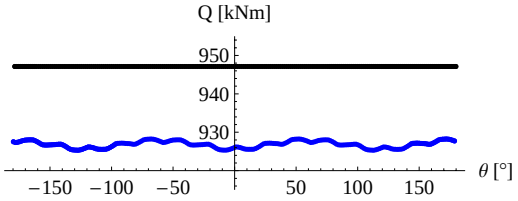

Figure 3.9: *Total torque as a function of the azimuth position. Black: no shear; Blue: power law profile with shear exponent of 0.5.*

Figure 3.10 shows the relative difference between the power output obtained for a sheared profile ($P^{(\alpha)}_{u_{hub}}$) and the power output obtained with a uniform inflow for the same wind speed at hub height, ($P^{(0)}_{u_{hub}}$):

$$\Delta P = \frac{P^{(\alpha)}_{u_{hub}} - P^{(0)}_{u_{hub}}}{P^{(0)}_{u_{hub}}} \tag{3.2}$$

According to HAWC2Aero, the power output depends on the shear exponent, mainly resulting in a decrease of the power when the shear exponent increases. These results are consistent with Walter (2007) and Antoniou et al. (2009) who carried out the same kind of simulations with BEM models and power law profiles. Moreover, it coincides with the measurements presented in (Albers et al., 2007), where high shears gave smaller power outputs than low shear. This shows that power law profiles are expected to give lower power than constant profiles. However it does not mean that large shear necessarily results in lower power. Antoniou et al. (2009) and VanLuvanee et al. (2009) showed that profiles influenced by low level jets, characterised with higher shear above hub height than below hub height, resulted in higher power than other profiles (constant or power law).

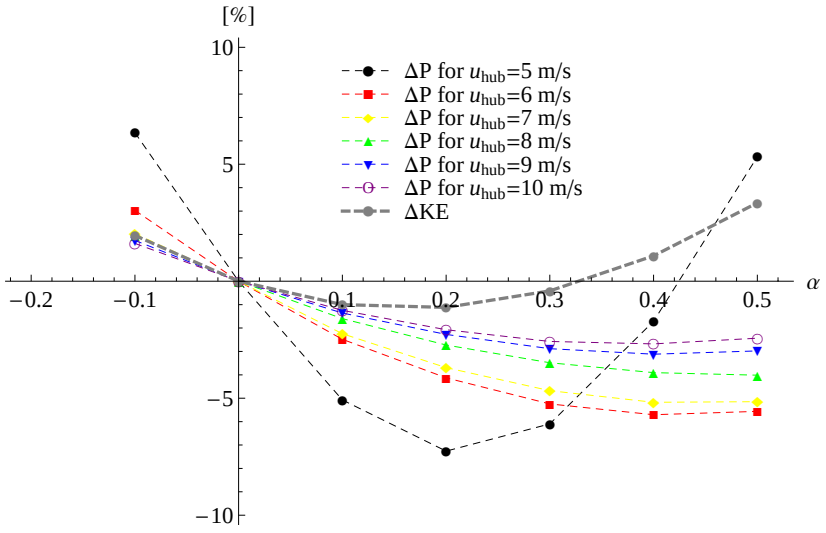

Figure 3.10: *Normalised difference in power output and in kinetic energy flux between sheared inflow and uniform inflow as function of the shear exponent, for various wind speeds at hub height. (The difference in kinetic energy flux is explained in section 5.2.1.)*

3.5 Consequences on the power curve

3.5.1 With power law profiles

As explained in chapter 1, a power curve shows the power output of the turbine as a function of the wind speed at hub height. However, as shown previously, for a given wind speed at hub height, the power output of a turbine is expected to vary with the wind speed shear. This variation in the power output results in a significant scatter in the power curve plot as the shear varies during the power curve measurement. Indeed, if only the wind speed at hub height is considered, all the points corresponding to profiles with the same wind speed at hub height appear with the same abscissa but with different ordinates, since the different profiles result in different power outputs. As an example, the power curve and C_P curve obtained with the results of the simulations described in the previous section are shown in Figure 3.11. C_P was defined as in the IEC 61400-12-1 standard (IEC, 2005):

$$C_P = \frac{P}{\frac{1}{2}\rho u_{hub}^3 A} \tag{3.3}$$

where P is the 10 minute mean turbine power output, ρ is the air density, u_{hub} the speed at hub height and A the rotor swept area.

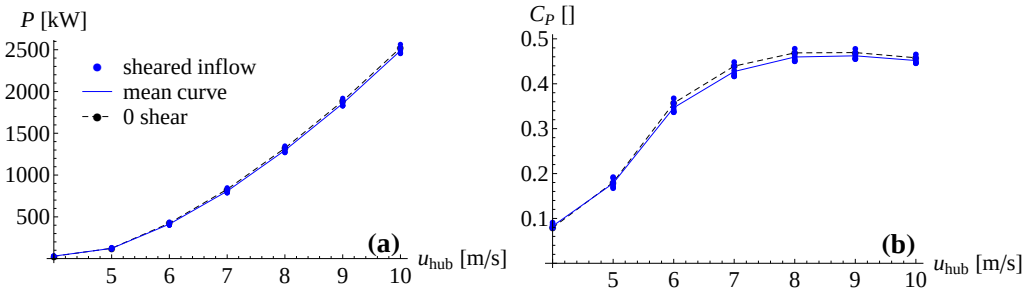

Figure 3.11: *(a): Standard power curve and (b): C_P curve, i.e. plotted as function of the wind speed at hub height and where only the wind speed at hub height is taken into account in the C_P evaluation. Results obtained with the same simulations cases described in section 3.4 (laminar flow with wind speed shear)*

As these results were obtained with results of simulations, the scatter seen in Figure 3.11 are only due to the variations of wind shear as any other possible sources of scatter in the power curve was eliminated (no turbine error and no measurements error).

3.5.2 With other wind speed profiles

One could argue that the scatter in Figures 3.11 (a) and (b) is rather small, but these results were obtained with theoretical power law profiles. Because of their simplicity, use of these theoretical profiles was convenient in order to establish a relation between shear and power performance. However, as it was argued in chapter 2, the power law cannot represent all the wind speed profiles.

In **Paper I**, given in appendix, similar simulations were carried out with profiles different from the power law. 173 profiles were derived from measurements at Høvsøre. The process of derivation of the profiles is fully described in **Paper I**. These profiles were used as inputs for the aerodynamic simulations. The model used was AE_N_WIND, a simplified version of HAWC2Aero, which does not include a controller algorithm (constant rotational speed and constant pitch). It was shown in the paper that this simplification was reasonable for the small range of wind speeds considered. Furthermore AE_N_WIND (as HAWC2Aero) offers the user the possibility of describing any speed profile by giving the wind speed at various heights, thus the approximation of the wind profile with a model was not necessary.

Figures 10 (a) and (b) in **Paper I** show the partial power curve and C_P curve obtained with the 173 profiles. For a standard power curve ("one point"), the scatter is very large. Not only does this confirm that the speed shear can increase the scatter in the power curve but it also shows that profiles deviating from the power law can generate a much larger difference in power output than the power law profiles.

3.6 Summary

The speed shear was shown to have an effect on the response of the wind turbine. According to BEM simulations, a power law profile results in a smaller power output than that obtained with a uniform inflow with the same wind speed at hub height. Moreover the deviation can be larger for other kinds of profiles (different from the power law).

On one hand, different shear types result in different mean power curves. On the other hand, the wind speed profile depends on numerous mechanisms. Hence, most power performance measurement data sets are expected to contain a distribution of profiles resulting in a significant scatter in the power curve and therefore in a significant uncertainty.

Chapter 4

Effect of turbulence intensity on the power performance

In the previous chapter, only simulations with laminar inflow were considered in order to isolate the effect of wind shear. However real inflows are not laminar, and a wind turbine is subjected to the combined effect of shear and turbulence. This chapter presents a short investigation of the influence of the turbulence intensity on the power performance and the power curve in the first part, and the influence of wind shear combined with turbulence intensity in the second part. The turbulence intensity (TI) is defined as :

$$TI = \frac{\sigma}{u} \tag{4.1}$$

where u is the 10 minute mean wind speed and σ the standard deviation.

In HAWC2Aero, the time variations of the three components of the wind speed are simulated by using the Mann model of turbulence (Mann, 1998). This is a spectral tensor model for the atmospheric surface layer turbulence under neutral stratification. The model assumes that the turbulence is homogeneous in space but non-isotropic. The method generates a full three-dimensional turbulence field with all three components. The wind speed time variations are superimposed to the mean wind speed profile. In order to obtain statistically significant results, each shear case is run with 10 different time series created by the Mann model using different seedings. In all simulations presented here, the turbulence intensity is assumed constant with height, in order to focus on the effect of shear.

4.1 Isolated turbulence

4.1.1 Simple aerodynamics

The simulations cases considered in this section correspond to a statistically uniform flow - i.e. same average and turbulence intensity everywhere - with a mean wind speed of 8 m/s and a turbulence intensity of 10%. Figure 4.1 shows the time series of the wind speed at 3 points at 3 different heights observed from a stationary frame of reference. The wind speed varies with time at all points and is not exactly the same at all three points at each time step but the mean and turbulence properties are nominally identical.

Figure 4.2 (Top) shows the free wind speed from a point rotating at rotor speed. Higher variance is added to that due to the wind turbulence by the rotational sampling of the wind speed as the point repeatedly passes through coherent structures. This larger variance is consequently also evident in the angle of attack variations (see Figure 4.2 (Bottom)), and hence on the loads on the turbine rotor.

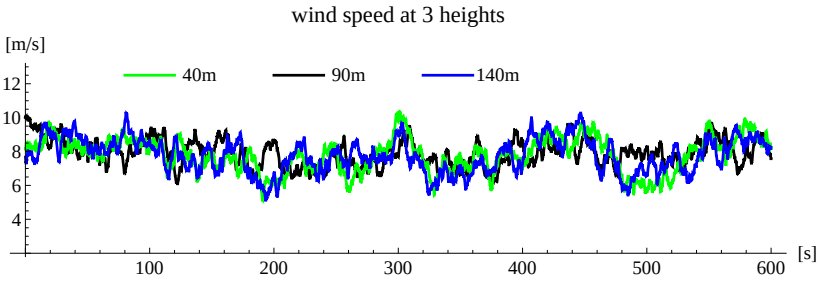

Figure 4.1: *Time series of the longitudinal wind speed at three heights for a statistically uniform inflow (i.e. no shear) and TI=10%*

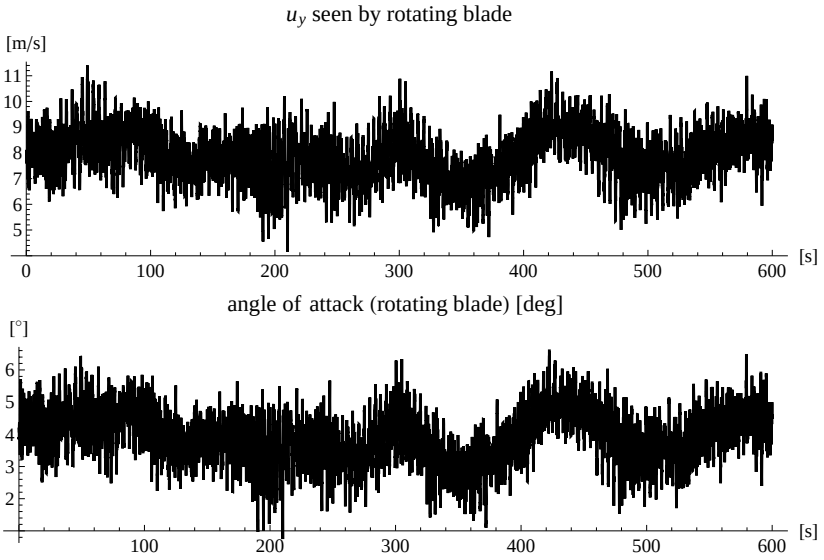

Figure 4.2: *(Top): Time series of the longitudinal free wind speed from a rotating point at a radius of 36m from the rotor center; (Bottom): Times series of the angle of attack from point at a radius of 36m on a rotating blade - for a statistically uniform inflow (i.e. no shear) with a mean wind speed of 8 m/s and TI=10%*

4.1.2 Consequences on the power curve

A standard power curve is derived from 10 minute averaged values of the speed at hub height and the power output of the turbine. The wind speed used in the power curves presented in this chapter comes from the average of the time series generated by the Mann model. Figure 4.3 shows the power curve scatter plot obtained with various turbulence intensities from 5% to 20% for different mean wind speeds between 3 and 13 m/s. For a given mean wind speed value used as input to the model, the mean speed output can vary slightly from one seed to another as it can be seen in Figure 4.3. Hence the standard deviation of the mean wind speed in each speed bin is not zero and increases with the turbulence intensity. The response of the turbine to the speed fluctuations depends on the internal dynamics of the turbine. According to HAWC2Aero simulation results shown in Figure 4.3, the standard deviation of the power increases with the turbulence intensity.

When the wind speed fluctuates around the rated wind speed, the power extracted is limited to the rated power. Therefore only "negative fluctuations" (i.e. the instantaneous wind speeds below rated speed) of the wind are transformed into power fluctuations. Consequently, 10 minute mean power obtained with a given turbulence intensity is generally smaller than the power that would be obtained with the same mean wind speed and a laminar flow (TI=0%), and the mean power decreases as the turbulence intensity increases (Hunter et al., 2001; Albers et al., 2007) , see Figure 4.4. In the same way, as

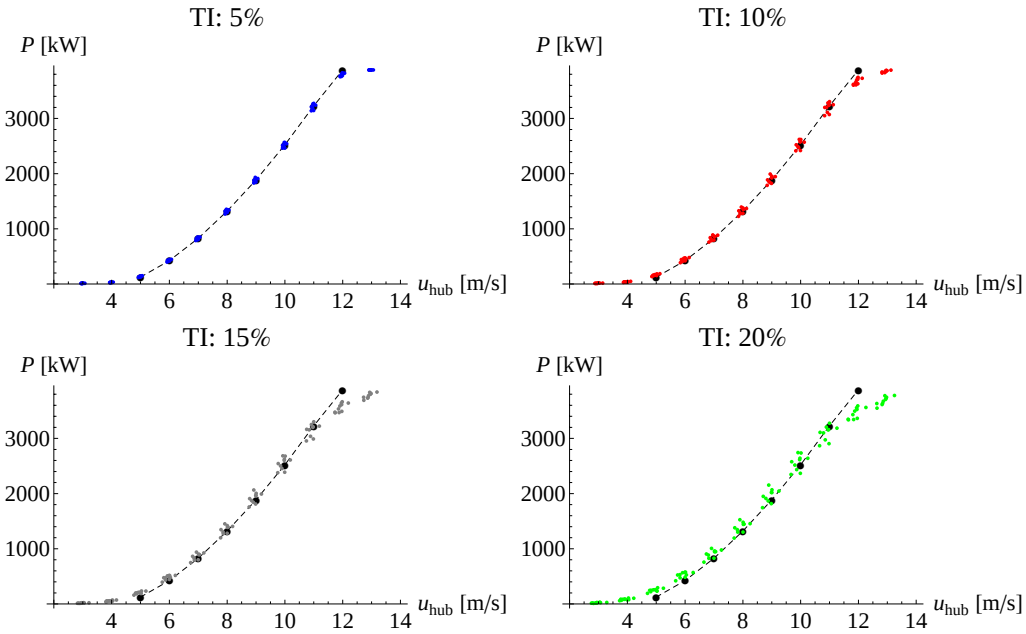

Figure 4.3: *Power curve scatter plots obtained for various turbulence intensities from 5% to 20%. Black points: points obtained for uniform inflow; line: interpolation line considered as representation of the zero-turbulence power curve; colored dots: points obtained for turbulent inflow. The scatter increases with the turbulence intensity.*

the wind speed fluctuates around the cut-in wind speed, only the positive fluctuations are transformed in power fluctuations. Therefore, near the cut-in wind speed, the mean power is expected to increase with the turbulence intensity. Between the cut-in and rated speeds, the turbine is expected to respond to any wind speed fluctuations (positive or negative). Within the wind speed range where the C_P is constant (or varying very little, as between 6 and 10 m/s in this example, see Figure 3.11), the turbine power increases with the turbulence intensity as the power is then proportional to the cube of the wind speed:

$$P = \frac{1}{2}\rho u^3 A C_P \tag{4.2}$$

Indeed, the average of the cube of the wind speed increases with the turbulence intensity. The wind speed can be decomposed as the 10 minute average, $\langle u \rangle$, and the fluctuations, u', defined as: $\langle u' \rangle = 0$:

$$u = \langle u \rangle + u' \tag{4.3}$$

The cube of the wind speed then becomes:

$$u^3 = (\langle u \rangle + u')^3 = \langle u \rangle^3 + 3\langle u \rangle^2 u' + 3\langle u \rangle u'^2 + u'^3 \tag{4.4}$$

and the average of the cube of the wind speed becomes:

$$\langle u^3 \rangle = \langle u \rangle^3 (1 + 3\frac{\langle u'^2 \rangle}{\langle u \rangle^2} = \langle u \rangle^3 \left(1 + 3\frac{\sigma^2}{\langle u \rangle^2}\right) = \langle u \rangle^3 \left(1 + 3TI^2\right) \tag{4.5}$$

where $\sigma^2 = \langle u'^2 \rangle$ is the 10 minute wind speed variance and TI the turbulence intensity defined by eq. (4.1). The second term of eq. (4.4) disappears by definition of the fluctuations and the last term disappears if the fluctuations distribution is assumed to be Gaussian. According to this approximation, the average of eq. (4.2) is:

$$\langle P \rangle = \frac{1}{2}\rho \langle u \rangle^3 \left(1 + 3TI^2\right) A C_P \tag{4.6}$$

The effect of the turbulence intensity on the power curve can be seen as the combination of one effect on the mean power curve that varies with the turbulence intensity (especially around rated speed) and one effect on the scatter that increases with the turbulence intensity. The scatter in the power curve results from both effects as it usually results from a distribution of turbulence intensities.

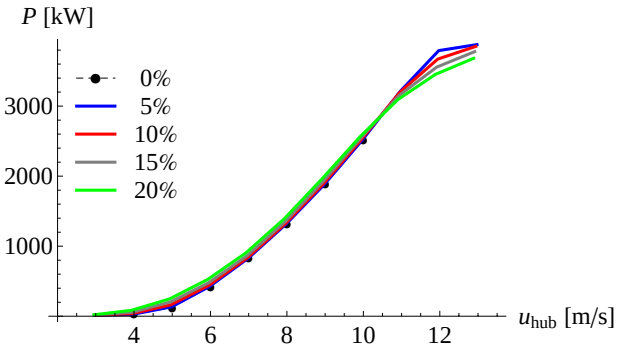

Figure 4.4: *Mean power curves for various turbulence intensities*

4.2 Turbulence and shear

4.2.1 With power law profiles

In this section, the inflow for the simulations consists of a sheared mean speed profile (following the power law with 8 m/s at 90m (hub height) and a shear exponent of 0.5) superimposed with turbulence (with a turbulence intensity of 10%).

Figure 4.5 shows the time series of the wind speed at three heights (as in Figure 4.1 with no shear). The effect of the speed shear is that the wind speeds now fluctuate around three different mean values (for the three different heights). The consequences are an increase of the fluctuation amplitude of the wind speed seen by the blade and of the angle of attack, as shown in Figure 4.6, and therefore of the loads on the turbine rotor.

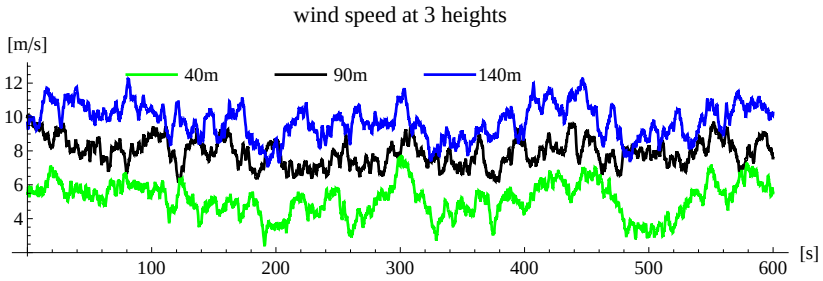

Figure 4.5: *Time series of the longitudinal wind speed at three heights for an inflow combining a mean speed profile following the power law with* $\alpha = 0.5$ *and TI=10%.*

Figure 4.7 shows the longitudinal free wind speed as a function of the azimuth angle (as done in the shear effect analysis in Figure 3.4). The cyclic fluctuation of the speed due to shear appears clearly in spite of the fluctuations due to the turbulence. This shows that, even though the scatter due to turbulence can be larger than the scatter due to shear, the shear effect is not overwhelmed by the turbulence. This is obviously relative to the shear and turbulence magnitudes. However, for the case of flat terrain, the turbulence intensity is limited and only a few values exceeding 15% are expected (based on westerly wind observation at Høvsøre).

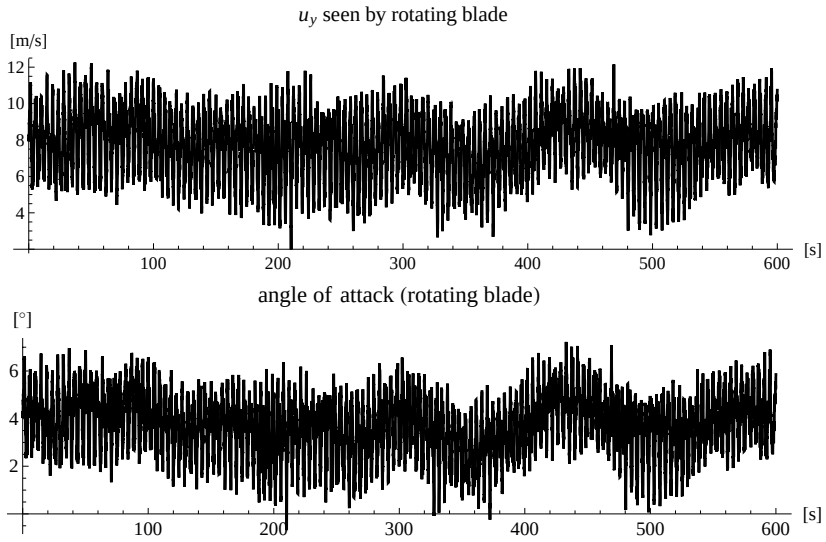

Figure 4.6: *(Top): Time series of the longitudinal free wind speed from a rotating point at a radius of 36m from the rotor center; (Bottom): Times series of the angle of attack from point at a radius of 36m on a rotating blade - for a sheared inflow with a power law profile with* $\alpha = 0.5$ *and TI=10%*

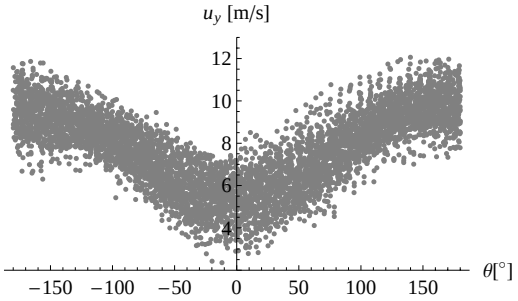

Figure 4.7: *Longitudinal free wind speed seen from rotating point as function of the azimuth angle. TI=10%, power law profile with* $\alpha = 0.5$.

4.2.2 With other wind speed profiles

Paper I presents results from simulations combining wind shear and turbulence intensity. The profiles are the same as from the laminar cases (see section 3.5.2) and the turbulence intensities were likewise derived from the measurements at Høvsøre. The turbulence intensity was therefore not constant with altitude. However, it was generally rather small as the Høvsøre site is located in flat terrain and surrounded by grassland and the sea.

Figure 10 (c) and (d) in **Paper I** show the partial power curve and C_P curve obtained with the output of these simulations. The range of power outputs is similar to the laminar inflow simulations, although the standard deviation is slightly larger. The impact of moderate turbulence remained rather small compared to that of the large range of wind shears.

4.3 Summary of the turbulence effect

The turbulence intensity globally increases the mean power output except near rated speed where the power output decreases for increasing turbulence intensity. Moreover, the turbulence intensity increases the scatter in the power curve, first, because it increases

the power standard deviation, and secondly because the time averaging results in different power curves for different turbulence intensities.

In spite of the fluctuations due to turbulence, the fluctuations due to shear are still visible. A reduction of the scatter due to shear in the power curve would therefore reduce the global scatter in the power curve even if part of the scatter is due to turbulence.

Chapter 5

Equivalent wind speed

Wind farm developers demand site specific power curves in order to reduce annual energy production (AEP) uncertainties. The only way to achieve this goal is to introduce the influence of secondary parameters in the power performance measurement through the definition of generalised power curves. Frandsen et al. (2000) and Eecen et al. (2006) presented such a generalised power curve defined as a multivariable linear function. However, such a model presents some difficulties from a technical and marketing point of view, as the power curve is presented as a multivariable function of independent parameters and the calculation of the energy production then requires to estimate the combined probability density function, which can be a serious challenge. Another possibility to generate a generalised power curve which accounts for the influence of other wind descriptors additionally to the wind speed at hub height consists in defining a unique generalised parameter which explains the variability of ten minutes average electrical power in a better way than the wind speed at hub height.

In this thesis, the focus has been on the role of wind shear as a secondary parameter. The goal is to define a generalised wind speed parameter that would account for the variability of the turbine power output due to the wind shear. A power curve presented as a function of such a parameter would be more repeatable than the standard power curve (function of the wind speed at hub height). The aim is to reduce the sensitivity to shear and this is equivalent to reducing the scatter due to shear in the measured power curve.

5.1 Definition

The idea is to define a wind speed that would be representative for the whole wind profile generating the rotor torque; i.e. a wind speed "equivalent" to the whole wind profile for the turbine power performance. Different definitions for this "equivalent wind speed" are conceivable. Elliott and Cadogan (1990) found that, for strong shear, the power curves obatined with hub height wind speed and disk-averaged wind speed were substantially different. Sumner and Masson (2006) obtained a more consistent power curve by using the integral of the wind profiles over the rotor swept area.

Another idea is to consider the kinetic energy of the wind profile through the turbine rotor swept area. As mentioned earlier, the current IEC standard (IEC, 2005) for power performance measurement takes the wind speed at hub height as the unique wind speed reference. The power coefficient is defined as in eq. (3.3). The denominator, assumed to represent the kinetic energy flux through the rotor swept area, corresponds to the kinetic energy flux of a constant profile with the wind speed u_{hub}:

$$KE_{hub} = \frac{1}{2}\rho u_{hub}^3 A \tag{5.1}$$

where ρ is the air density, u_{hub} the wind speed at hub height and A the rotor swept area. However, the kinetic energy flux does not only depend on the wind speed at hub height

but on the whole wind speed profile. For a horizontally homogeneous boundary layer, the wind speed only depends on the altitude z. The kinetic energy flux through the rotor swept area is then given by:

$$KE^{Th}_{profile} = \int_{z_{hub}-R}^{z_{hub}+R} \frac{1}{2}\rho u(z)^3 c(z-(z_{hub}-R))dz \tag{5.2}$$

where z_{hub} is the turbine hub height, R the rotor radius and $c(z)$ is the chord (of the circle defined by the rotor swept area) as a function of height z:

$$c(z) = 2\sqrt{2Rz - z^2} \tag{5.3}$$

Note that eq. (5.2) is accurate if u is the component of the wind speed vector which is orthogonal to the turbine rotor plan. As the rotor is usually tilted upward, the horizontal component of the wind speed vector is not exactly orthogonal to the rotor plane. However the tilt angle being very small(about 6°), it is acceptable to disregard the non-orthogonality.

Three simple definitions for an equivalent wind speed taking the speed shear into account are then:

- a simple average:
$$U_{avg} = \frac{1}{2R}\int_{z_{hub}-R}^{z_{hub}+R} u(z)dz \tag{5.4}$$
- the integral of the wind speed profile over the rotor swept area, i.e. a linear average weighted with the rotor area:
$$U_{disk} = \frac{1}{A}\int_{z_{hub}-R}^{z_{hub}+R} u(z)c(z-(z_{hub}-R))dz \tag{5.5}$$
- an equivalent wind speed giving the same kinetic energy flux as the whole profile based on the approximation given by eq. (5.2) - a cubic average weighted with the rotor area:
$$U_{KE} = \left(\frac{1}{A}\int_{z_{hub}-R}^{z_{hub}+R} u(z)^3 c(z-(z_{hub}-R))dz\right)^{1/3} \tag{5.6}$$

5.2 Equivalent wind speed for shear

5.2.1 With power law profiles

U_{disk} (eq. (5.5)) and U_{KE} (eq. (5.6)) were tested with the outputs of the simulations described in section 3.4, i.e. laminar inflows with power law shear for various wind speeds at hub height between 5 and 10 m/s and α between -0.1 and 0.5. The results are shown in Figure 5.1.

The idea of using an equivalent wind speed in the power curve is to get a new distribution of the points which is more consistent with the relation between the wind profile input to the turbine and the power output. This new points distribution is expected to decrease the dispersion of the points around the mean power curve (or C_P curve), called the scatter hereafter. However, the modification of the points distribution also involves a modification of the mean power curve. Figure 5.2 shows the mean power curves and C_P curves obtained with the different wind speed definitions: the wind speed at hub height (u_{hub}), U_{disk} and U_{KE}.

The linear average (U_{disk}) gives a mean power curve very close to the zero-shear power curve and results in an obvious reduction of the scatter as the points are well aligned with the mean power curve. However this is strongly suspected to be due to the approximation made in the aerodynamic model. In HAWC2Aero, the local torque coefficient, i.e. the torque for one computational cell of the swept rotor area normalised with the dynamic

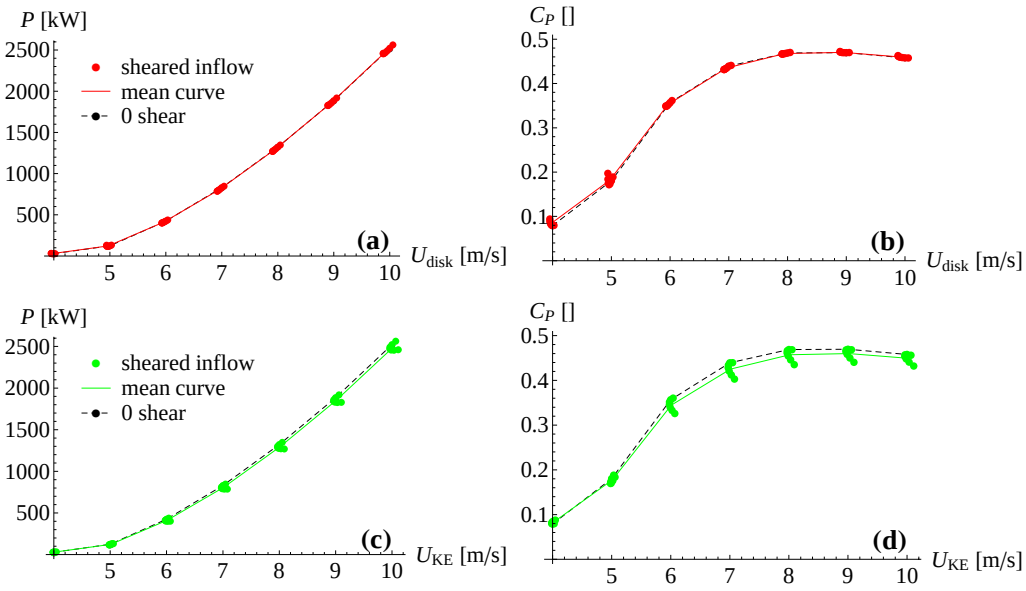

Figure 5.1: *Power curve and C_P curve obtained using different wind speed definitions in abscissa. Black points: points obtained for uniform inflow; dashed line: interpolation line considered as representation of the zero-shear power curve. (a): power as function of U_{disk}; (b): C_P as function of U_{disk}; (c): power as function of U_{KE}; (d): C_P as function of U_{KE}. The results shown in this figure were obtained from the same simulation cases as the results displayed in Figures 3.10 and 3.11, laminar inflows with power law shear.*

force, is normalised using the mean wind speed over the rotor swept area (Bak, 2006). More realistic results may be obtained by using the wind speed averaged over the cell area.

The cubic average (U_{KE}) gives a mean power curve similar to the mean power curve obtained with the wind speed at hub height. The scatter is slightly reduced for this example. Figure 3.10 shows the relative difference between the kinetic energy flux obtained with eq. (5.2) for a power law profile [1] and that obtained when assuming a constant wind speed profile (eq. (5.1)). The relative difference is defined by:

$$\begin{aligned} \Delta KE &= \frac{KE^{(\alpha)}_{profile} - KE^{(0)}_{hub}}{KE^{(0)}_{hub}} \\ &= \frac{1}{A}\int_{z_{hub}-R}^{z_{hub}+R}\left(\left(\frac{z}{z_{hub}}\right)^{3\alpha} - 1\right) c(z-(z_{hub}-R))dz \end{aligned} \tag{5.7}$$

This quantity does not depend on the wind speed at hub height, but on the turbine rotor radius and hub height, hence it varies from one turbine to another. However for a given wind turbine, this quantity only depends on the shear exponent (α). Figure 3.10 shows that, for the turbine simulated here, the kinetic energy flux decreases down to a minimum around $\alpha = 0.2$ and increases again for larger shear exponents. The simulated turbine power output does not follow the kinetic energy flux variations as it remains smaller than P^0_{hub} for any positive shear exponent for most values of u_{hub}.

On the other hand, using U_{KE} results in a way of plotting the power output of the turbine as a function of the power input. This could show the true efficiency of the turbine, i.e. its ability to extract the power available in the wind.

[1] The kinetic energy flux is not an output of HAWC2Aero, it has been calculated manually.

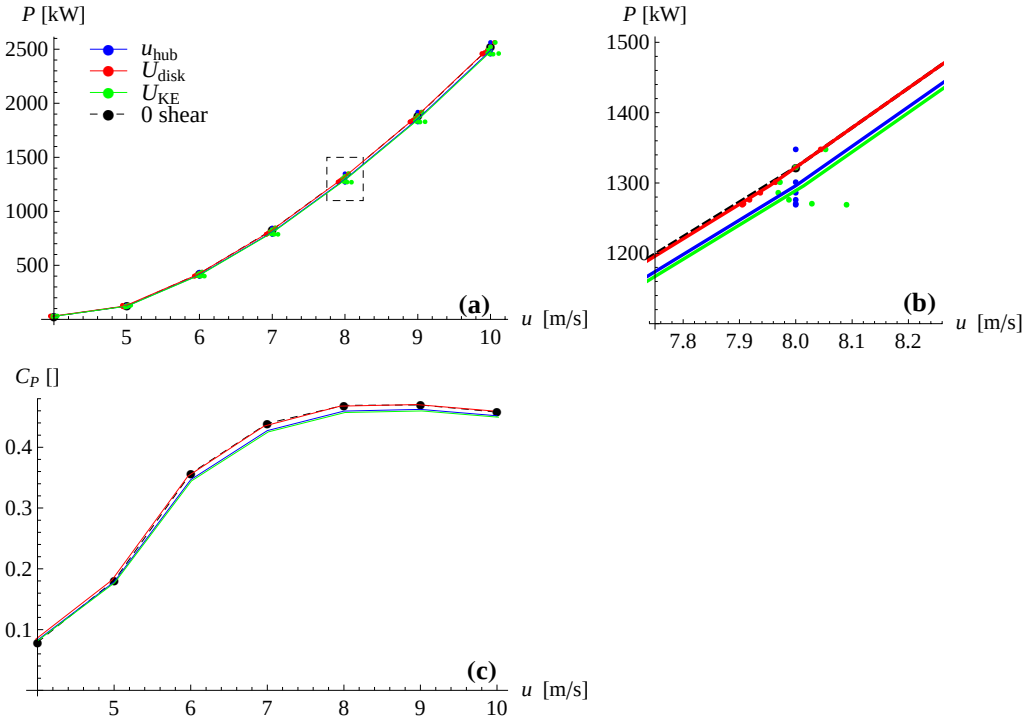

Figure 5.2: *(a): Scatter and mean power curve obtained for the various wind speed definitions together with the 0 shear power curve; (b): Zoom in power curve figure around 8m/s at hub height; (c): C_P mean curves obtained for the different wind speed definitions.*

5.2.2 With other wind speed profiles

The equivalent wind speed U_{disk} was also investigated in **Paper I**; it was named U_{eqM1}. In order to be applied with wind speed profile measurements, eq. (5.5) was approximated by:

$$U_{disk} = \sum_{i=1}^{N} u_i \frac{A_i}{A} \tag{5.8}$$

where N is the number of wind speeds per profile, u_i the wind speed at the i_{th} height and A_i the area of the corresponding segment of the swept rotor area (see Figure 2 in **Paper I**). Figure 10 (a) and (b) shows the results obtained with laminar inflow simulations for $N = 3$ ("3 points") and $N = 5$ ("5 points") together with the standard scatter plot ("1 point"). The use of the equivalent wind speed U_{disk} results in a greater reduction of the scatter than for the theoretical profiles in Figure 5.1. However, this is strongly suspected to be due to the way the aerodynamic model computes the rotor torque for a sheared inflow, as mentioned earlier.

The scatter in the power curve resulting form using U_{KE}, defined by eq. (5.6), was not investigated in **Paper I**, so it is done here. Figure 5.3 compares the partial power curve scatter plot obtained with u_{hub}, U_{disk} and U_{KE}, with the same simulations outputs as in Figure 10, in **Paper I**. Eq. (5.6) was approximated by

$$U_{KE} = \left(\sum_{i=1}^{N} u_i^3 \frac{A_i}{A} \right)^{1/3} \tag{5.9}$$

Both equivalent wind speeds were evaluated with $N = 5$.

The use of U_{KE} does not decrease the scatter as much as U_{disk}. However, the scatter is significantly smaller than that obtained with the wind speed at hub height. Moreover, in this plot, like in the plots in **Paper I**, the reference power curve is an approximation

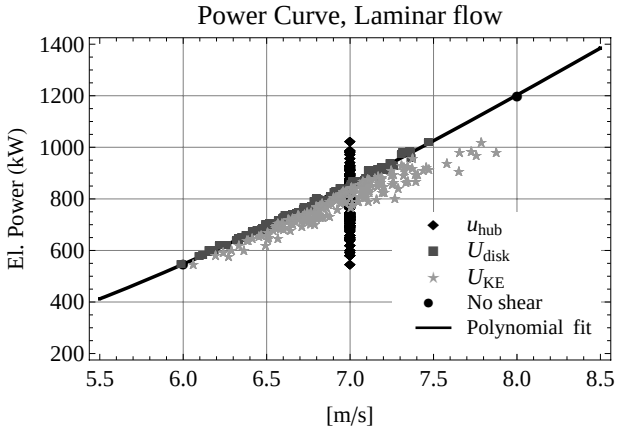

Figure 5.3: *Power curve scatter plot obtained with u_{hub}, U_{disk} as defined by eq. (5.8) and U_{KE} as defined by eq. (5.9). The wind speeds and power values are the output of the simulations from* ***Paper I*** *with laminar inflow.*

of the 0-shear power curve. The mean power curve (obtained with the bin method of the IEC standard) may have been more relevant, but this would not have been meaningful as only a small range of wind speeds was covered by these simulations.

The power curve obtained with an equivalent wind speed, such as U_{KE} and U_{disk}, remains shear dependant as the power extraction of a turbine is usually not optimized for sheared inflows. None of these equivalent wind speed definitions fully accounts for the aerodynamics of the turbine in a non uniform inflow. Only an equivalent wind speed that accounts for the aerodynamic changes due to the sheared inflow would give a power curve independent of the wind speed shear. However, this is very difficult (probably impossible) to define, as it requires a full understanding of the aerodynamics variation in an inflow with vertical shear, and this can vary from one single speed profile to another.

5.3 Equivalent wind speed and turbulence

The previous section showed that an equivalent wind speed taking the wind shear into account can reduce the scatter in the power curve. However, the results were obtained with laminar inflow so the wind shear was the only source of scatter. It was shown in chapter 4 that turbulence is another important secondary parameter responsible for the scatter in the power curve.

5.3.1 Reduction of the scatter with turbulent inflow

Figures 10 (c) and (d) in **Paper I** show the results obtained with the output of the simulation cases with turbulent inflow. As for the laminar cases, the use of the equivalent wind speed U_{disk} reduced the scatter. However, the turbulence intensities were rather low. Figure 5.4 compares the results obtained with u_{hub}, U_{disk} and U_{KE}, derived from the same simulations output as used in Figures 10 (c) and (d). As for the laminar cases, U_{KE} does not reduce the scatter as much as U_{disk} but reduces the scatter significantly compared to the standard scatter plot.

5.3.2 Scatter due to turbulence

The equivalent wind speed definitions proposed previously cannot reduce the scatter due to the turbulence itself since they are based on 10 minute mean speeds. The turbulence intensity can be taken into account in the equivalent wind speed by considering the

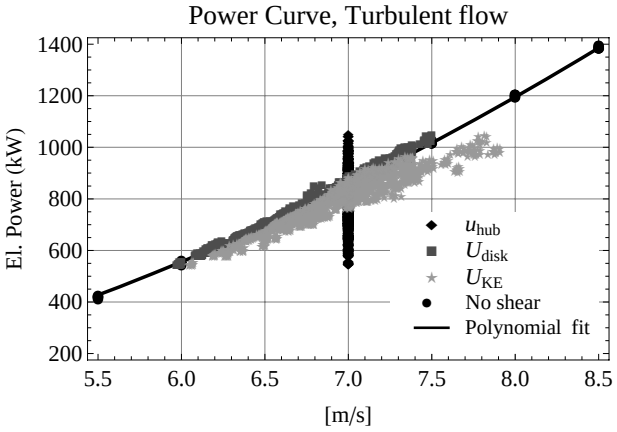

Figure 5.4: *Power curve scatter plot obtained with u_{hub}, U_{disk} as defined by eq. (5.8) and U_{KE} as defined by eq. (5.9). The wind speeds and power values are the output of the simulations from* ***Paper I*** *with turbulent inflow.*

average of the cube of the wind speed given by eq. (4.5):

$$U_{disk\_TI} = \sum_i \langle u_i \rangle \left(1 + 3\frac{\sigma_i^2}{\langle u_i \rangle^2}\right)^{1/3} \frac{A_i}{A} \tag{5.10}$$

$$U_{KE\_TI} = \left(\sum_i \langle u_i \rangle^3 \left(1 + 3\frac{\sigma_i^2}{\langle u_i \rangle^2}\right) \frac{A_i}{A}\right)^{\frac{1}{3}} \tag{5.11}$$

Figure 5.5 shows the power curves obtained for the different speed definitions: u_{hub}, U_{KE_TI} and U_{disk_TI}, with the simulations described in section 4.1.2, i.e. with wind speeds between 3 and 13 m/s and various turbulence intensities: 5%, 10%, 15% and 20%.

The problem is that the turbulence modified equivalent wind speeds simply increase with the turbulence intensity for any wind speed. As noticed previously, where the power curve follows the cube of the wind speed (i.e. C_P almost constant), the power output increases with the turbulence intensity. Thus for this wind speed range, the scatter is reduced when using U_{disk_TI} or U_{KE_TI}, see Figures 5.5 (c) and (d). However, near rated speed, the 10 minute average of the turbine power output decreases with the turbulence intensity. U_{KE_TI} and U_{disk_TI} cannot reduce the scatter around rated wind speed.

These equivalent wind speed definitions were used in **Paper I**: U_{disk_TI} was named U_{eqT1} and U_{KE_TI} was named U_{eqT3}. The results are shown in Figures 10 (g) and (h). As those results are limited to a small speed range within the medium load range and with low turbulence intensities, the scatter is reduced but no significant difference appears between the equivalent wind speeds that take the turbulence intensity into account and the definitions that ignore it.

The use of an equivalent wind speed taking the turbulence intensity into account cannot normalise the power curve for the turbulence effect. Gottschall and Peinke (2008) emphasized the impact of short-time dynamics for a proper description of the power conversion process of a wind turbine. Simple sample statistics are not sufficient to capture the characteristics of this process. The authors suggested a dynamical approach, based on fast sampled data, estimating the stationary power curve representative of the deterministic dynamics of the wind turbine (separated from the stochastic influences). However such a method is rather different from that suggested here, as the equivalent wind speed method does not account for the turbine dynamics but only for the natural wind power.

Based on the 10 minute average values, Kaiser et al. (2003) and Albers (2010) suggested two methods aiming at representing the non linear relation between the 10 minute

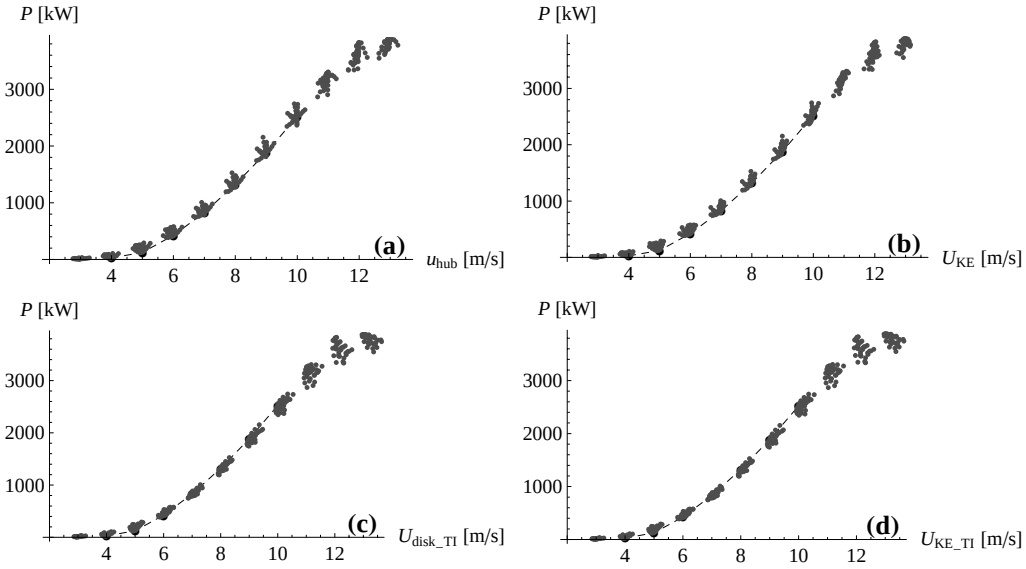

Figure 5.5: *Power curve scatter plot obtained with the output of the simulations cases with various turbulence intensities between 5% and 20% and no shear : power as function of (a): u_{hub}, (b):U_{KE}, (c): U_{disk_TI}, (d): U_{KE_TI}*

mean power and the 10 minute mean wind speed. Both methods require that the power curve for 0% turbulence intensity (0%-TI power curve) is retrieved from the measurements obtained with turbulence intensity which was not 0%. In the method discussed in (Kaiser et al., 2003), the 10 minute mean power for a given TI is based on the 0% TI power curve and its second derivative that changes sign according to the bend of the power curve.

Albers (2010) went a step further as his method is based on the fact that the 10 minute average of the power is not linearly related to the mean wind speed but to the wind speed distribution during the considered 10 minute and the shape of the power curve. According to these assumptions, if the shape of the 0%-TI power curve was known, it would be possible to calculate the 10 minute mean power that would be obtained with a given turbulence intensity ($TI > 0\%$) as it only changes the wind speed distribution. Albers' method therefore consists of 2 steps:

1. The estimation of the 0%-TI power curve;

2. The simulation of the power curve for a chosen turbulence intensity.

This method was applied to the simulated data set used in Figure 5.5 (including various turbulence intensities between 5% and 20%) in order to obtain the power curves normalised to 0% and 20% turbulence intensity. The results, displayed in Figure 5.6, show that this method solves the problem of the bending at rated speed: a sharp bend is obtained for 0% turbulence intensity and a smooth bend is obtained for 20%. Albers' method takes only the wind speed at hub height into account. Furthermore, Albers' method changes the power value (the power curve y-axis), contrary to the equivalent wind speed method which modifies the wind speed definition (therefore influences the x-axis) in the power curve.

Therefore both the equivalent wind speed method and Albers' turbulence normalisation method can be applied together quite easily. The combination of the two methods was tested with experimental data and the results are presented on section 9.3. Albers' method is described in more details and further discussed in that section.

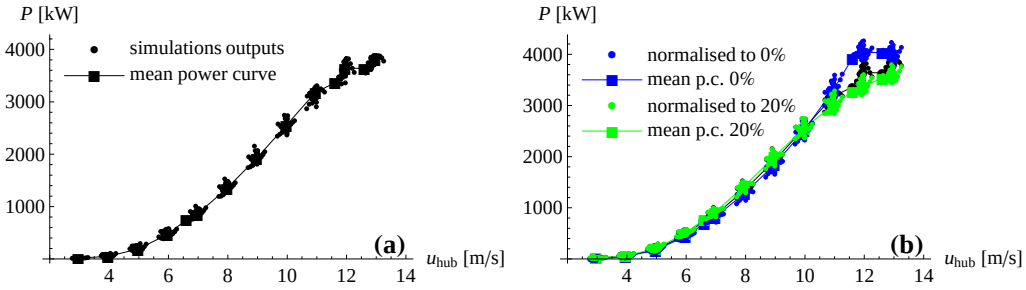

Figure 5.6: *(a): Power curve scatter plot obtained with the output of the simulations cases with various turbulence intensities between 5% and 20% and no shear; (b): Results of the normalisation of the power curve shown in(a) to 0% and 20% turbulence intensity with Albers' method*

5.4 Summary of equivalent wind speed investigation with aerodynamic simulations

The scatter due to the wind speed shear could be decreased by using an equivalent wind speed accounting for the shear. Such an equivalent wind speed can be defined in several ways. Two definitions were investigated: the integral of the wind speed over the rotor swept area and an approximation of the kinetic energy flux taking the wind shear into account, i.e. the integral of the cube of the wind speed profile over the rotor swept area. However, due to the uncertainties in the modeling, the simulations did not enable us to conclude about the best definition. The linear average resulted in a smaller scatter but this is almost certainly due to an artefact of the aerodynamic model. The BEM simulations do not appear as an ideal tool to find the best equivalent speed definition. It would require a more advanced model with fewer assumptions in the response of the turbine to a non-uniform inflow and better validated.

Secondly, simulations with sheared and turbulent inflow showed that the equivalent wind speed method reduced the scatter in the power curve even if it is affected by turbulence. However only the scatter due to shear is reduced, not the scatter due to turbulence.

Finally an equivalent wind speed accounting for the turbulence intensity in addition to the shear cannot normalise the power curve for the turbulence intensity. On the other hand the method suggested by Albers (2010) does normalise the mean power curve but does not seem to reduce the scatter. This is further discussed in section 9.3.

Chapter 6

Lidar

A wind sensing LiDAR (Light Detection And Ranging) is an instrument measuring the wind speed and direction remotely using coherent laser light. Wind sensing lidar profilers (called simply lidars hereafter) entered the wind power market in 2006 when Qinetiq released their production version ZephIR wind lidars. Subsequently, Leosphere introduced the Windcube in 2007, and the Gallion from Sgurr appeared on the market in 2009.

Lidars are presently used in the wind power sector to assess wind resource prior to wind farm installation. The site development process can be accelerated - and therefore the cost potentially decreased - as a lidar can be deployed in very short time compared to the time needed for the planning and erection of a mast. Moreover, the costs rise rapidly, as the height of the mast increases. A lidar therefore gives the possibility not only to measure at any height (within some limitations explained later in this chapter), but also to measure the wind speed at several heights simultaneously for a fixed cost. A further advantage is that while masts are difficult to redeploy, a lidar is designed to be mobile.

Lindelöw-Marsden et al. (2009) showed that a lidar measurements at hub height can results in AEP prediction close to that obtained with a cup anemometer. Moreover, for a wind turbine with a hub above 60m, the wind speed at hub height is usually estimated by extrapolation from measurements with a short mast. The use of a lidar offers the possibility of measuring the wind speed at hub height instead of extrapolating. The present study aims at showing that lidar measurements can even improve power performance measurement as the lidar provides a measurement of the wind speed profile, eliminating the need for models and extrapolation.

As Windcube lidars were used in both experiments described in this thesis, the following description of lidar principle of operation concentrates on pulsed systems, such as the Windcube.

6.1 Principle of operation of a pulsed lidar

The basic principle of operation of a lidar is based on the Doppler effect of a coherent signal reflected against a moving target. A lidar emits a near-infrared signal with a wavelength of 1.55 micrometer. Along its path the light is scattered by aerosols (e.g. dust, pollen) which are transported by the wind, and therefore assumed to move with the speed of the wind. Because of the Doppler effect, the backscattered signal has a different frequency than the emitted signal. The difference in frequency, known as the Doppler frequency, is proportional to the radial wind speed (v_r), i.e. the component of the wind speed along the laser beam direction, usually called the ***line-of-sight***:

$$f_D = \frac{2f_E}{c} v_r \tag{6.1}$$

where f_D is the Doppler frequency, f_E the emitted frequency and c the speed of light. The full 3-dimensional (3D) wind speed vector (horizontal component, vertical component and

Figure 6.1: *Picture of a Windcube lidar (on the left) and a ZephIR lidar (on the right)*

wind direction) can be retrieved by combining several radial speeds measured in different directions under the assumption of horizontal homogeneity.

6.1.1 Measurement range

The range where a pulsed lidar measures is selected by ***range-gating***, i.e. by sampling the backscatter within the time window corresponding to the range of interest. Indeed, as a light pulse propagates through a dispersed target, like the particles in the atmosphere, backscatter return continuously after the pulse has left the system. As the pulse travels at the speed of light, the backscatter sampled at time t arrives from the range $ct/2$ (as during the time t, the signal reached the target and came back to the sensor).

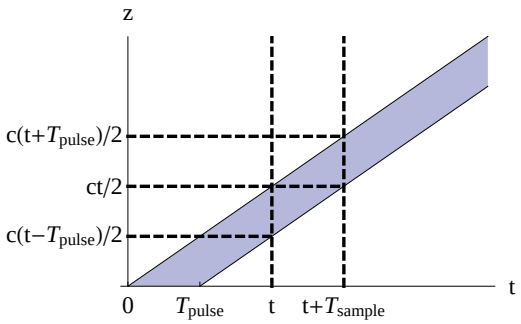

Figure 6.2: *Distance to the origin of the received scatter as a function of collection time*

As the pulse has a finite duration, T_{pulse}, every sample point is constructed from the superposition of backscatter generated from a volume having the shape of a long thin cylinder with the width of the laser beam (typically with a diameter of a few centimeters) and of length $cT_{pulse}/2$. Indeed, at a time t, the lidar receives scatter from the beginning of the pulse which is generated at a distance $ct/2$, but also backscatter from the rest of the pulse, which is between $c(t - T_{pulse})/2$ and $ct/2$. This is illustrated in Figure 6.2.

Backscatter distances do not contribute with the same amount of energy to a Doppler spectrum. The contribution distribution can be represented by a triangular function with its summit (maximum weight) at the middle of the range gate (Lindelöw, 2007).

Furthermore, the effective sample volume length depends mainly on the pulse shape. Hence, for a pulsed system, the effective sample volume length is constant with height. For a Windcube, the pulse duration is 200 ns, corresponding to a pulse length of 60 m, and the effective range resolution is about half the pulse length, i.e. about 30 m along the line-of-sight.

6.1.2 Radial speed retrieval

The time series from each range-gate of each pulse are Fourier transformed into a power spectrum. As explained previously, the backscatter are actually coming from a volume defined by the width of the laser beam (a few centimeters) and the pulse length. In theory, if the wind within this volume was perfectly homogeneous (same speed everywhere), the backscatter signal would have a narrow distribution of frequencies with its maximum at the Doppler frequency corresponding to the component of the aerosols speed along the beam direction within the sample volume. However, as the wind in this volume is not homogeneous (due to turbulence and wind shear), the received backscatter is the superimposition of many reflections with a distribution of frequencies. The resulting spectrum has a larger width than for a uniform wind. The spectrum width depends on the turbulence and the wind shear within the sampling volume. The peak of the spectrum is assumed to correspond to the speed at the middle of the range gate.

Furthermore, the spectrum obtained for each individual pulse is very noisy and the low signal to noise ratio prevents the Doppler frequency from appearing clearly. The signal to noise ratio has to be improved by averaging a large number of spectra in order to obtain a reliable speed estimate. This is why, the emitted signal is actually a train of 10000 pulses. The resulting 10000 spectra are block averaged. Due to the short recording duration (200 ns), the resulting spectra have a poor frequency resolution and the frequency peak of the block-averaged spectrum is obtained with a maximum likelihood estimator based on a proprietary algorithm developed by Leosphere.

6.1.3 Three-dimensional vector

With the range gating, a pulse-train sent in one line-of-sight results, after processing of the backscattered signal, in radial speeds at various ranges quasi simultaneously. In order to obtain a 3-dimensional wind speed vector, a Windcube lidar measures radial speeds successively in four line-of-sights separated azimuthally by 90 degrees from each other: $Vr_0, Vr_{90}, Vr_{180}, Vr_{270}$, by rotating the laser beam with an angle ϕ from the vertical, see Figure 6.3. Simple trigonometric considerations are used to calculate the three components of the wind speed (2 horizontal and 1 vertical):

$$\begin{aligned} u_1 &= \frac{v_{180} - v_0}{2sin(\phi)} \\ u_2 &= \frac{v_{270} - v_{90}}{2sin(\phi)} \\ w &= \frac{v_0 + v_{90} + v_{180} + v_{270}}{4sin(\phi)} \end{aligned} \tag{6.2}$$

At each direction step, the Windcube combines the four most recent radial speeds at each height in order to obtain the horizontal and vertical speeds and wind direction. In this way, a full 3-dimensional vector is obtained every 1.5s.

6.1.4 Carrier to Noise Ratio

The carrier to noise ratio (CNR) is defined as the ratio between the peak power level in the Doppler spectrum to the power of the photodetector noise. The noise from the photodetector is measured as a dummy range-gate corresponding to the period immediately before each pulse is emitted. The CNR therefore gives an indication of the strength of the backscattered signal. The CNR is calculated for each block-averaged spectrum.

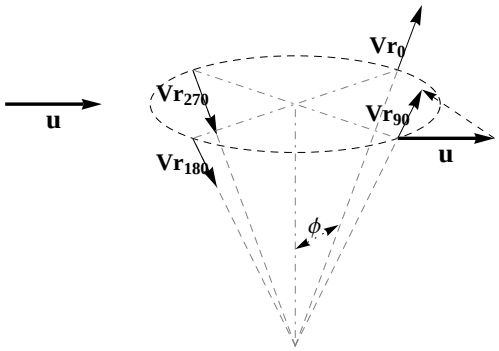

Figure 6.3: *Lidar conical scan.* $\boldsymbol{u}$ *is the wind speed vector;* ϕ *is the cone angle and* $Vr_0, Vr_{90}, Vr_{180}, Vr_{270}$ *are the radial speeds in four successive line-of-sights.*

As the power of light decreases with the square of the distance (because of the dispersion of the backscatter), the CNR decreases with height and this limits the maximum range where a lidar can measure. The laser power cannot be increased because of the physical limitations of the optical fiber and to comply with eye-safety regulations. The power of the backscatter signal could be increased by increasing the pulse length, but this would reduce the vertical resolution and increase the minimum height. Another way of increasing the useable range is to focus the laser beam rather than using a colimated beam. In the Windcube, the laser beam is focused at about 80m giving a peak CNR around that height, see Figure 6.4 (a). This extends the range of the instrument to around 300m, depending on the background aerosol concentration.

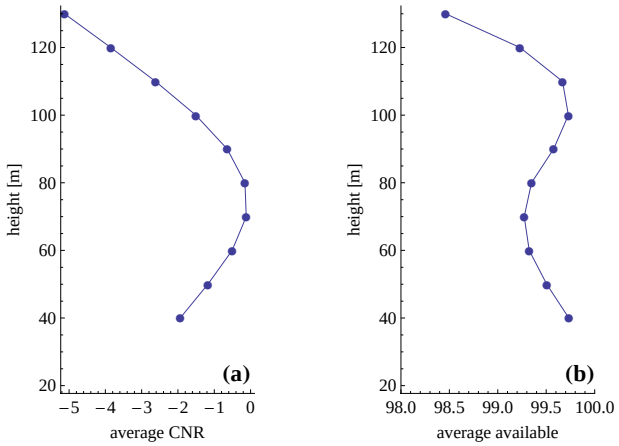

Figure 6.4: *(a): Averaged CNR profile; (b): Average availability profile*

Lidar measurements assume homogeneous distribution of the aerosols in the lower part of the boundary layer. The aerosol concentration changes from time to time and from place to place and drops dramatically above the ABL. If the CNR is below a predetermined threshold (usually -22dB in the Windcube), the uncertainty of the radial speed estimate is deemed to be large and no radial speed is returned.

A 10 minute CNR is defined by averaging the CNR measured at a given height in all four line-of-sights during 10 minutes. The CNR actually gives an idea of the backscattered power but one may be interested only in whether or not a signal could be detected (i.e. whether the CNR was above the acceptance threshold). Thus, the ***availability*** parameter is defined as the ratio between the number of speeds actually measured and the total number of speeds theoretically possible. Figure 6.4 (b) shows the availability parameter as function of height.

6.2 Limitations of a pulsed lidar in measuring the wind speed profile

6.2.1 Horizontal homogeneity

A lidar actually measures the radial speed (along the line-of-sight) and the combination of at least 3 radial speeds measured in 3 different directions is required to derive the full wind speed vector. The best way to achieve this would be to have three lidars, at three different positions, with their beams crossing at the point of interest. However, the use of a single instrument is preferred as it is less costly. The measurement of radial speeds in different directions is then achieved by shooting in different directions from one fixed point on the ground, by rotating the laser beam around the vertical with an angle ϕ (usually $\phi = 30°$). A Windcube lidar successively measures the radial speeds at 4 positions, by rotating the laser beam in 90° increments. The four radial speeds are therefore taken on a circle of diameter

$$D = 2\,h\,Tan(\phi) = \frac{2}{\sqrt{3}}h \tag{6.3}$$

where h is the measurement height. Consequently the radial speeds are measured at locations rather distant from each other. For instance, when the lidar measures the wind speed at $h = 100\,m$, two radial speeds taken at points radially opposed are separated by about 115 m. Therefore the combination of those radial speeds to retrieve the full 3 dimensional wind speed vector only makes sense if the layer of air at 100 m is horizontally homogeneous. Lidar wind speed measurements thus require the horizontal homogeneity of the wind in the lower part of the atmosphere; i.e. the wind speed should not vary horizontally. This assumption is fair in flat terrain, but is a limitation for measurement in complex terrain.

6.2.2 Precipitation

Rain can affect lidar measurements. Since the rain drops are falling, they cannot be said to be transported by the wind. The horizontal wind speed retrieval is not affected on average. However, the scatter in the regression between lidar measurements and cup anemometer measurements is increased, which is not desirable for the purpose of reducing the scatter in the power curve measurement. The periods with rain were therefore excluded from the data sets used in the experimental analyses.

6.2.3 Shear

Cone angle

An error in the cone angle (ϕ) would affect both the retrieval of the 3-D wind speed vector from the measured radial speeds and the sensing range. Indeed, to accurately retrieve the 3-D wind speed vector from the measured radial speeds according to eq. (6.2), the cone angle used in the equation (implemented in the software) must be the actual cone angle. Secondly, an error in the cone angle results in measuring at the wrong height since the line-of-sight range is incorrect ($2Tan(\phi) \times h$). For contemporary lidars this angle is determined for the prism present individually for each lidar as a part of the manufacturing process.

Range gating

One inherent problem with remote sensing is to accurately know the distance it is sensing at. In case of wind shear, an error in sensing distance can introduce a measurement bias. For pulsed systems, the trigger time (i.e. the time the pulse leaves the lidar) has to be known to an accuracy higher than 10 ns in order to get an accuracy for the range gating with an accuracy of 1m (Lindelöw et al., 2008).

Uneven backscatter contribution within the range-gate

A lidar measures the wind distribution from a sample volume of some length. The radial wind speed is estimated from the measured wind spectra, which corresponds to the wind distribution within the sample volume weighted with the appropriate function. It is assumed that the dominant line-of-sight wind velocity is representative of the wind velocity at the altitude which corresponds to the peak (or the centroid) of the weighting function in the sample volume. For this reason, the estimation of the dominant wind signal slightly depends on the wind shear in the sample volume, i.e. about 26 m high vertically.

Range gate distortion

Another inherent error could be due to unadjusted distortion of the range gates. Fiber based lidars typically use a focused telescope to collect more backscatter from the intermediate range. The range dependent collection efficiency of the focused telescope will shift the classical weighting function in the range gate, as illustrated in Figure 6.5 (Lindelöw et al., 2008).

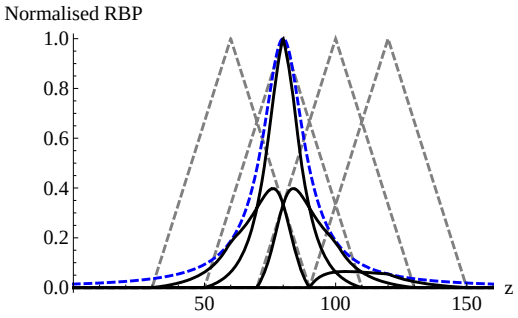

Figure 6.5: *Weighting of the backscatter for a pulsed focused lidar.*

Wind shear proportional error

In Høvsøre, a difference of more than 1% in the 1-parametric regression[1] was observed between lidar measurements for easterly and westerly winds. This deviation is strongly suspected to be due to the influence of shear as these two sectors present very different shear (see section 2.2.2). According to Lindelöw et al. (2008) most of these errors are linearly dependant on the shear and can be detected with a 2-parametric regression.

6.3 Other remote sensing wind profilers

For the sake of comparison, the main differences between a pulsed lidar system and two other remote sensing (RS) instruments, a continuous wave lidar and a sodar, are now described.

6.3.1 Continuous wave lidar

As indicated by its name, a continuous wave (cw) lidar emits the infrared signal continuously. The principle of range gating cannot be applied. The range of measurement is defined by the focusing of the laser beam at a specific range. The backscattered energy then comes from the focused volume, weighted according to the appropriate Lorentzian function centered at the focal distance. The obtained radial wind speed distribution in this case is ideally dominated by the signal from the set focus distance.

[1] Lidars are usually compared to cup anemometers with a linear regression between the speed measured simultaneously by both instruments at the same height; see examples in Figures 7.2, 8.2 and 11.6.

This is the cause of the main differences with a pulsed lidar system. First, the sample volume length is not constant with height, according to the Lorentzian function model, it increases with the measurement range. Although, it is smaller than for the pulsed system at low heights, it is larger at high heights. According to Mikkelsen (2009) the sample range for both instruments is equal at about 150m. However, the Windcube sample range has been modelled in a different way than in (Lindelöw, 2007), resulting in a larger sample range (37.5m). Moreover, as the sample range increases with height, cw lidar measurements become significantly less accurate above 200m.

Secondly, with a cw system, we are obliged to assume a sensibly flat vertical profile of aerosol concentration. The assumption of vertical aerosol homogeneity unfortunately fails completely in the fairly common case of low level clouds (under 1500m). Here, the relatively huge backscatter from the cloud base can be detected even though the cloud is far above the focus distance. The resulting Doppler spectrum has two peaks – one corresponding to the radial speed at the focused height and a second corresponding to the (usually) higher speed of the cloud base. Unless corrected for, this will introduce a bias to the wind speed measurement. For this reason, the ZephIR has a cloud-correction algorithm. Two extra scans at 38m and 800m are inserted into the height cycle and used in order attempt to remove the influence of the clouds at the desired measuring heights.

Since the cloud-correction algorithm is only partially successful, it is necessary to remove periods where low clouds are present in order to achieve the best possible data analysis. Then, additional equipment such as a met. mast and/or a ceilometer is required and the lidar is only used as an auxiliary equipment. Furthermore, the filtering of the lidar data reduce significantly the amount of usable data as pointed out in (Montes et al., 2009).

Thirdly, as the laser beam must be focused at the measurement range, the radial speed can be measured only at this height. Thus for a ZephIR, once the laser beam is focused at the first measurement height, it scans the air conically in order to measure several (50 per rotation) radial speeds in different line-of-sights (that are then used to retrieve the 3-D wind speed vector). Then, in order to measure to the next range, the laser beam must be refocused and scan the air and so on. Therefore, with a cw system the radial speeds at different heights are measured successively (contrary to the pulsed lidar that measured the radial speeds at all heights simultaneously before rotating the beam).

6.3.2 Sodar

A SoDAR (Sound Detection And Ranging) measurement is based on the Doppler effect of the sound when reflected against a moving target. However, unlike light, the sound is not reflected by the aerosols in the air but by the changes in refractive index of air due to temperature inhomogeneity. A sodar therefore measures the speed of turbulence patches transported by the wind. All sodars are pulsed system and, like pulsed lidars, the measurement range is defined by range-gating, the radial speeds at the different heights are measured simultaneously, the probe length is constant (about 20m).

The AQ500 sodar (sodar used in the measurement campaign described in chapter 7) is a 3-beams monostatic sodar using parabolic dishes to direct the beams with a beam angle of 15 degrees from the vertical. Such a sodar is cheaper than a Windcube or Zephir lidar, but has more limitations than a lidar. First, a sodar needs some thermal structure to measure any radial speed, therefore the signal availability drops close to neutral conditions.

Then, as a sodar detects backscattered sounds, it is sensitive to surrounding noise (such as that due to cars or planes) and to surrounding obstacles (such as trees or buildings) that can create fixed echoes. Rain is also a problem because of the noise of the rain drops impacting the microphones.

Furthermore, even without surrounding noise and obstacles, sodar measurements are inherently noisier than lidar measurements, as is shown in chapter 7. This is mainly due to two reasons. First, unlike light, the sound does not propagates in a straight line

but readily refracts. The sound beams hence spread out and the location from where the backscatter arrives is not accurate. Secondly, as the sound travels much slower than light, one sodar "shot" takes much longer. We need many shots (averaged spectra) to reduce the noise to an acceptable level. For this reason a sodar can only provide a wind speed measurement every 10 minutes. The uncertainty on each 10 minute mean value is hence much larger than for lidars.

Figure 6.6: *Picture of a AQ500 sodar*

Chapter 7

First experiment: comparison between a lidar, a sodar and a cup anemometer

In chapter 5, the use of an equivalent wind speed taking the shear into account was shown to reduce the scatter in the power curve. The experimental validation of this method requires a measurement of the wind profile in front of a large wind turbine simultaneously with measurement of the turbine power output. A remote sensing instrument capable of measuring the wind speed profile up to the higher tip of the turbine rotor is an attractive alternative to a met. mast as it is relatively easily installed. Hence, a measurement campaign was conducted with a lidar and a sodar in front of a multi-MW wind turbine.

7.1 Description of the measurement campaign

The experiment took place at Risø DTU's Test Station for Large Wind Turbines, located at Høvsøre, described in section 2.2, in spring 2008. The wind directions considered were within the 90° sector delimited according to the IEC standard for performance testing (IEC, 2005) in order to avoid wakes from other turbines: $230° - 320°$. This experiment was initially designed to measure the power performance of two of the five wind turbines located at Høvsøre (named turbine A and B in Figure 7.1). A Windcube lidar and an AQ500 sodar were placed close to each other between the masts A and B, as shown in the sketch in Figure 7.1. However, data from turbine A were not suitable for the experiment. The wind turbines at Høvsøre are test turbines. Therefore they are subjected to numerous changes in settings according to the manufacturer needs. For this reason, it was not possible to have a data set suitable for a power curve test. Therefore, only the results obtained with turbine B are presented here. Mast M_B is equipped with a top-mounted cup anemometer fulfilling the requirements of the IEC 61400-12-1 standard.

The principle of operation of the RS instruments is described in chapter 6. The Windcube lidar measured in this location for 3 months (from 25/02/08 to 20/05/08) at 10 heights chosen to match the five heights: $0.5z_{hub}$, $0.75z_{hub}$, z_{hub} , $1.25z_{hub}$, $1.5z_{hub}$ where z_{hub} is the wind turbine hub height. The AQ500 sodar measured at this location, with a constant setting, for about 2 months (from 15/04/08 to 20/05/08). The sodar AQ500 was located 5 m west of the lidars (see Figure 7.1). The sodar measured at every 15m including the turbine hub height.

The data were selected according to the operational status of the turbine. Periods with a temperature below $2°C$ were excluded in order to avoid measurements with ice affected cup anemometers. For lidar and sodar quality data, periods with rain were excluded. Finally, only 10 minute lidar data with an availability of 100% (see section 6.1.4) were selected.

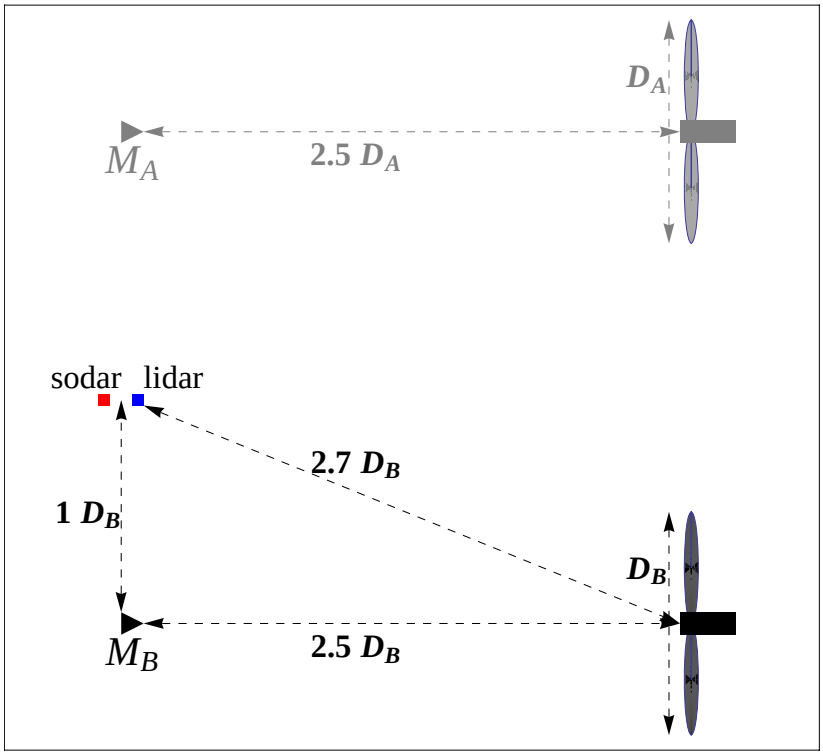

Figure 7.1: *Sketch of the experimental set up. M_A: mast A, M_B: mast B, D_A (D_B): Rotor diameter of wind turbine A (B).*

For reasons of confidentiality, no more information is given concerning the wind turbine. The data were normalised: the turbine power output using the rated power P_{rated} and the wind speed using the rated speed u_{rated}.

7.2 Comparison Lidar-Sodar

Figure 7.2 (a) and (b) show the comparison of the simultaneous 10 minute mean wind speed at hub height measured by a RS instrument (lidar and sodar, respectively), and the cup anemometer. Both data sets include the same 10 minute periods. The sodar measurements overestimated the wind speed in comparison to the speed reported by the cup anemometer. Figure 7.2 (c) and (d) show the RS instruments error, i.e. the difference between the simultaneous RS and cup anemometer measurements, at hub height. The standard deviation of the sodar error (0.82 m/s) is much larger than the standard deviation of the lidar error (0.26 m/s). The sodar data are significantly noisier than the lidar data.

There was no indication of any major problem with the sodar during this experiment. The difference in measurements from the two instruments can be explained by the difference in the way they operate. Because sodar measurements are based on the Doppler shift of backscattered sound, they are sensitive to surrounding noise and obstacles, which is not the case for light beams. Moreover, the sampling frequency of a sodar is much lower than that of a lidar. Each radial speed measured by the sodar is derived from the averaged Doppler spectra over 10 minutes, whereas, for a pulsed lidar, a radial speed in one line-of-sight is obtained every 6 seconds and each radial speed is derived from the average of thousands of Doppler spectra (see chapter 6).

The overestimation of the wind speed measured by the sodar shifts the power curve to the right, see Figure 7.2 (f). Moreover the noisy measurements (at hub height) from the sodar results a much larger scatter in the power curve than the power curve obtained

with the cup anemometer; whereas the scatter in the power curve obtained with the lidar is similar to that obtained with the cup anemometer, see Figure 7.2 (e). If the RS instrument increases the scatter in the power curve compared to a cup anemometer, it is unlikely that the speed profiles from that same instrument can help to reduce the scatter.

The large standard deviation of sodar error was observed at every height resulting in a random distortion of the profiles. According to the estimation of the uncertainty of measurements suggested in chapter 11, sodar measurements would have a larger uncertainty than lidar measurements, since the standard deviation of the residuals in the linear regression between sodar and cup anemometer measurements is larger than that of lidar. Assuming that the sodar has the same residuals standard deviation at all heights, an equivalent wind speed derived from these measurements may reduce the scatter in the power curve in comparison to the sodar measurements at hub height, but hardly in comparison to the cup anemometer measurements or to the lidar measurements. Therefore, the profiles measured by the AQ500 sodar were found not to be suitable for equivalent wind speed calculation.

7.3 Power curve measurement with the lidar

7.3.1 Direct comparison to the standard power curve

Figure 7.3, plot (a) shows the scatter plot of the power curves measured with the cup anemometer and with the lidar at hub height. Plot (b) shows the scatter plot of the power curves obtained with lidar wind speed measurements at hub height and U_{disk} derived from the lidar wind profile measurements, according to eq. (5.8). The three scatter plots are very similar. Plot (c) shows the mean power curve for all three wind speeds. The curve obtained with the lidar at hub height is slightly different from the standard curve. The power curve obtained with the equivalent wind speed is very close to that obtained with the lidar measurement at hub height.

Different power curves are obtained for different wind speed definitions in abscissa, as already mentioned in section 5.2 and as it can be seen in Figure 7.3 (c). The scatter has to be defined for each speed definition relative to the corresponding mean power curve. Plot (d) displays the scatter per wind speed bin. The scatter was quantified as the mean residual relative to the mean power curve. As the measured power curve is actually a succession of segments, the mean residual was calculated for each segment. One segment is defined by 2 points of coordinates (v_{i-1}, P_{i-1}) and (v_i, P_i) where v_i is the i^{th} wind speed in the mean power curve and P_i the corresponding average power. Thus the mean residual for the j^{th} segment or bin is defined as:

$$err_j = \sqrt{\frac{1}{N_j}\sum_{k=1}^{N_j}(y_{j,k} - f_j(u_{j,k}))^2} \tag{7.1}$$

where N_j is the number of data in the j^{th} bin (corresponding to the j^{th} segment, e.g. $v_{i-1} \leq u_{j,k} \leq v_i \, \forall k \epsilon [1, N_j]$), $u_{j,k}$ the measured wind speed of the k^{th} point in the j^{th} bin , $y_{j,k}$ the corresponding power output and

$$f_j(u) = \left(\frac{P_i - P_{i-1}}{v_i - v_{i-1}}\right) u + \left(P_i - \left(\frac{P_i - P_{i-1}}{v_i - v_{i-1}}\right) v_i\right) \tag{7.2}$$

is the equation of the j^{th} segment. This way of evaluating the scatter in the power curve scatter plot has the weakness of being influenced by the slope of the mean power curve segment - this explains the general trend of increasing scatter up to normalized wind speed in Figure 7.3 (d). However, quantified according to this simple method, the scatters obtained with the different wind speeds can be compared.

The scatter obtained with the lidar measurement at hub height is slightly smaller than the scatter for the cup anemometer measurements. This is further discussed in section 7.3.3. On the other hand, the scatter obtained with the equivalent wind speed is

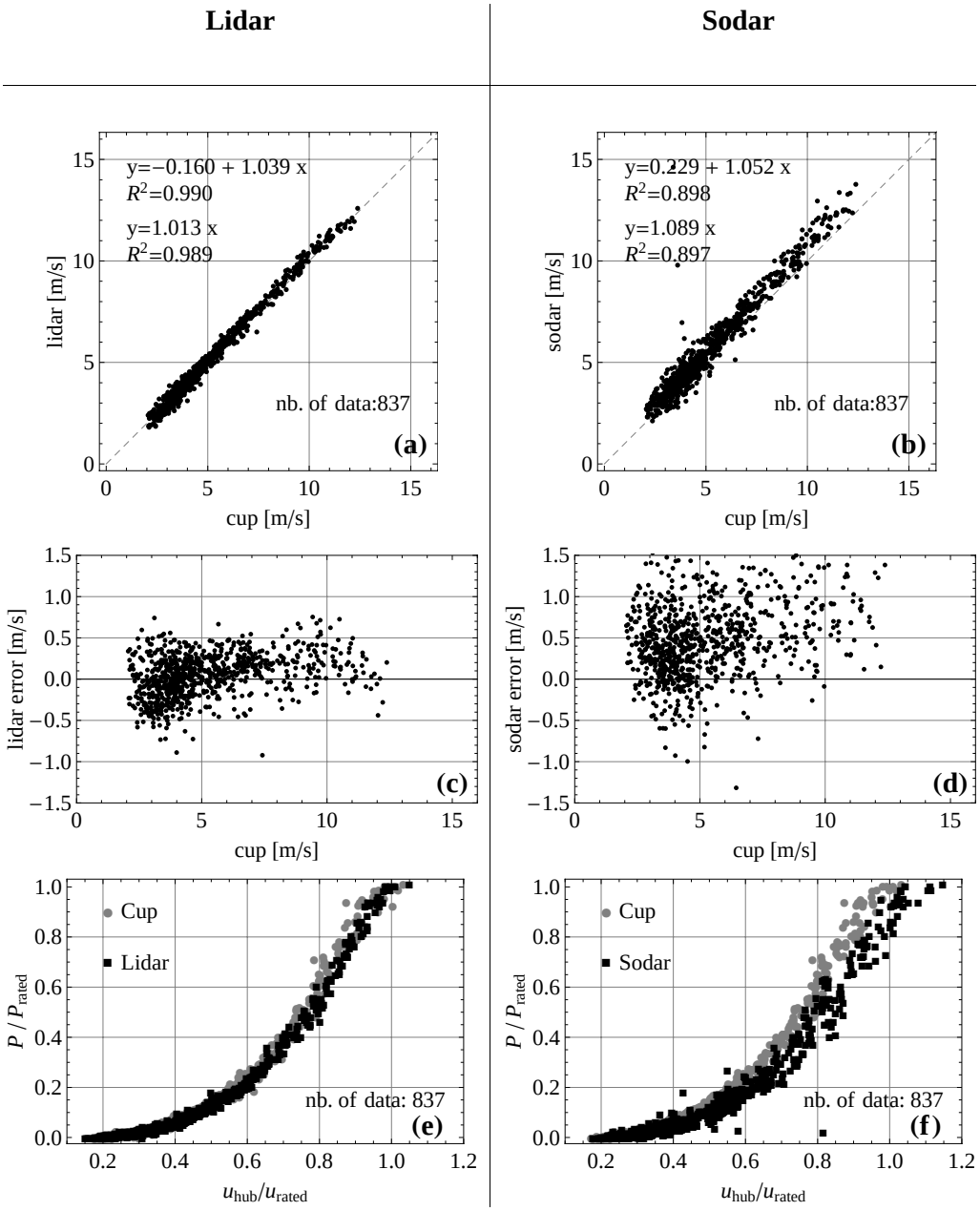

Figure 7.2: *(a): Comparison of the lidar 10 minute mean wind speed measurements at hub height with the cup anemometer measurements, (b): Comparison of the sodar 10 minute mean wind speed measurements at hub height with the cup anemometer measurements, (c): Lidar error (d): Sodar error, (e): Power curve scatter plots obtained with the wind speed at hub height measured by the cup anemometer and the lidar; (f): Power curve scatter plots obtained with the wind speed at hub height measured by the cup anemometer and the sodar*

not smaller than the lidar measurements at hub height contrary to what was expected from the aerodynamic simulations (see chapter 5).

7.3.2 Lidar correction with the cup anemometer measurements

Lidar measurements at a given height are generally not exactly equal to cup anemometer measurements at the same height. A lidar measurement is generally different from a cup measurement since a lidar measures over a large volume whereas a cup anemometer

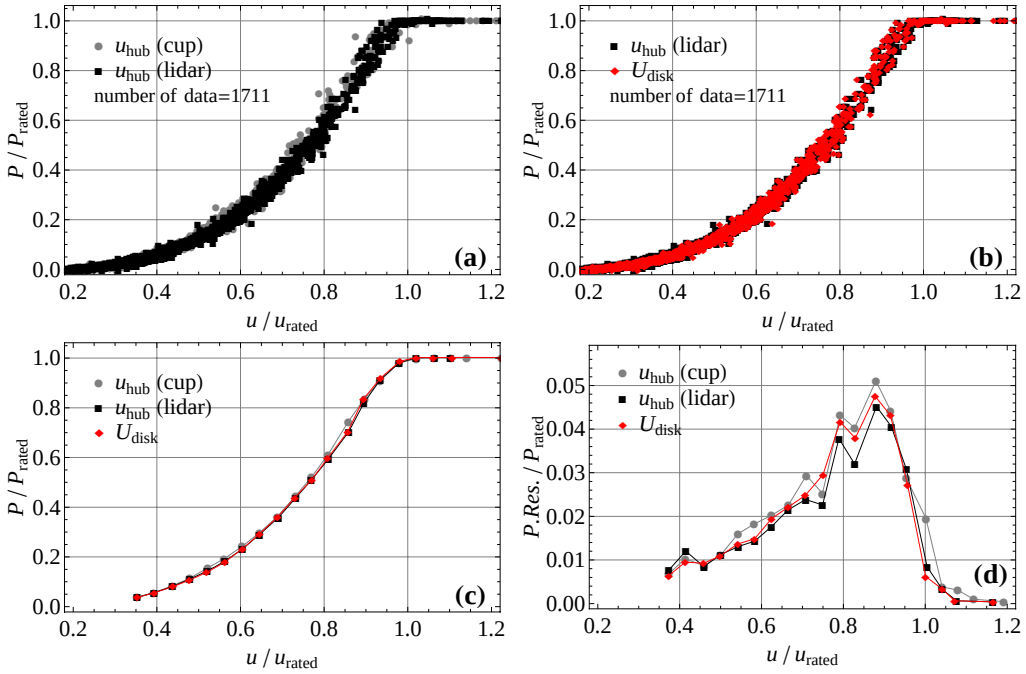

Figure 7.3: *(a): Power curve scatter plot obtained with the wind speed at hub height measured by the cup anemometer and the lidar; (b): Power curve scatter plot obtained with lidar wind speed at hub height and U_{disk}; (c): Mean power curves for the 3 wind speed definitions; (d): Mean residuals as a function of wind speed for the 3 wind speed definitions.*

performs a point measurement. As the lidar technology is still recent compared to cup anemometers, one could prefer to use the lidar as a relative instrument, i.e. keeping the cup anemometer measurements for the wind speed at hub height and using the lidar to provide information about the shear. This can be achieved by shifting the wind profile measured by the lidar so the hub height wind speed from the lidar is equal to the cup measurement at hub height, for each ten minutes average measurement, see Figure7.4.

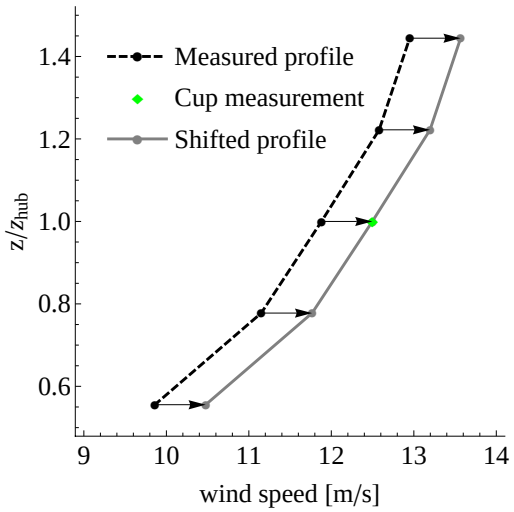

Figure 7.4: *Profile shifting. Black dots and dashed black line: measured wind speed profile, large black dot: cup anemometer measurement at hub height, Gray dots and gray line: shifted profile.*

Figure 7.5 shows the same results as in Figure 7.3 but obtained with "shifted" profiles. The profile correction results in identical power curves for lidar measurements at hub

height and cup anemometer measurements. Therefore, only the results obtained with the wind speed at hub height and the equivalent wind speed are shown. The mean power curve obtained with U_{disk} is almost identical to that obtained with u_{hub} (plot (c) in Figure 7.5). Regarding the scatter, there is no significant difference (plot (d)).

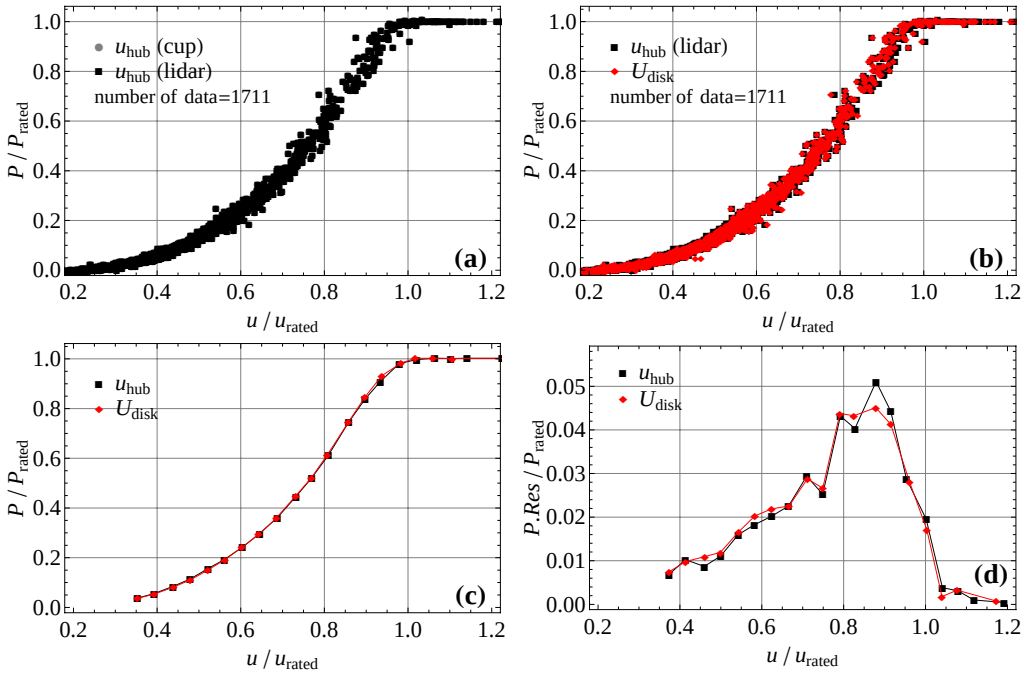

Figure 7.5: *(a): Power curve scatter plot obtained with the wind speed at hub height measured by the cup anemometer and the lidar; (b): Power curve scatter plot obtained with lidar wind speed at hub height and U_{disk}; (c): Mean power curves for the 2 wind speed definitions; (d): Mean residual as a function of wind speed for the 2 wind speed definitions. The results displayed in this figure were obtained with the lidar profiles shifted to match the cup anemometer measurements at hub height.*

7.3.3 Spatial correlation

A closer look at Figure 7.3 (a) reveals a few outliers that appear for the cup anemometer measurements but not for the lidar measurements. These outliers caused a scatter larger than for the lidar measurement at hub height. Indeed peaks appear in the mean residual plot (Figure 7.3 (d)) for the same wind speeds as the outliers in plot (a) (at u=0.55 u_{rated}, 0.7 u_{rated}, 0.8 u_{rated} and 0.9 u_{rated}). Further investigations showed that these outliers were appearing only for winds coming from North-West (wind direction between 285° and 320°) as shown in Figure 7.6. The difference between power curves is probably due to a difference in wind speed between the locations of the two instruments. For the North-Westerly winds, the lidar is directly upwind of the turbine (which is not the case for the cup anemometer). The speed measured by the lidar is then probably better correlated to the wind experienced by the turbine than the speed measured by the cup anemometer.

The design of this experiment was therefore not optimal to compare the scatters in power curve obtained with a cup anemometer and a lidar. Moreover, in these conditions, shifting the lidar profile measurements according to the cup anemometer measurements, as performed in 7.3.2, increases the confusion since the cup anemometer de-correlation with the wind speed at the turbine was transferred to the lidar measurements increasing the scatter of the power curve measured with the lidar.

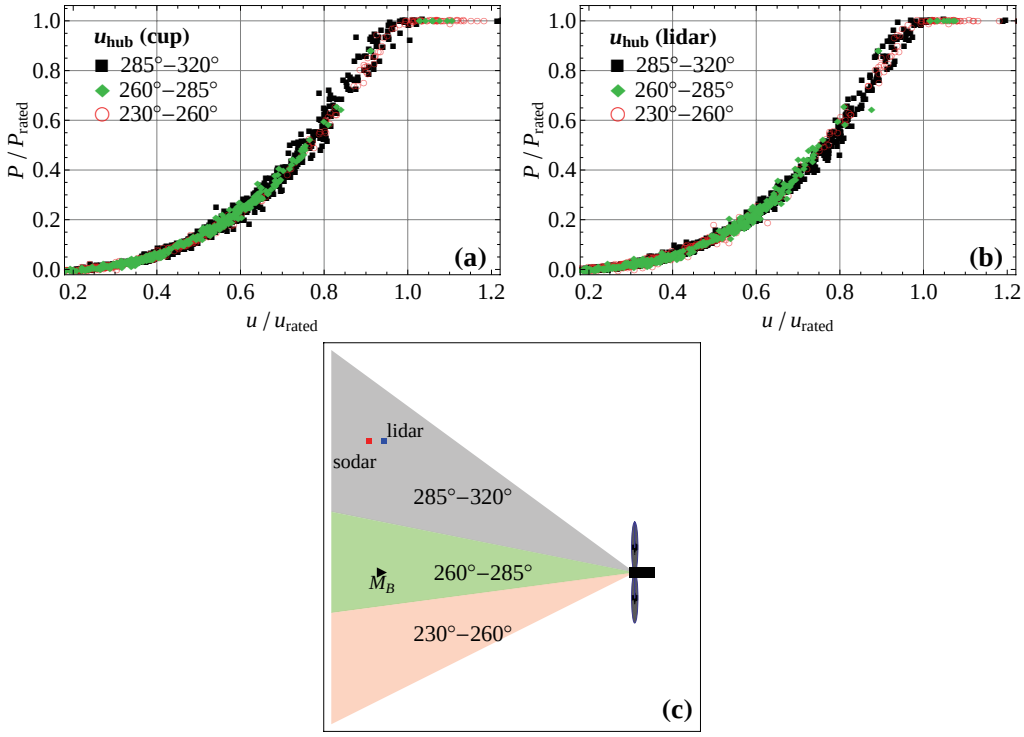

Figure 7.6: *Power curve scatter plot obtained (a): with wind speed measurements at hub height with the cup anemometer, (b): with the lidar; (c): Sketch of the wind sectors considered in graphs (a) and (b) relative to the experimental set up*

7.3.4 Shear distribution

In this experiment, the use of an equivalent wind speed did not reduce the scatter in the power curve contrary to the predictions from the numerical simulations (see chapter 5). However, the standard power curve did not have much scatter to start with. The question was then to determine whether there was any scatter due to wind shear. The wind profiles measured by the lidar during this campaign were analysed. As it was explained in chapter 2, it is not straight forward to classify the wind speed profiles. The power law model is very convenient as it characterises a wind speed profile with one number: the shear exponent. However, this model cannot represent all kinds of profile, especially profiles occurring at a coastal site.

In this experiment, the lidar measured the wind speed at 9 heights equally distributed between 0.5 and 1.5 z_{hub}. Each wind speed profile measured by the lidar was fitted to the power law with a least mean square method in order to find the most representative shear exponent for this profile (α_{fit}). The fit is forced through the point of coordinate (u_{hub}, z_{hub}) where u_{hub} the wind speed at hub height:

$$u_{fit}(z) = u_{hub}\left(\frac{z}{z_{hub}}\right)^{\alpha_{fit}} \tag{7.3}$$

α_{fit} is believed to be more representative of the wind profile than the shear exponent derived from 2 or 3 speed measurements. Moreover, the goodness of fit was evaluated with the residual sum of squares (RSS) by applying eq. (2.8) with u_{fit} the fit function defined by eq. (7.3), u_i the wind speed measured by the lidar at height z_i and $N = 9$.

Figure 7.7 shows the distribution of the shear exponents (α_{fit}) for all the profiles and the proportion of RSS smaller than 0.1, i.e. profiles for which the power law approximation is relatively acceptable. It appears from this analysis that most of the profiles measured during this campaign had a shape close to a power law profile and that there is a large majority of small shear exponents ($0 < \alpha_{fit} < 0.2$). According to the simulations

results, these kinds of shear are expected to have only a moderate influence on the power curve (see chapter 3).

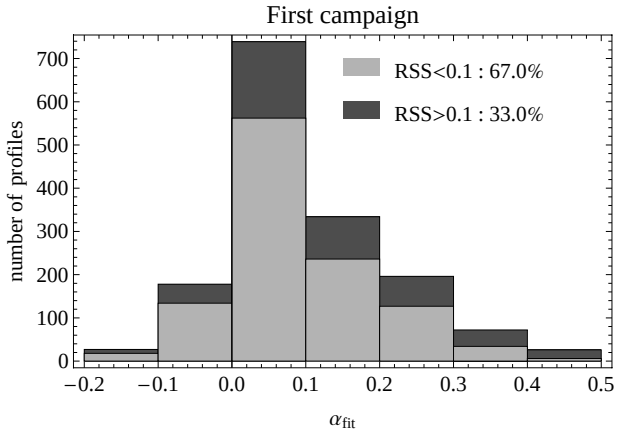

Figure 7.7: *Distribution of the shear exponents and proportion of good fits*

7.4 Conclusions of the first measurement campaign

This measurement campaign did not result in a clear validation of the equivalent wind speed method. However it pointed out several things that should be carefully considered when investigating power curve measurement with remote sensing:

1. Power performance verification requires measurements with high absolute accuracy and low noise. The sodar used during this experiment did not meet the requirements and it did not make sense to use the sodar measurements to estimate a wind speed average over the rotor swept area. This was confirmed by VanLuvanee et al. (2009) who applied the equivalent wind speed method with sodar measurements. The scatter in the power curve obtained with the equivalent wind speed was larger than the scatter obtained with the cup anemometer measurements. With shifted profiles, as explained in section 7.3.2, the scatter in the power curve obtained with the equivalent wind speed and cup anemometer measurements were comparable. However, the authors observed a reduction of the scatter when the LLJ profiles were isolated. Perhaps in the case of these specific profiles, the uncertainly in power curve due to shear was larger than the uncertainty in the sodar measurements.

2. The lidar measurements appeared to be more suitable for the application of the equivalent wind speed method as they were rather accurate and noise-free compared to the cup anemometer measurements. However, since the lidar technology is relatively immature, a comparison to met. mast measurements is still required before using a lidar for power curve measurements.

3. Comparing the power curve measurement obtained with lidar measurements to that obtained with a cup anemometer must be done carefully, keeping in mind that the spatial correlation decreases with distance between the instruments. The comparison is expected to be best if the instruments are positioned close to each other.

4. Although the cup anemometer only is accepted as a stand-alone instrument and it should be used as a reference for comparison, a systematic correction of the lidar measurements to match the cup anemometer measurements is not always a good solution when the instruments are spatially separated.

Although no significant reduction in the power curve scatter was observed when using the equivalent wind speed, the conventional and the equivalent wind speed power curves were at least as good as each other. This is what is expected for the power law profiles with small shear exponents, that have dominated during the measuring campaign, according to the simulations results (see chapters 3 and 5).

Chapter 8

Second experiment: Validation of the method

8.1 Introduction

Learning from the conclusions of the first experiment, a new measurement campaign was undertaken at Høvsøre. A Windcube lidar, first compared to the tall met. mast for a few months, was installed in front of a multi-MW wind turbine. It was installed next to the mast located to the west of the turbine and which is equipped with a top-mounted cup anemometer used for the standard power performance measurement[1].

8.2 Description of the experiment

The measurements took place at Risø DTU's Test Station for Large Wind Turbines (see section 2.2.1). A Windcube lidar was installed at 5m from the mast in front of one of the turbines (different from turbine B in the first experiment), see experimental set up in Figure 8.1. The selected wind directions were within $225° - 315°$ ($\pm 45°$ around the west direction). The measurements were taken during the early spring 2009, the season during which unusual shears are often observed at this location (see section 2.2.2).

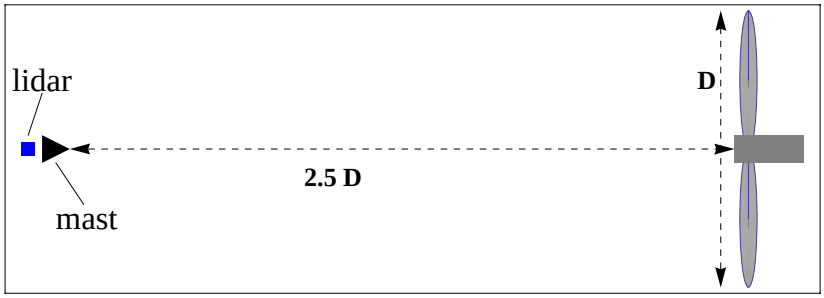

Figure 8.1: *Sketch of the experimental set up*

Moreover, it is important for a power curve measurement that the turbine settings remain constant during the whole measurement period. As the turbine considered here is a test turbine, the settings are often modified by the manufacturer. For this reason, the measurement period has been limited to about a month (from 25/02/2009 to 21/03/2009), during which the turbine kept the same settings.

[1]The main results presented in this chapter are the subject of **Paper II** given at the end of the thesis. Since these results are central to the work presented in this thesis, and the paper is still under revision, the results are also fully described in this chapter.

For reasons of confidentiality, no more information are given concerning the wind turbine. The data were normalised: the turbine power output using the rated power P_{rated}, the wind speed using the rated speed u_{rated} and the power coefficient using the maximum value of C_P observed in the standard power performance measurement ($C_{P_{Max}}$).

The data were first selected according to the turbine status. The initial data set was reduced because the lidar stopped twice for a period of a few days. The lidar measured the wind speed at 9 heights from $0.5z_{hub}$ to $1.5z_{hub}$, where z_{hub} is the turbine hub height. In order to select the best-quality data from the lidar, the time periods with rain were excluded. Moreover, only the 10 minute time periods during which horizontal speeds were "available" (see section 6.1.4) at all heights, i.e. only the complete profiles, were taken into account.

Figure 8.2 shows the regression of the wind speed at hub height simultaneously measured by the lidar and by the cup anemometer. After the filtering described above, two outliers remained. They occurred immediately after a rainy period and are probably due to an error or a delay of the rain sensor. These outliers were removed from the data set manually. Figure 8.2 shows the final data set, 87% of the exploitable data. This data set consists in 907 data, therefore it does not meet the amount of 180 h of measurements required by the IEC standard for power performance measurement (IEC, 2005), but the requirement of at least 3 data per wind speed bin has been met for the wind speeds below rated speed.

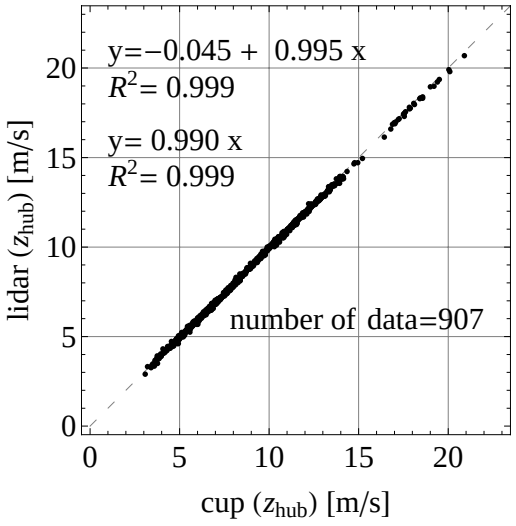

Figure 8.2: *Comparison of lidar to cup anemometer wind speed measurement at hub height*

According to Figure 8.2, the lidar showed a very good agreement to the cup anemometer (regression slope very close to unity and high R^2) with a slight underestimation of the wind speed on average.

8.3 Using the lidar to measure a standard power curve

First of all, the power and C_P curves obtained with the lidar wind speed measurements at hub height were compared to those obtained with the cup anemometer. Figure 8.2 shows that the lidar compares very well to the cup anemometer, however it slightly underestimates the wind speed. A direct consequence of this is the slight shift to the left of the power curve obtained with the lidar compared to the curve obtained with the cup anemometer and the C_P obtained with the lidar is globally higher than the C_P obtained with the cup anemometer, see Figure 8.3.

A method to combine the lidar profile measurements with the cup anemometer measurements was suggested in 7.3.2 in order to eliminate this difference. For this measure-

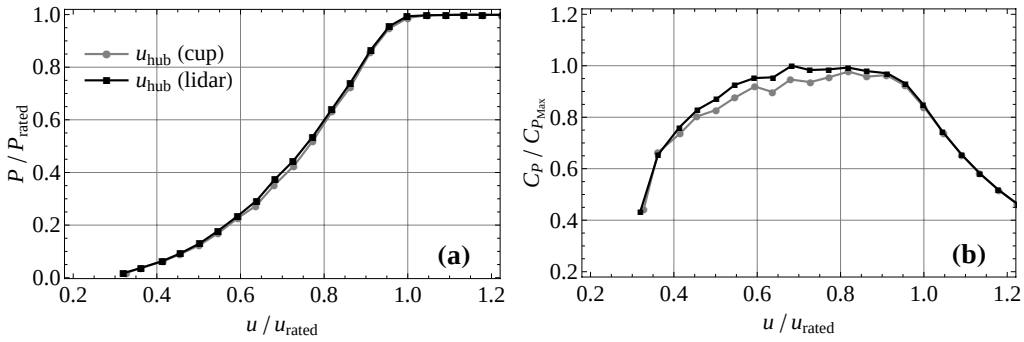

Figure 8.3: *(a): Mean power curve, (b): mean C_P curve, obtained with the cup anemometer and the lidar wind speed measurements at hub height.*

ment campaign, this is dealt with in section 8.7. The primary aim here is to investigate the difference in scatter between the power curves (and C_P curves) obtained with the wind speed at hub height and the equivalent wind speed. The scatter was quantified with the mean residual relative to the mean power curve as defined by eq. (7.1). However, as it can be seen in Figure 8.4 (a), this quantity depends on the slope of the power curve which increases with the wind speed up to the rated speed. So, in order to facilitate the comparison, the mean residual error was normalised with the segment slope $\left(\frac{P_i - P_{i-1}}{v_i - v_{i-1}}\right)$. This is shown in Figure 8.4 (b). Figure 8.4 (c) shows the residual error for the C_P, as defined by eq. (7.1), but with:

$$f_j(u) = \left(\frac{C_{Pi} - C_{Pi-1}}{v_i - v_{i-1}}\right) u + \left(C_{Pi} - \left(\frac{C_{Pi} - C_{Pi-1}}{v_i - v_{i-1}}\right) v_i\right) \tag{8.1}$$

Unlike the power curve, the C_P curve has a low slope for the medium load range of wind speeds, so it was not necessary to use a normalisation.

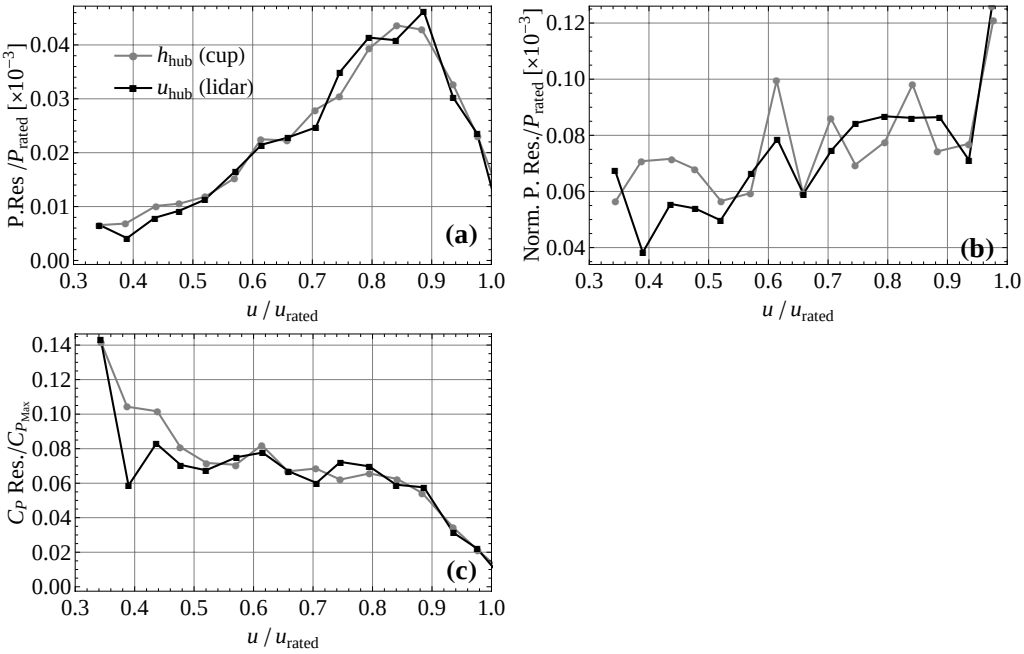

Figure 8.4: *(a): Mean residual in the power curve (P. Res.); (b): Normalized residual in the power curve (Norm. P. Res.); (c): Mean residual in the C_P curve (C_P Res.)*

Figure 8.4 shows that the scatter in the power curve (resp. the C_P curve) obtained with lidar measurement at hub height is comparable to the one from the cup anemometer

measurement. Therefore, in the next sections (up to 8.6 included), only the power (resp. C_P) curve obtained with the lidar measurements, either at hub height or with the equivalent wind speed, are considered in order to focus on the application of the equivalent wind speed method rather than the differences between cup anemometer and lidar measurements.

8.4 Wind shear effect on the power performance measurement

For each speed profile measured by the lidar, the shear exponent (α_{fit}) and the RSS were estimated according to eq. (7.3) and eq. (2.8), respectively, with $N = 9$.

The profiles were divided into two groups according to the RSS:

- Group 1: $RSS \leq 0.1$; the profiles from this group have a shape close to a power law profile;
- Group 2: $RSS > 0.1$; the profiles from this group have a shape that cannot be well represented by a power law profile.

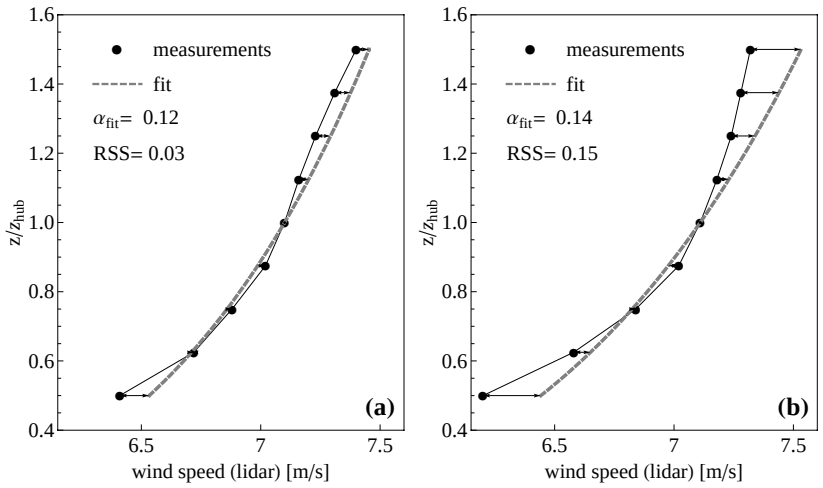

Figure 8.5: *Example of measured profiles and their fit to a power law profile; (a): $RSS \leq 0.1$, (b): $RSS > 0.1$*

Figure 8.5 shows two examples of measured profile with its shear exponent and RSS. According to this classification, profile (a) in Figure 8.5 would be in group 1 and profile (b) in group 2. The value of 0.1 was arbitrarily chosen here as threshold for the RSS, because it gave two groups of data showing two trends (shown in Figure 8.7) while being statistically comparable (as they count similar numbers of data: 511 in group 1 and 396 in group 2).

For comparison purposes with the first experiment, Figure 8.6 presents the distribution of the shear exponent (α_{fit}) for the two groups of profiles. The second data set (second experiment) contained more profiles with a high RSS, i.e. non power law profiles than the first data set. Moreover, the shear exponents are higher than in the first experiment.

Figure 8.7 shows the scatter plot of the standard power curve (a) and the C_P curve (b) as function of the wind speed at hub height. In this figure, C_P is defined as in the IEC 61400-12-1 standard, see eq. (3.3). The two colours represent the two groups of profiles. In Figure 8.7 (a) and (b) two trends appear (one for each group) leading to two

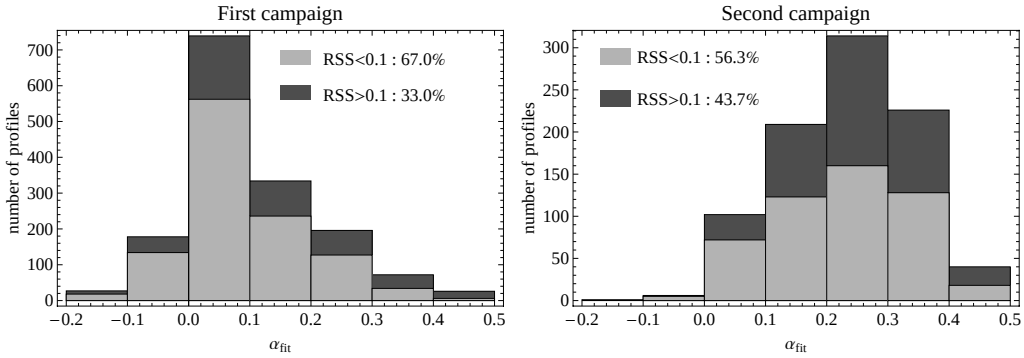

Figure 8.6: *Distribution of the shear exponents and proportion of good fits (i.e. low RSS) for the first and the second measurement campaigns*

mean power curves and C_P curves[2] shown in Figure 8.7 (c) and (d). The power output of the turbine for a given wind speed at hub height is smaller on average for the data from group 2 (non power-law profiles) than for the data from group 1, and the data from group 2 generally give a lower C_P.

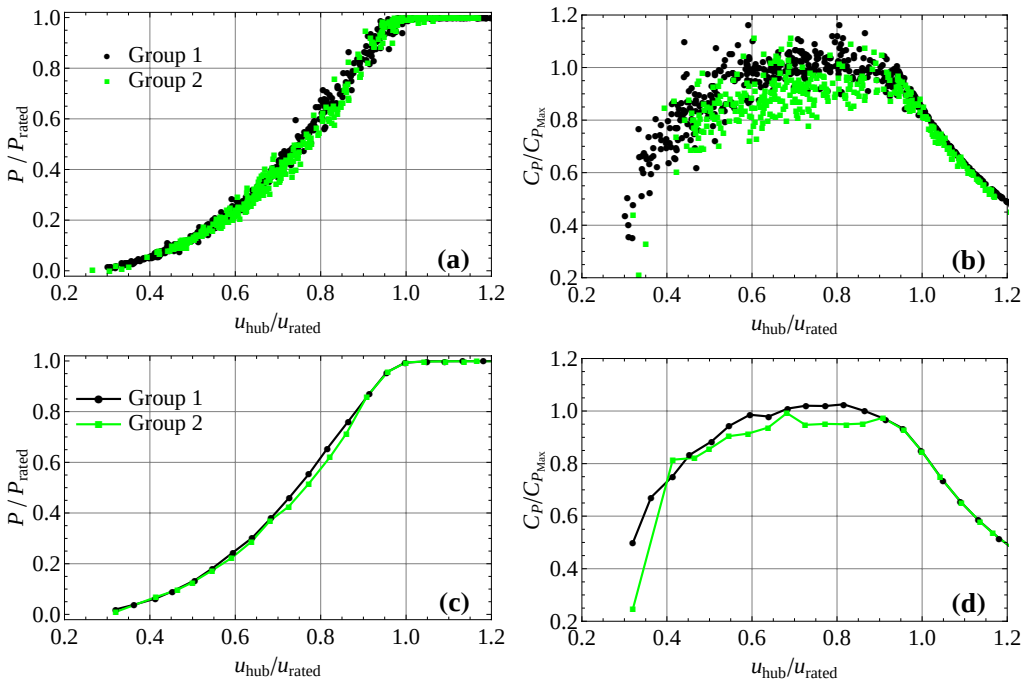

Figure 8.7: *(a): Power curve scatter plot, (b): C_P curve scatter plot, (c): Averaged power curves for each group of profile, (d): Averaged C_P curves. These plots were obtained by using the wind speed at hub height only and C_P defined as in the IEC 61400-12-1 standard.*

What might appear here as an under-performance of the wind turbine (especially for the data from group 2) is actually due to an overestimation of the kinetic energy flux of the wind. Indeed, the kinetic energy flux, KE_{hub} defined in eq. (5.1) used to calculate the C_P in eq. (3.3) implicitly assumes that the wind speed is constant over the entire rotor swept area. Or, in other words, the wind speed shear is ignored.

[2]obtained after binning the data into 0.5 m/s wind speed bins and averaging as required by the IEC 614000-12-1 standard

8.5 A better approximation of the kinetic energy flux

As already mentioned in chapter 5, a better approximation of the kinetic energy flux can be obtained by considering the wind speed profile over the rotor swept area. For a theoretical profile, the kinetic energy flux is given by eq. (5.2). Here this equation was applied with a power law profile. The variation of the ratio KE^{Th}_{prof}/KE_{hub} as a function of the shear exponent is shown by a blue line with diamonds in Figure 8.9 (KE_{hub} is given by eq. (5.1)). According to this theoretical analysis, the ratio between the two kinetic energy approximations is below 1 for a shear exponent between 0 and 0.3 with a minimum around 0.2. However the ratio remains quite high as it is 0.988 for $\alpha = 0.2$. For negative shear exponents and shear exponents higher than 0.3, the ratio is larger than 1. This shows that an error of up to 1% is made in the evaluation of the energy available in the wind for a power law profile with a usual shear exponent (between 0 and 0.4).

For the measured profiles, the kinetic energy flux was approximated by:

$$KE_{prof} = \frac{1}{2}\rho \sum_{i=1}^{N} u_i^3 A_i \tag{8.2}$$

where u_i is the wind speed measured at the i^{th} height in the profile and corrected for the air density and A_i is the area of the corresponding segment of the rotor swept area, see Figure 8.8.

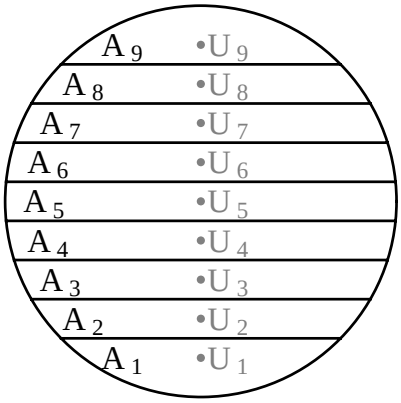

Figure 8.8: *Rotor swept area divided into 9 segments corresponding to the 9 heights where the lidar measured*

The ratio KE_{prof}/KE_{hub} for the measured profiles is also displayed in Figure 8.9. The profiles from group 1 follow rather well the analytical results; i.e. they show a moderate different in kinetic energy flux with the constant profile assumption. The profiles from group 2, on the other hand, do not follow the analytical curve at all and demonstrate a much bigger difference between the two ways of evaluating the kinetic energy flux. The approximation of a constant wind speed over the whole rotor swept area overestimates the kinetic energy flux for most of the data of group 2 and underestimates it for a few of them.

Two wind speed profiles can have the same wind speed at hub height but different kinetic energy. In a standard power curve, such profiles would have the same abscissa (hub height wind speed) whereas they would almost certainly result in different power outputs. This is partially why the two groups of profiles give two different power curves. The kinetic energy flux overestimation has even more impact on C_P which explains why C_P for the group 2 profiles is generally lower than for group 1.

Another contribution to the differences between the power curves can be the true influence of the wind speed shear on the efficiency of the wind turbine and hence on the power output. Indeed, two profiles possessing the same kinetic energy may give different

turbine power output, because for some wind speed shear conditions (for example, a power law profile with a large shear exponent) the turbine is not able to extract as much energy as in other shear conditions (for example a constant profile). This depends on the design and the operational characteristic of the turbine, which the kinetic energy flux says nothing about.

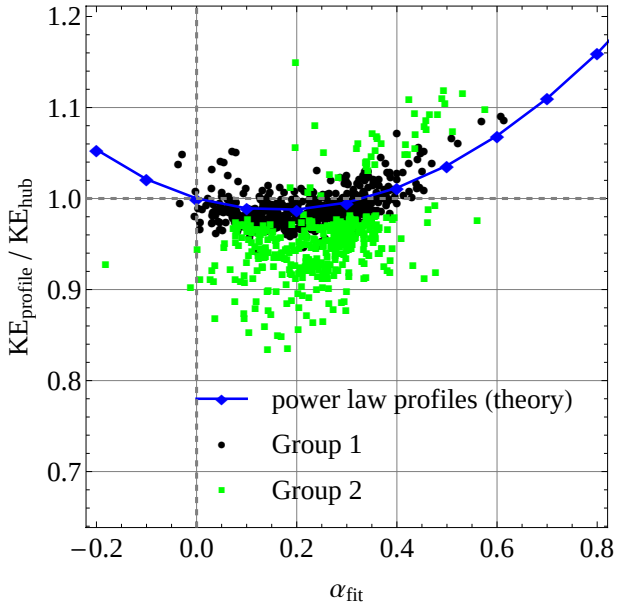

Figure 8.9: *Ratio between the kinetic energy flux accounting for the wind speed profiles and the kinetic energy assuming a constant wind speed with height equal to the hub height wind speed*

8.6 Application of the equivalent wind speed method

The equivalent wind speed giving the same kinetic energy flux as the speed profile (U_{KE}) was derived from each profile measured by the lidar according to eq. (5.9) with $N = 9$.

8.6.1 Application to the classified profiles

Figure 8.10 shows plots comparable to the plots in Figure 8.7. In Figure 8.10, the power and C_P are plotted as a function of the equivalent wind speed defined by eq. (5.9) - instead of the wind speed at hub height in Figure 8.7 - and C_P is calculated as:

$$C_P = \frac{P}{KE_{prof}} = \frac{P}{\sum_{i=1}^{N} \frac{1}{2}\rho u_i^3 A_i} \tag{8.3}$$

- instead of eq. (3.3) in Figure 8.7. In Figure 8.10, profiles from both groups follow the same trend. The mean power and C_P curves obtained with each group of points overlap each other. This shows that the difference in power curves between the two groups seen in Figure 8.7 was mainly due to the error in kinetic energy flux.

8.6.2 Application to the unified data set

In a conventional power performance measurement, the data would not be grouped according to the profile shapes, but all the data would be considered together irrespectively. The effect of assuming a constant wind speed over the whole rotor disc (or ignoring the wind speed shear) in the kinetic energy flux estimation then appears as a scatter in the power and C_P curves. The use of the equivalent wind speed results in the reduction of

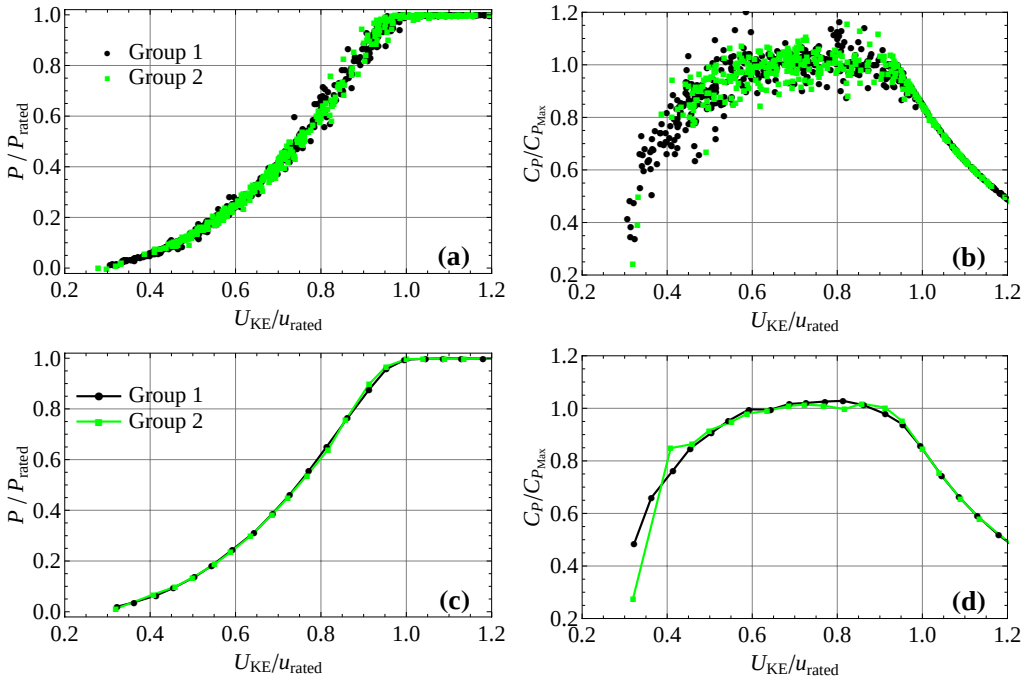

Figure 8.10: *(a): Power curve scatter plot, (b): C_P curve scatter plot, (c): Averaged power curves for each group of profiles, (d): Averaged C_P curves. These plots were obtained using the equivalent wind speed defined by eq. (5.9) and C_P defined by eq. (8.3)*

this scatter. This can be seen directly by comparing Figure 8.10 (a) (resp. (b)) to Figure 8.7 (a) (resp. (b)).

In order to make the difference clearer, the scatter was quantified with the mean residuals as explained in section 8.3. Figure 8.11 shows the residuals as a function of the wind speed. It confirms that the use of the equivalent wind speed resulted in a reduction of the scatter in both the power curve and the C_P curve.

8.7 Lidar profiles corrected with cup anemometer measurements

In chapter 7, it was suggested to shift the profiles measured by the lidar so the wind speed at hub height would match the cup anemometer measurement. However, as the scatter in power curves obtained with the two instruments were different, this kind of "correction" was questioned in the conclusion. The main problem in the experiment described in chapter 7 was that the lidar was located at a significant distance from the cup anemometer (about one rotor diameter), which made the comparison difficult if not meaningless. In the new experiment presented here, the lidar was installed as close as possible to the mast: at about 5m, and oriented so the beam would avoid most of the mast wakes. A direct comparison of the measurements by the two instruments at hub height (Figures 8.2, 8.3, 8.4) showed close agreement. The question is then whether or not the "correction" of the lidar measurement with the cup anemometer measurement is meaningful in this case.

The profiles were classified into two groups, the equivalent wind speed was derived from the profiles, the power and C_P curves were obtained for both groups and the scatter was evaluated as described in section 8.4 and 8.6, but considering, this time, the wind speed profiles shifted in order to match the wind speed measured by the cup anemometer at hub height.

The results are very similar to those obtained without profile correction:

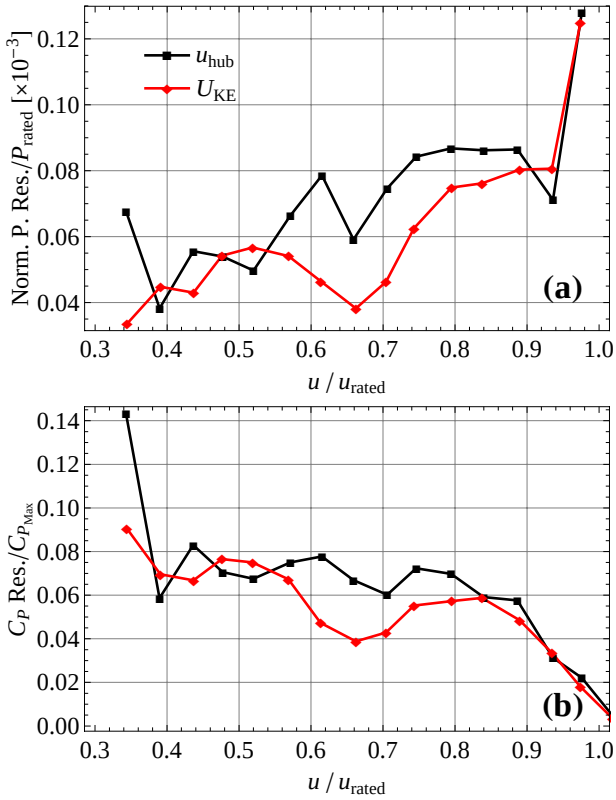

Figure 8.11: *(a): Normalised mean residuals in the power curve (Norm. P. Res.); (b): Mean residuals in the C_P curve (C_P Res.)*

- the 2 groups of profiles resulted in two different power (and C_P) curves when using the wind speed at hub height, see Figure 8.12;
- when using the equivalent wind speed , the two curves are much closer to each other, see Figure 8.13;
- the scatter in the power curve was reduced when using the equivalent wind speed, see Figure 8.14.

Moreover, Figure 8.14 shows that the scatter is similar in both cases: with and without "correction" of the profile. The main difference occurs where the largest difference appear between the measurement at hub height with the lidar and the cup anemometer (at wind speeds below 0.5 u_{hub}). Shifting of the lidar speed profiles did not reduce the scatter in comparison to the uncorrected lidar measurements.

8.8 Conclusions of the second experiment

The wind shear was demonstrated to have an influence on the wind turbine power performance. The error in power performance measurement due to the wind shear is larger for profiles deviating from the power law than for those having a shape comparable to a power law profile. This result points out the necessity of measuring the wind profile in front of the turbine and not to assume the wind profile to follow a model such as the power law. This is further investigated in chapter 9. The equivalent wind speed methods resulted in the reduction of the scatter due to the wind shear in the power and C_P curves.

This investigation also demonstrated a successful application of the equivalent wind speed method with lidar measurements. The lidar measurement at hub height showed

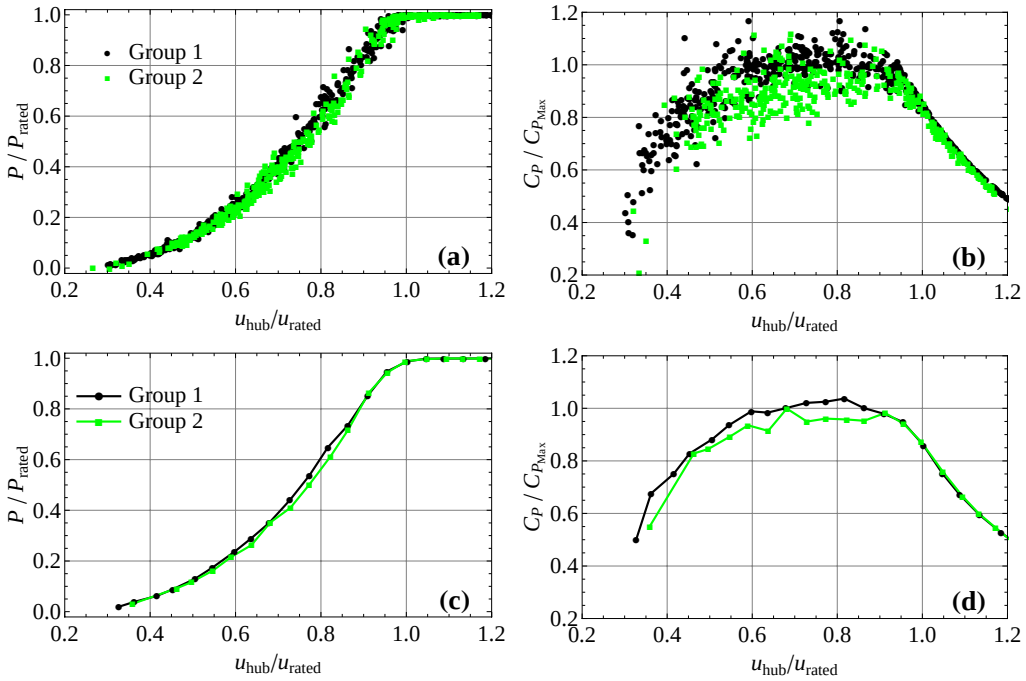

Figure 8.12: *(a): Power curve scatter plot, (b): C_P curve scatter plot, (c): Averaged power curves for each group of profile, (d): Averaged C_P curves. These plots were obtained by using the wind speed at hub height measured by the cup anemometer and C_P defined as in the IEC 61400-12-1 standard.*

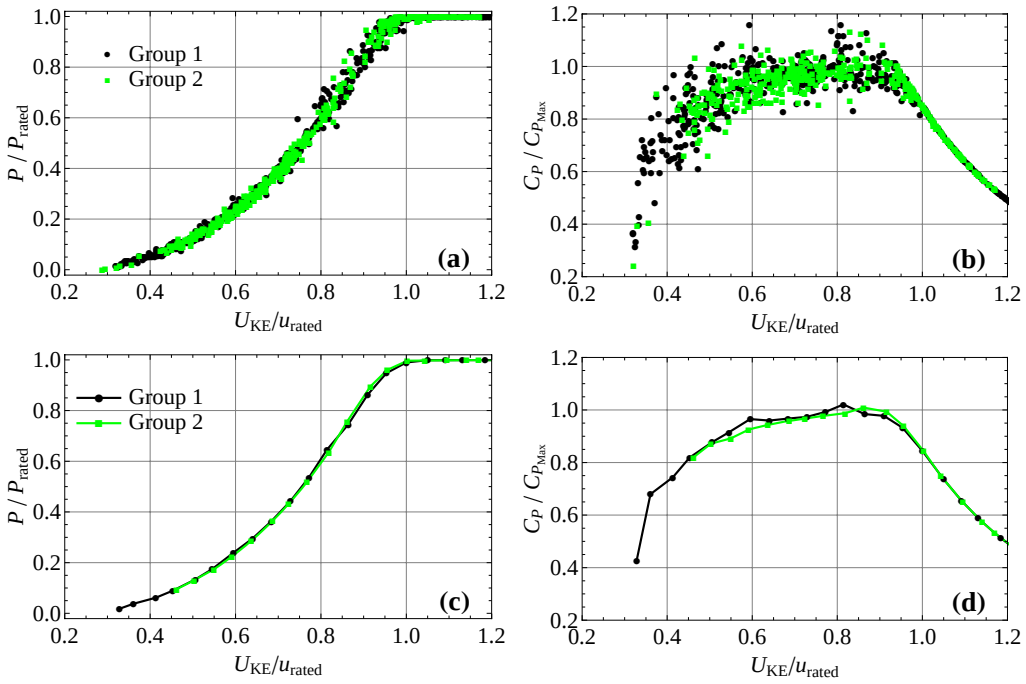

Figure 8.13: *(a): Power curve scatter plot, (b): C_P curve scatter plot, (c): Averaged power curves for each group of profile, (d): Averaged C_P curves. These plots were obtained using the equivalent wind speed derived from the profiles shifted in order to match the cup anemometer measurement at hub height.*

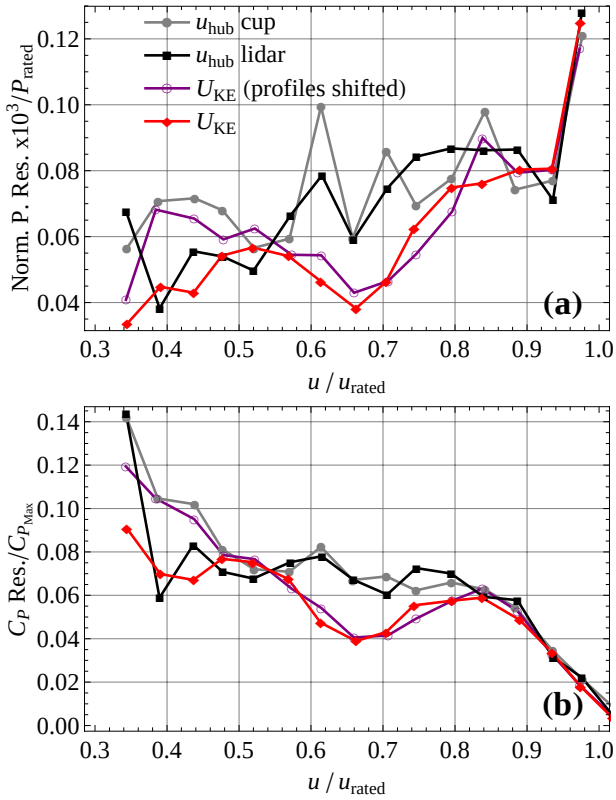

Figure 8.14: *(a): Normalised mean residuals in the power curve (Norm. P. Res.); (b): Mean residuals in the C_P curve (C_P Res.) obtained with the shifted profiles*

a very good comparison to those of the cup anemometer. Conventional power curve obtained with both instruments were very similar and the scatter comparable.

Chapter 9

Further investigations of the equivalent wind speed using real data

In the previous chapter, the equivalent wind speed method was tested with the definition of equivalent wind speed given by eq. (5.9) using speed measurements at 9 heights. These measurements validated the method as less scatter in the power curve and the C_P curve were obtained with the equivalent wind speed than with the wind speed at hub height. Using this dataset, some more subtle aspects of the method are now investigated. Indeed, questions were raised with the results from aerodynamic simulations and answers may be obtained from the experimental results.

The first question was about the equivalent wind speed definition, as several definitions were suggested in chapter 5. Therefore, the analysis is now made with other definitions than the one used in chapter 8.

Secondly, a question concerning the application of the equivalent wind speed method (especially experimentally) is to determine how many measurement points in the profiles are necessary to obtain a significant reduction of the scatter in the power curve. The method was applied with various number of measurement points, first, over the whole turbine rotor vertical span and,secondly, within its lower half only.

Thirdly, regarding the effect of turbulence, it was suggested to use the method described in (Albers, 2010). In chapter 5, this method was shown to "normalise" the mean power curve according to the chosen turbulence intensity, with aerodynamic simulations using turbulent inflow but no shear. In the present chapter, this method is tested with measurements including both wind shear and turbulence, and is applied in combination with the equivalent wind speed.

9.1 Various definitions of equivalent wind speed

In chapter 5, four equivalent wind speed definitions were investigated with aerodynamic simulations, they are summed up in Table 9.1:

	mean speed shear	turbulence intensity
U_{disk}	X	
U_{KE}	X	
U_{disk_TI}	X	X
U_{KE_TI}	X	X

Table 9.1: *List of the equivalent speed definitions investigated in chapter 5*

It was previously pointed out that one advantage of using U_{KE} was that the power

coefficient C_P then shows the ability of the turbine to extract the energy available in the wind. U_{KE_TI} can give a better approximation of the efficiency of the turbine than U_{KE}. The quantity $\frac{1}{2}\rho U_{KE\_TI}^3 A$ gives an improved approximation of the wind kinetic energy flux, accounting for both the shear and the turbulence intensity. Moreover, U_{KE_TI} and U_{disk_TI} gave very similar results with the aerodynamic simulations. For these reasons, only U_{KE_TI} was retained for this investigation.

U_{KE_TI}, as defined in eq. (5.11), is based on the measurements of the turbulence intensity at all heights (TI_i with $i \,\epsilon[1, N]$) in the wind speed profile. However, the standard deviation that can be measured by a lidar can deviate significantly from cup anemometer measurements. Indeed, it was shown that this deviation was typically 20% in average for a continuous wave lidar in (Wagner et al., 2009). Most of this deviation is due to the volume averaging and the influence of the vertical wind speed fluctuations. The investigation for a pulsed lidar system has yet to be performed. It was therefore chosen to use the wind speed standard deviation measured by the cup anemometer at hub height and assume the turbulence intensity profile to be constant in the U_{KE_TI} calculation.

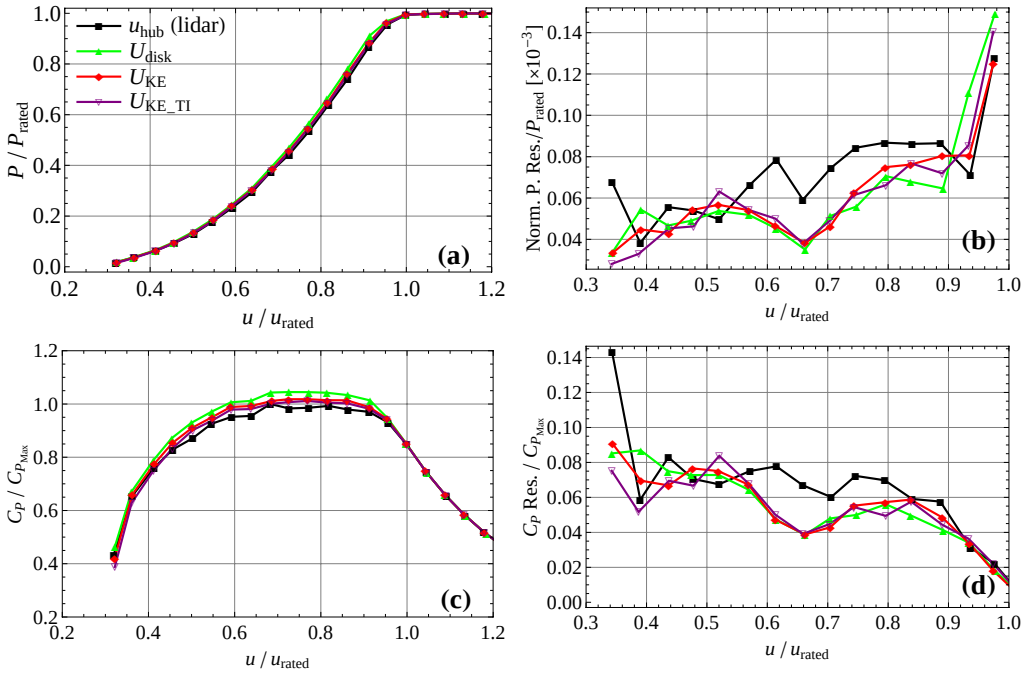

Figure 9.1: *(a): Mean power curves; (b): Normalised mean residuals in power (Norm. P. Res.); (c): Mean C_P curves; (d): Mean residuals in C_P (C_P Res.), for the wind speed measured at hub height by the cup anemometer and the lidar and the equivalent wind speeds U_{KE}, U_{disk} and U_{KE_TI}*

Figure 9.1 shows the power curves, the C_P curves and the residuals obtained for the wind speed measured at hub height (with the lidar) and for the equivalent speed definitions: U_{KE}, U_{disk} and U_{KE_TI} defined by eq. (5.6), eq. (5.5) and eq. (5.11), respectively. The mean power and C_P curves are slightly different from each other. The difference is again due to a good or bad approximation of the kinetic energy flux. Indeed, if U_{disk} is used to calculate the power in the wind, it is not consistent with the kinetic energy flux: the quantity $\frac{1}{2}\rho U_{disk}^3 A$ has no physical meaning. As U_{disk} is on average smaller than u_{hub} and the other equivalent speeds, the power curve is shifted to the left and it gives on average a higher C_P. U_{KE} gives a better approximation of the kinetic energy flux than the wind speed at hub height. The introduction of turbulence intensity (U_{KE_TI}) increases slightly the available power in the wind and therefore decreases slightly the mean C_P. But the difference is very small, mainly because the turbulence intensity was

rather low: 5.6% on average for this dataset, see Figure 9.2.

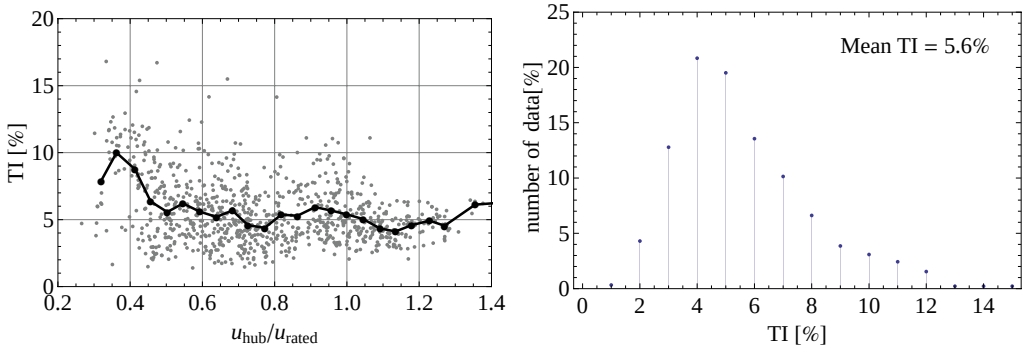

Figure 9.2: *Measured turbulence intensity during the second campaign*

All three definitions resulted in reducing the scatter with a reduction of the same range of magnitude. Therefore any of these three equivalent wind speed definitions results in a power curve less dependant on wind shear than the standard power curve. There is very little difference in the scatter obtained with the three equivalent wind speeds. The best definition can therefore not be deduced from this criterion.

U_{KE} enables us to better estimate the efficiency of the turbine to extract the power from the wind. U_{KE_TI} gives an even better estimation of the turbine efficiency as the kinetic energy flux then also accounts for the turbulence. However, as already pointed out in section 5.3.2, it does not normalise the power curve for the turbulence effect as it results in different power curves for different turbulence intensities due to the asymmetric influence of the turbulence close to the cut-in and rated wind speed. Therefore, U_{KE} still appears as the most appealing definition.

Nevertheless, such a power curve remains dependant on wind speed shear as the turbine's ability to extract energy from different shear conditions depends on the wind turbine design and control strategy. In order to get a power curve completely independent of the vertical wind shear, the equivalent wind speed should be the wind speed for a constant profile (i.e. with no shear) which gives the same turbine power output as the measured profile, meaning an equivalent wind speed that would account for not only the wind speed shear but also its effect on the turbine efficiency.

9.2 Speed profile description for the application of the equivalent speed method

In the second measurement campaign, 9 measurement points were used in order to get as much information as possible about the speed profiles. Indeed, a Windcube lidar can measure up to 10 heights[1]. The measurement at hub height was necessary in order to compare the scatter in the power curve obtained with he equivalent wind speed to that obtained with these measurements. Hence, the hub height was selected as a mandatory measurement height and the other measurement heights were then evenly distributed above and below hub height.

However, depending on the equipment available, it is not always possible to measure the wind speed at 9 heights. For instance, a ZephIR lidar offers a maximum of 5 measurement heights. The question is then whether the equivalent wind speed method can give good results with less than 9 measurement points. Another case is the lack of measurements above hub height - when using a met. mast with cup anemometers at hub height and below, for example - where the profiles need to be extrapolated.

[1]More than 10 is actually possible but the data processing would then be longer.

In order to investigate the influence of the number of measurement points, the equivalent wind speed was derived from 2, 3 or 5 measurement points - by ignoring the measurements at other heights.

9.2.1 Number of measurement points in the speed profile

Figure 9.3 shows the various configurations that were considered. For a given number of measurement points, two parameters can be tuned: the position of each measurement point, i.e. the height relative to rotor swept area, and the weighting function then applied to each measurement in the equivalent wind speed definition. The weighting function is defined as the ratio between the segment area adjacent to the measurement point and the whole rotor swept area.

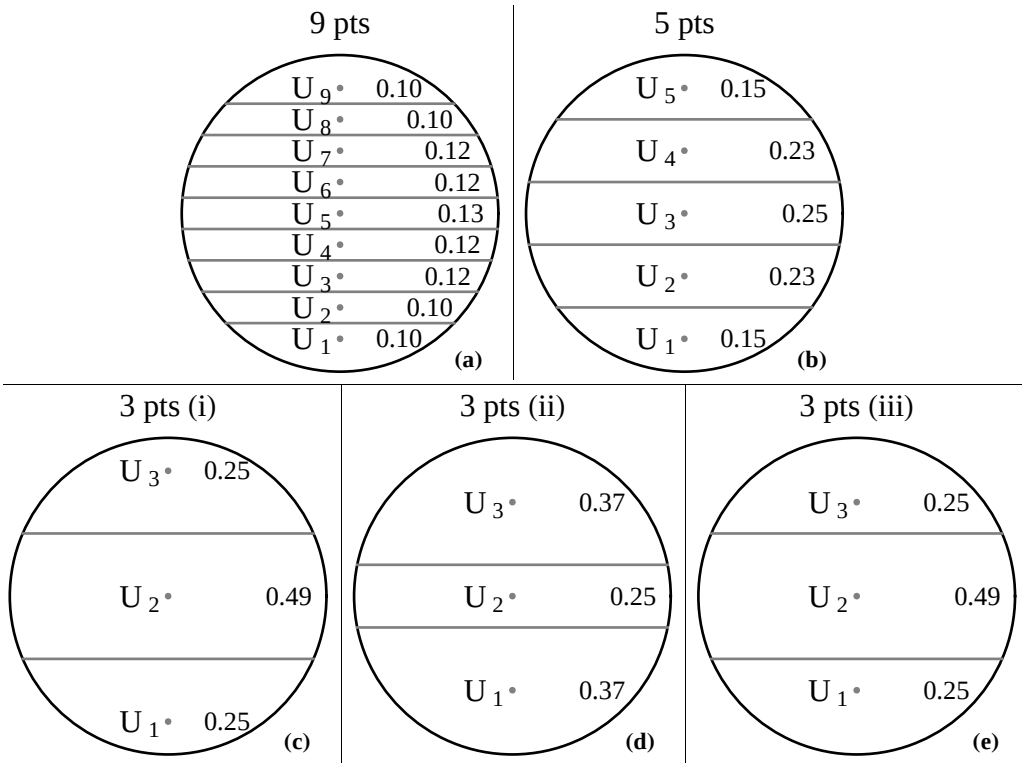

Figure 9.3: *Five configuration tested for the application of the equivalent wind speed method for a given rotor swept area. (a): 9 points (as used in chapter 8); (b): 5 points; (c): 3 points including the highest and lowest measurement points; (d): 3 points with small weight for measurement at hub height; (e): 3 points, same points as case 4 but same weighting as case 3. The number on the right in each segment is the weight given to the corresponding wind speed, based on the segment area*

Figure 9.4 shows the mean power curves and C_P curves and the scatters obtained for the various configurations. The scatter was calculated as described in section 8.3. The scatters obtained with the various configurations are all close to each other and smaller than the scatter obtained with a wind speed at hub height on average. Hence three measurement heights are enough to get a satisfactory result.

Amongst the 3 different configurations using 3 speed measurements, case (i) seems slightly worse than the others. The equivalent wind speed is probably more representative of the speed over the rotor if it based on measurements taken inside the rotor swept area, i.e. not too close to the higher and lower tip heights. Case (iii) appears to be the best, resulting in the smallest scatter, with sometimes unexpected smaller scatter than the 9 measurements points configuration. However, the dataset used in this analysis is rather

small, therefore small differences in the scatter may not be significant. This should be tested with other data sets.

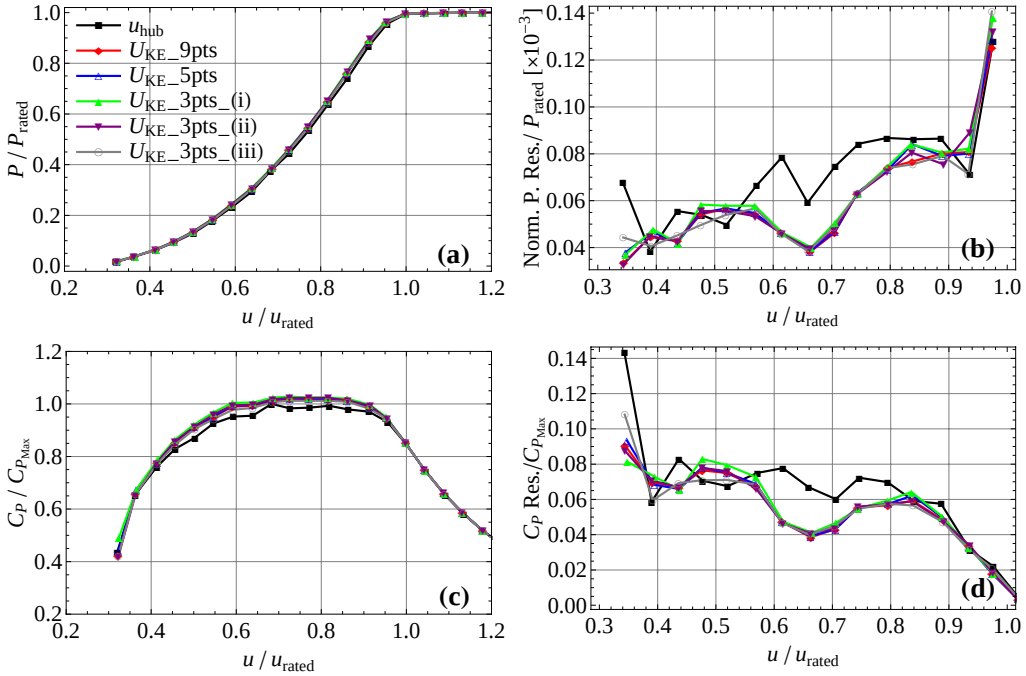

Figure 9.4: *(a): Mean power curves; (b): Normalised mean residuals in power (Norm. P. Res.); (c): Mean C_P curves; (d): Mean residuals in C_P (C_P Res.), obtained with the wind speed at hub height and the 5 different measurement configurations shown in Figure 9.3.*

Figure 9.5 shows the relative difference in the kinetic energy flux approximation obtained with various number of measurement heights,i.e. KE_{prof} given by eq. (8.2) was evaluated with various values of N. The value obtained with 9 measurement heights was taken as a reference as it was the best approximation of the kinetic energy flux one could get with these measurements. Figure 9.5 shows that the approximation obtained with 3 wind speed measurements is much better than that based on the wind speed at hub height only. The approximation obtained with 5 points is even better, nevertheless the improvement is smaller than from 1 point to 3 points.

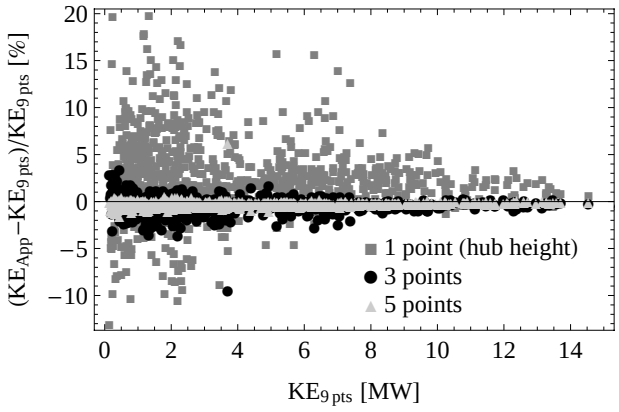

Figure 9.5: *Difference in wind kinetic energy flux approximation relative to that obtained with 9 measurement heights: with 1 measurement at hub height, with 3 measurement heights (config. (e) in Figure 9.3) and with 5 measurement heights*

9.2.2 With extrapolated profiles

It is assumed now that the wind speed is measured at 1 or 2 heights below hub height (in addition to the measurement at hub height). If no lidar or tall met. mast is available, and no wind speed above hub height can be used to characterise the speed profile, it is then necessary to extrapolate the wind speed profile.

Stefanatos et al. (2008) fitted the speed measurements at hub height and two heights below to a power law. These power law profiles were then used to derive various equivalent wind speeds, but the scatter in the power curves remained the same as that obtained with wind speeds at hub height.

A similar analysis was done here. First, the shear exponent was derived from the lowest wind speed measurement and the wind speed at hub height according to eq. (2.7). Secondly, one additional measurement point, between the lower tip and hub height, was considered and the shear exponent was obtained by fitting the 3 points to a power law.The equivalent wind speed was then derived by integrating the cube of this speed profile over the rotor swept area as in eq. (5.6).

Figure 9.6 shows the results obtained with the equivalent wind speed for a shear exponent derived from 2 or 3 speed measurements compared to the results obtained with the wind speed measurement at hub height. The figure shows that the scatter is larger on average than the scatter in the reference power curve and the results are very similar for shear exponents derived from 2 and 3 measurements. This means that, regardless of the way the shear exponent is derived, for this dataset, the assumption of a power law profile induces an error in the wind speed profile and therefore in the kinetic energy flux and in the equivalent wind speed for this dataset.

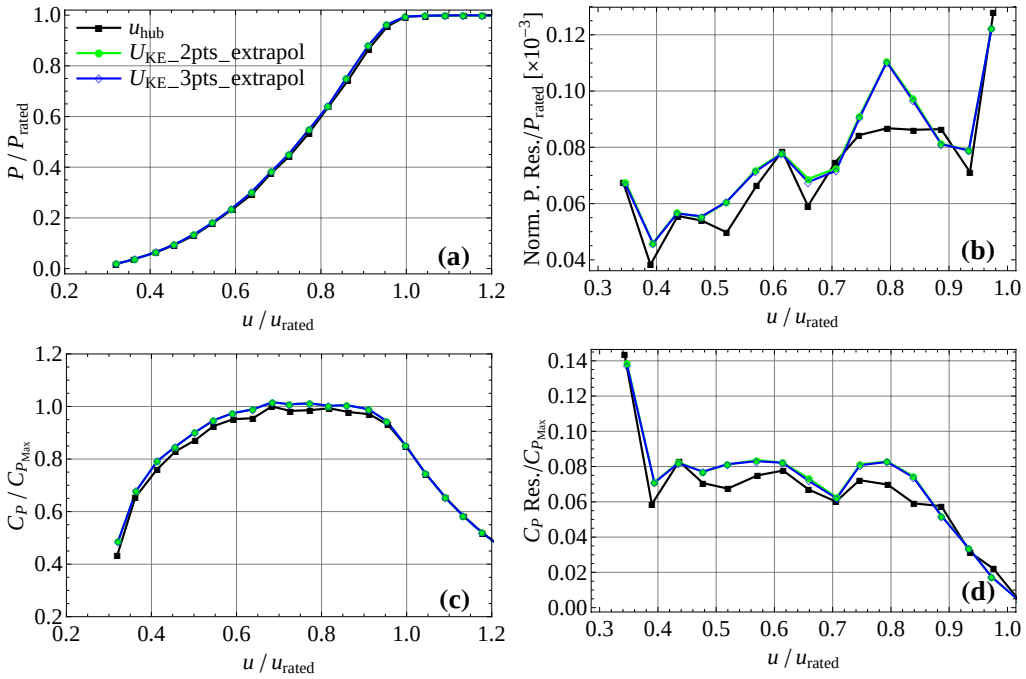

Figure 9.6: *(a): Mean power curves; (b): Normalised mean residuals in power (Norm. P. Res.); (c): Mean C_P curves; (d): Mean residuals in C_P (C_P Res.), obtained with the wind speed at hub height and profiles extrapolated from 2 and 3 measurements.*

Figure 9.7 shows the difference in the kinetic energy flux approximation between the values obtained by applying eq. (5.2) with a power law and α derived from 2 or 3 measurement points and the values obtained by applying eq. (8.2) with 9 measurement heights. The results obtained with the extrapolated profiles are not better than those obtained with speed measurements at hub height. Moreover, the results obtained in section 9.2 with speed measurements at 3 heights (1 at hub height, 1 below and 1 above)

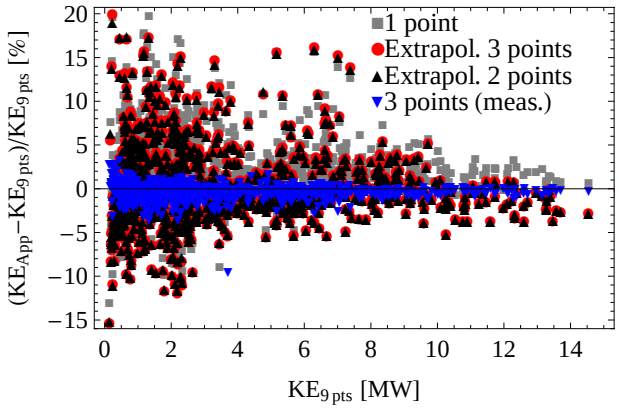

Figure 9.7: *Difference in wind kinetic energy flux approximation relative to that obtained with 9 measurement heights: with 1 measurement at hub height, with 3 measurement heights with extrapolated profiles from 2 measurement heights and 3 measurement heights below hub height.*

are much better than the results obtained with extrapolated profiles. It is probable that this conclusion is site dependent since the extrapolation could give good results in inland sites where the power law is a better approximation to the speed profile than at the coastal site considered here.

9.2.3 Conclusions

This investigation showed that 3 measurement points (including one above hub height) were enough to improve the wind turbine power performance measurement. Then, the more the measurement points, the better the evaluation of the kinetic energy flux. However, the difference in scatter obtained with 3, 5 or 9 wind speeds in the profile was rather small for this dataset. Moreover, if only 3 heights must be selected, it is probably more relevant to measure the wind speed at half of the radius (or maybe at 70% of the radius) rather than close to the edge of the rotor swept area. Finally, an equivalent wind speed derived from wind speed profile extrapolated from measurements at 2 or 3 heights below and at hub height did not decrease the scatter in the power curve. This shows that, more than the number of measurement points, it is important to actually measure the wind speed profile in front of the whole rotor swept area. It is therefore necessary to measure the wind speed at, at least, one height above hub height.

9.3 Combination of the equivalent wind speed method with Albers' method

In section 5.3.2, it was suggested to use the method described in (Albers, 2010) in order to "normalise" the power curve for the turbulence intensity. This method is made of two main steps: 1) the definition of the 0%-TI power curve, 2) the simulation of the power output for the chosen turbulence intensity (TI_{target}). This method was designed to normalise the standard power curve for the TI_{target}. As, on the other hand, the equivalent wind speed method "normalises" the power curve for the effect of shear, the combination of these two methods would result in a power curve less sensitive to the wind characteristics, and therefore less dependent on the site and season.

9.3.1 Description of Albers' method

The model is based on the assumption that the wind turbine follows the same power curve at each instant. This power curve would be the measured power curve if the turbulence

intensity was 0. According to this assumption, the power output of the turbine for any turbulence intensity can be simulated by:

$$P_{sim}(v, TI) = \int_{v=0}^{\infty} P_{0\%}(v) f(v) dv \tag{9.1}$$

where $P_{0\%}(v)$ is the power given by the 0% TI power curve for the wind speed v, and $f(v)$ is the wind speed distribution. This distribution is assume to be Gaussian [2], denoted by $f(v) = \mathcal{N}(v, \sigma^2)$, it only depends on the 10 minute wind speed average, v, and variance, σ^2. The variance here is given by $\sigma^2 = TI^2 \times v^2$.

Step1: definition of the 0%TI power curve

The 0%-TI power curve is derived from a few parameters characteristic of the turbine: the rated power, the cut-in wind speed and the maximum C_P (Albers, 2010). The values taken for these parameters are tuned with an iterative process in order to minimize the error between the simulated mean power curve and the measured mean power curve . The simulated mean power curve is the power curve obtained by applying eq. (9.1) to each wind speed bin[3] statistics: $P_{sim}(v_i, TI_i)$ where v_i is the bin-averaged speed and TI_i is the bin-averaged turbulence intensity in the i^{th} bin. Figure 9.8 shows the mean measured power curve, the final mean simulated power curves and the final 0%-TI power curve obtained with the first step of the method.

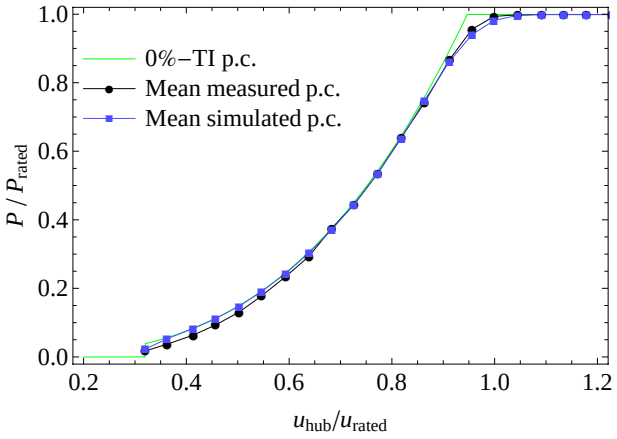

Figure 9.8: *Measured mean power curve, 0%-TI power curve and simulated mean power curve*

Step2: Simulation of the power output with TI_{target}

Once the 0%-TI power curve has been determined, each 10 minute measured power output is corrected for the TI_{target} by applying the formula:

$$P^{(10)}_{TI_{target}}(v^{(10)}_{meas}) = P^{(10)}_{sim}(v^{(10)}_{meas}, TI_{target}) + P^{(10)}_{meas} - P_{sim}(v^{(10)}_{meas}, TI^{(10)}_{meas}) \tag{9.2}$$

where $P^{(10)}_{meas}$ and $v^{(10)}_{meas}$ are the simultaneous measured 10 minute mean power and wind speed and $TI^{(10)}_{meas}$ is the 10 minute measured TI. $P^{(10)}_{sim}(v_{meas}, TI_{target})$ is the power output expected if the assumption that the turbine follows the 0% TI power curve at each instant was true. But there is actually a difference between the actual power output and the simulated power output as the power curve is influenced by other parameters such as the speed shear for example. Albers' method can only reduce the scatter due to the

[2] Gaussian or normal distribution of the variable x: $f(x) = \frac{1}{\sqrt{2\pi\sigma^2}} e^{-\frac{(x-\mu)^2}{2\sigma^2}}$ where μ is the average and σ the standard deviation.

[3] i.e. the wind speed bins used to average the power curve as described in the IEC 61400-12-1 standard

distribution of the turbulence intensity during the power curve measurement. Eq. (9.2) implies that the error between the predicted power for TI_{target} ($P^{(10)}_{TI_{target}}(v^{(10)}_{meas})$) and the simulated power for TI_{target} ($P^{(10)}_{sim}(v^{(10)}_{meas})$) is the same as the error between the measured power ($P^{(10)}_{meas}$) and the simulated power for the measured turbulence intensity ($P_{sim}(v^{(10)}_{meas}, TI^{(10)}_{meas})$). Figure 9.9 shows the measured power curve scatter plot, the simulated power curve for $TI_{target} = 10\%$ and the predicted power curve scatter plot for $TI_{target} = 10\%$.

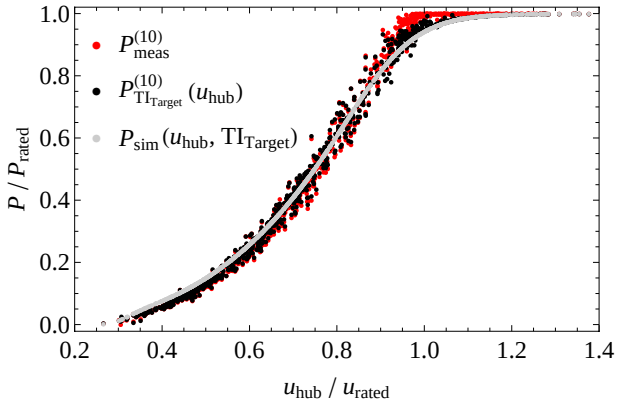

Figure 9.9: *Measured power curve scatter plot ($P^{(10)}_{meas}$), simulated power output for $TI_{target} = 10\%$ ($P^{(10)}_{sim}(v^{(10)}_{meas}, TI_{target})$), resulting simulated power curve scatter plot ($P^{(10)}_{TI_{target}}$)*

9.3.2 Combination with the equivalent wind speed

Albers' method was initially designed to normalised the standard power curve, i.e. based on wind speed measurements at hub height, for the turbulence intensity. In order to compare the results to those obtained by combining Albers' method with the equivalent wind speed, the turbulence normalisation was applied to both power curves: with hub height wind speed and with equivalent wind speed. As the mean power curve obtained with the equivalent wind speed is likely to be different from the mean standard power curve obtained with the hub height wind speed, it was necessary to derive the 0% TI power curve from the equivalent wind speed power curve as well.

The turbulence normalisation changes the power value whereas the equivalent wind speed method changes the wind speed. Therefore for a given TI_{target} value, four results can be compared:

	Measured power	**Normalised power**
u_{hub}	standard power curve	Albers' method
U_{KE}	equivalent wind speed power curve	combined methods

The exercise was done for two values of TI_{target}: 5% and 10 %; the results are shown in Figure 9.10. As shown in Figure 9.10 (a), for the case of normalisation to 5%, the normalised power curves are very similar to the measured power curve, as the mean measured turbulence intensity is 5.6%, see Figure 9.2. The mean turbulence intensity is around 5% for all the wind speeds except around $0.4 \times u_{rated}$ where the mean turbulence intensity is around 10%.

When the power curve is normalised to 10% TI, it is generally moved upwards as the TI increases the power output (see chapter 4) except around rated wind speed where it moved downward, see Figure 9.10 (b). Regarding the scatter (Figure 9.10 (d)), the turbulence normalisation results are very similar to the measurements with wind speed at hub height and equivalent wind speed respectively. Albers' method normalises the

mean power curve according to the turbulence intensity but does not reduce the scatter in the power curve.

A difference in normalised scatter is seen at around rated wind speed. This is the region where the mean power curve experiences the largest change from the turbulence intensity normalisation. The slope of the mean power curve around this wind speed is different from the measured power curve. As this affects the normalised scatter[4], the non-normalised scatter is also shown in Figure 9.10 (e) and (f). The graphs are very similar for 5% and 10%. In both cases, the scatter is close to that obtained with the measured power, both for hub height wind speed and equivalent wind speed, respectively. A local increase in scatter occurs near cut-in and rated wind speeds. They are probably due to the error in the power curve model, i.e. error in the 0%-TI power curve resulting in a difference in the mean measured power curve and the mean simulated power curve, which is larger in these wind speed ranges than in the rest of the power curve as seen in Figure 9.8.

According to the results shown in Figure 9.10, the equivalent wind speed method reduces scatter due to shear also when the power has been normalised for the turbulence intensity according to Albers' method except near rated speed where the mean power curve slope is significantly changed. The mean power curve obtained with the combination of both methods is less sensitive to shear and is representative for a given TI. Such a power curve can give a better representation of the power curve that would be obtained at another site, with different wind shears and turbulence intensities from the power curve measurement site. In this sense, it is transferable from one site to another. Therefore it would give a better AEP estimation (this is further discussed in chapter 10).

[4]The scatter in the power curve was normalised with the mean power curve slope, see section 8.3

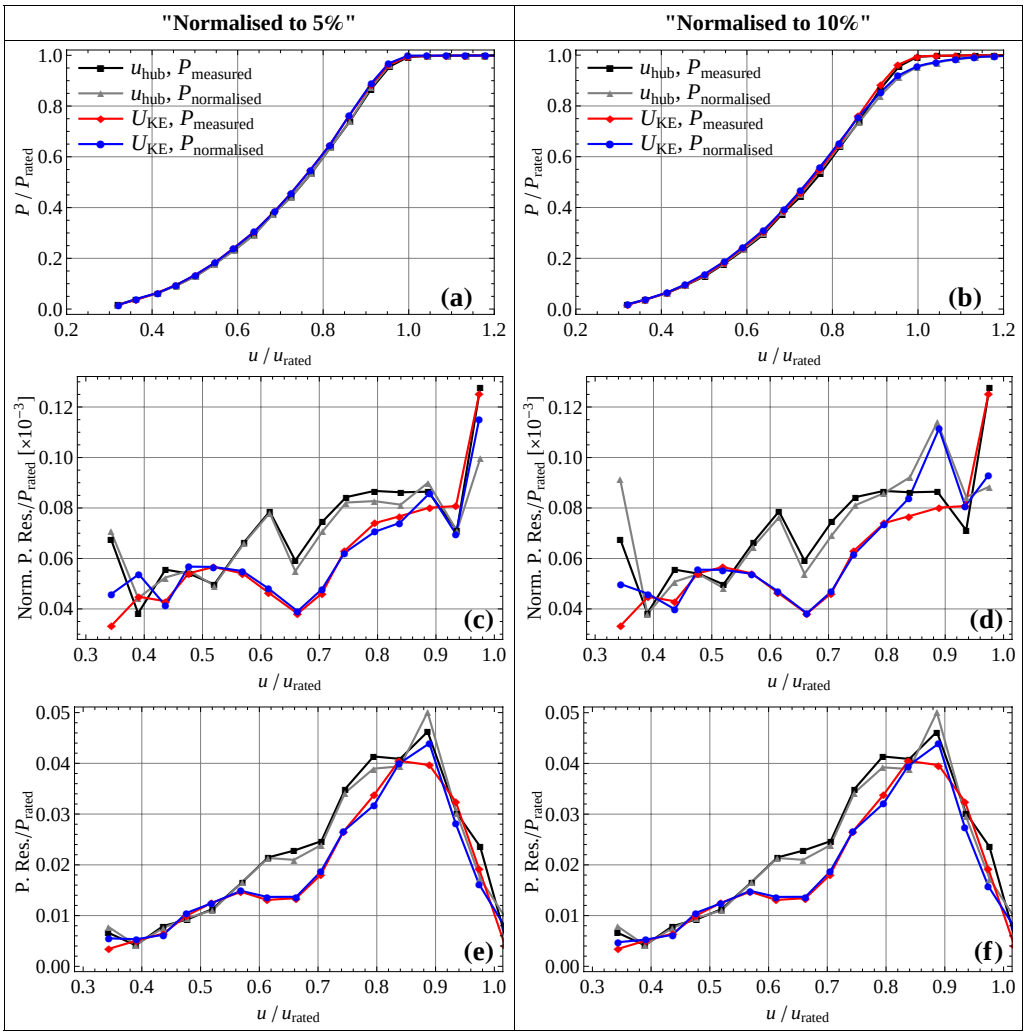

Figure 9.10: *Mean power curve and scatter in the power curve obtained with wind speed measurements at hub height and equivalent wind speed, both with and without turbulence normalisation using Albers' method*

Chapter 10

Annual Energy Production

An important purpose of the wind turbine power curve is for the estimation of the annual energy production (AEP). The AEP is basically the integration of the wind speed distribution times the power curve over the span of one year. However, the AEP usually needs to be predicted prior to the wind turbines installation at a potential wind farm site. Hence a reference power curve, measured at a different site, must be used for the AEP calculation. In that sense, the power curve is assumed to be transferable from one site to another.

The equivalent wind speed method defines a new power curve, different from the standard power curve, since it uses a different wind speed definition. This chapter addresses the difference between the AEP predicted with the standard power curve and with the equivalent wind speed power curve.

In the IEC 61400-12-1 standard, the Rayleigh distribution is used to estimate a generic AEP. For a particular wind farm site, the AEP is usually estimated using a wind speed distribution based on measurements. The AEPs based on both types of distributions are discussed here.

In order to focus on the differences between the results obtained with the equivalent wind speed and those obtained with the wind speed at hub height, the power curve obtained from lidar measurements at hub height is used as a representation of the standard power curve in this chapter. The difference between the power curve obtained from lidar measurements at hub height and that obtained from cup anemometer measurements is discussed in chapter 11.

10.1 Direct comparison of the standard and equivalent wind speed power curves

The power curve obtained with the equivalent wind speed is shifted to the left (towards lower wind speeds) compared to the power curve obtained with measurements at hub height, as shown in Figure 10.1. However this does not mean that the turbine has produced more power, since these two power curves were obtained with the same data set. The equivalent wind speed method modifies the wind speed used in the abscissa in the power curve but the wind turbine power output remains unchanged. This shift in the mean power curve actually shows that, for this dataset, the equivalent wind speed was on average smaller than the wind speed at hub height. Note that at another site with larger wind shear above hub height than below, such as in (Antoniou et al., 2009) and (VanLuvanee et al., 2009), the equivalent wind speed may be larger than the wind speed at hub height, so that the power curve would be shifted to the right.

To test the impact of the two different power curves on the AEP calculation, the power curves shown in Figure 10.1 were used to calculate the generic AEP as defined in the IEC 61400-12-1 standard, i.e. using the Rayleigh distribution. AEP estimations are then made for several average wind speeds from 4 m/s to 11 m/s according to the

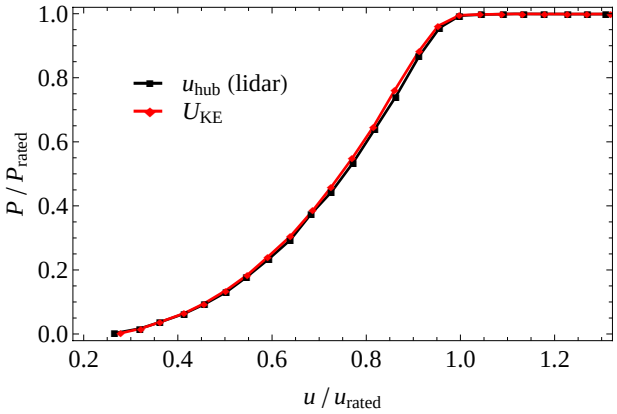

Figure 10.1: *Mean power curves obtained with the wind speed at hub height and the equivalent wind speed.*

equation:

$$AEP = N_h \sum_{i=1}^{N} [F(v_i) - F(v_{i-1})] \left(\frac{P_{i+1} + P_i}{2} \right) \tag{10.1}$$

where N_h is the number of hours in a year ($N_h = 8760$), v_i and P_i are respectively the mean wind speed and the mean power in the i^{th} wind speed bin and $F(v)$ is the Rayleigh cumulative probability distribution function for wind speed, v and the annual average wind speed, V_{avg}:

$$F(v) = 1 - exp\left(-\frac{\Pi}{4} \left(\frac{v}{V_{avg}} \right)^2 \right) \tag{10.2}$$

As shown in Figure 10.2, the AEP based on the equivalent wind speed is higher than that based on the hub height wind speed for all annual average wind speeds between 4 m/s and 11 m/s. This does not mean that the power produced at the test site is different with the two methods. This difference in AEP can be interpreted as follows: if an identical wind turbine was installed at a site where all the speed profiles were constant with height, then the power curve corresponding to this site would be different from the standard power curve measured at Høvsøre, but it would be close to the power curve obtained with equivalent wind speed. In other words, if the standard power curve measured at Høvsøre had been used to determine the AEP at a site with only constant profiles, the AEP would have been underestimated. With the equivalent wind speed power curve, on the other hand, the estimation would have been closer to the actual AEP.

The difference between the AEPs obtained with the two kinds of power curve should be interpreted carefully. Indeed, as mentioned earlier, at a site with different wind conditions, such as that described in (Antoniou et al., 2009) and (VanLuvanee et al., 2009), the power curve being shifted to the right, it would result in an overestimation of the AEP. The relation between the power curves depends on the wind shear conditions. Moreover such a simple interpretation is only valid for a site with predominantly constant profiles, which is not common.

Such a direct comparison of the AEPs obtained with wind speed measurements at hub height and equivalent wind speeds assumes an identical distribution, i.e. identical average and identical distribution shape, for both kinds of wind speed. This is not consistent, since it was noted that the equivalent wind speed was on average smaller than the wind speed at hub height for this dataset. A consistent comparison should account for the differences between the distributions of the two kinds of wind speed. For example, Sumner and Masson (2006) found an equivalent wind speed distribution shifted to the left compared to hub height speed distribution.

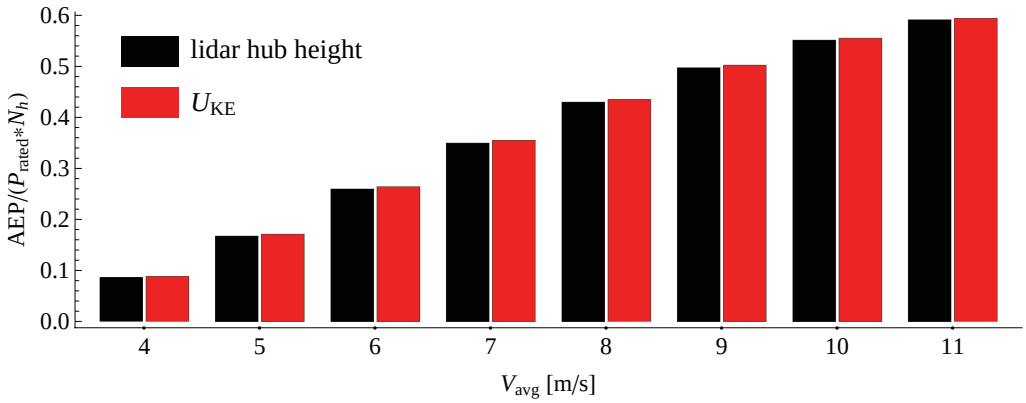

Figure 10.2: *Extrapolated AEP obtained with the wind speed at hub height and the equivalent wind speed.*

10.2 AEP prediction and transferable power curve

The estimation of the AEP at a potential wind farm site ideally requires the turbine power curve obtained at this site (preferably measured over a long period of time) and the wind speed distribution at the site. However, the AEP usually needs to be predicted prior to the actual installation of any turbine. Therefore, the power curve cannot be measured at the site. The power curve measured at a reference site is used instead. Regarding the wind speed distribution, long term measurements from the potential wind farm test site are usually well modelled by a Weibull distribution[1].

This procedure can give a good AEP prediction only if the reference power curve is sensibly transferable to the site, i.e. if the reference power curve is similar to the power curve that would be obtained at this site. However, as a standard power curve is sensitive to the wind shear, it is site dependant. Therefore the transfer of such a power curve from the reference site to another site is very probable to result in an error in the AEP.

This issue was illustrated using the power curves obtained with the two groups of profiles from section 8.6. The power curves obtained with the data from group 1 were considered as the reference power curves (one with the wind speed at hub height and one with the equivalent wind speed) as if they were measured at a reference site (site 1). These power curves were used to predict the power corresponding to the wind speeds of group 2, as if they had been measured at a different site (site 2). Both the estimated and measured power curve scatter plots are shown in Figure 10.3. The total power produced was then calculated by summing the 10 minute power outputs both for the power measured at site 2 and the power predicted with the reference power curves. The total power predicted with the hub height wind speed power curve overestimated the actual power production by 1.76%, whereas the power predicted with the equivalent wind speed power curve made an overestimation of only 0.005%.

By estimating the power obtained for group 2 with the power curve measured for group 1, the power curves were assumed to be identical for both groups (sites). However this assumption is wrong for the standard power curves, see Figure 8.13. This results in the wrong estimation of the total power at site 2. On the other hand, as the equivalent wind speed power curves obtained for the two groups of data are very similar, the transfer of the power curve obtained with one dataset to the other dataset is more acceptable and the prediction of the total power production was much better.

[1]Weibull distribution of the variable x: $f(x) = k\frac{x^{k-1}}{A^k} exp\left(-\left(\frac{x}{A}\right)^k\right)$. The Rayleigh distribution is actually a specific case of the Weibull distribution with $k = 2$.

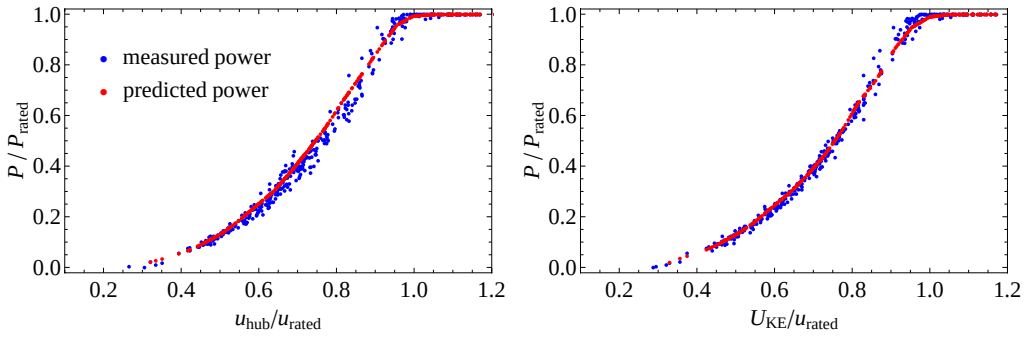

Figure 10.3: *Predicted and measured power scatter plots for the data from group 2. (a): with wind speed at hub height, (b): with equivalent wind speed.*

10.3 How should the equivalent wind speed be used to estimate the AEP?

The standard power performance measurement results in different power curves for different wind speed shear conditions. For a given turbine, different power curves can be obtained for different times of the year or of the day, different wind sectors or different sites. The problem is that different power curves give different AEPs, as shown in (Montes et al., 2009).

On the other hand, as the equivalent wind speed is representative of the speed profile, the power curve obtained with such a wind speed varies much less with shear. Similar power curves should be obtained for various shear conditions, and, for a given speed distribution, the power curve repeatability should result in a more consistent AEP.

However, the equivalent wind speed is quite likely to have a different value from the wind speed at hub height. Therefore, the equivalent power curve should be used with the equivalent wind speed measured at the wind farm site in order to obtain a consistent and accurate AEP prediction. Therefore, the wind profiles distribution needs to be estimated.

The issue is then what to do if no profile measurements are available and only the wind speed at hub height was measured at the new site.

One solution would be to establish a relation between the standard power curve and the equivalent wind speed power curve. This does not make sense because the standard power curve is shear dependant, therefore site dependant. In consequence the relation between the curves in also site dependent. To transfer the relation between the two types of power curve found at one site to another site is equivalent to transferring the standard power curve.

Another option would be to assume one kind of profile (one shear exponent, for example) for all profiles at one site. This is inconsistent with the equivalent wind speed method as its main advantage is to account for variability in shear. Assuming one speed profile shape is what is done in the current IEC standard (IEC, 2005), where a constant profile is implicitly assumed.

It may be better to make the AEP estimation by combining the hub height speed distribution with the equivalent wind speed power curve than with the standard power curve. Indeed, as explained in section 10.2 the equivalent power curve is more transferable from one site to another than the standard power curve. Combining the reference standard power curve with the distribution of wind speeds measured at hub height at the proposed wind farm site is equivalent to assuming a wind speed profile constant with height at both the reference site and at the wind farm site. On the other hand, if the reference equivalent wind speed power curve is combined with the distribution of the wind speed at hub height at the proposed wind farm site, the speed profile is assumed constant only at the wind farm site. As an example, the total power of group 2 was estimated by using the wind speed at hub height for the data from group 2 and estimating the power with the equivalent speed power curve obtained from group 1. This result, together with

the two results already shown in section 10.2, are given in Table 10.1. This estimation gives a slight underprediction of 0.5% but is better than the estimation with the standard power curve which gives an overestimation of 1.76%. Nevertheless in the specific case where the wind shear at the wind farm site is very similar to that at the reference site, the standard AEP prediction, using the standard power curve and the distribution of the wind speeds at hub height, would be better than that obtained by combining the equivalent wind speed power curve and the distribution of wind speeds at hub height.

	Standard p.c.	U_{KE} p.c.
u_{hub}	+1.76%	-0.5%
U_{KE}		0%

Table 10.1: *Error in the total power for group 2 data estimated with the power curves obtained with the data from group 1.*

In conclusion, the most sensible way to use the equivalent speed power curve to estimate the AEP is to also measure the equivalent wind speed at the assessment site, i.e to measure the wind speed at least 3 heights including one height above hub height (see section 9.2).

However, if only speed measurements at hub height are available at the proposed wind farm site, then the error in the AEP estimation can be reduced by using the equivalent wind speed power curve with these measurements.

Chapter 11

Measurement uncertainty

To be complete, a power curve measurement must include an evaluation of the measurement uncertainty. This chapter presents an analysis of the uncertainty in the equivalent wind speed power curve and a comparison to the standard power curve uncertainty. According to the IEC 61400-12-1 standard, the power curve uncertainty is the combined uncertainty of the measurements of the electrical power, the wind speed and the air density. As the equivalent wind speed method modifies the definition of the wind speed in the power curve, the uncertainty in the equivalent wind speed needed to be defined. However, as the equivalent wind speed was derived from lidar measurements, it was necessary to first define the uncertainty in lidar measurement. Hence, the uncertainty for three kinds of power curve are compared in this chapter: the standard power curve obtained with a cup anemometer, the power curve obtained with the lidar measurement at hub height and the power curve obtained with an equivalent wind speed.

The uncertainty in lidar wind speed measurements can be defined in several ways. A simple method is to use a calibrated instrument as a reference. Thus, in a first attempt to define the uncertainty in lidar measurement, it was chosen to be defined relative to a calibrated cup anemometer from which the uncertainty is known. The systematic part of the error in lidar measurements was corrected by calibrating the lidar and the stochastic part of the error was interpreted as the uncertainty.

For clarity, a different notation was adopted in this chapter: u denotes an uncertainty and v a wind speed.

11.1 Power curve uncertainty in the IEC 61400-12-1 standard

In the IEC 61400-12-1 standard, the power curve measurement uncertainty is defined as the combination of the measurement uncertainties of the turbine power output, the wind speed, the temperature and the pressure. Thus the power curve uncertainty combines category A uncertainty, i.e. uncertainty derived from the observed frequency distribution, and category B uncertainties, i.e. uncertainties derived from an assumed probability density function which cannot be derived directly from the observations (GUM, 1999). The combined uncertainty is calculated for each wind speed bin.

The uncertainty in electric power measurement combines a category A uncertainty, the standard deviation of the power in each bin, and category B uncertainties related to the current and voltage transformers and the data acquisition system. The uncertainties in wind speed, temperature and pressure are all of category B. These uncertainties account for the instruments uncertainty[1], the mounting effect, the site effect and the data acquisition system.

[1]For example, the cup anemometer for the wind speed measurements. A cup anemometer used for wind turbine power performance measurement must be calibrated in a wind tunnel. The cup anemometer uncertainty is derived from the this calibration.

In this investigation, three kinds of wind speed were considered, implying three different values of the uncertainty. The uncertainty in wind speed measured by the cup anemometer is estimated according to the procedure described in the IEC standard (IEC, 2005). A way of estimating the uncertainty in lidar measurements was defined and is described below. The uncertainty in equivalent wind speed is the combination of the uncertainty of several lidar measurements.

The uncertainty in temperature and pressure measurements is the same for all three kinds of power curve, as well as the category B uncertainty in electric power. On the other hand, the category A uncertainty in power is expected to be different for a power curve obtained with the equivalent wind speed than for the power curve obtained with the wind speed measurements at hub height as the scatter in the power curve is related to the power standard deviation in each bin.

11.2 Lidar calibration

The lidar used in this experiment was verified between 10/07/08 and 26/10/08 with the met. mast at Høvsøre (see Appendix). The wind speed measured by the lidar was compared to cup anemometer measurements at 5 heights (40, 60, 80, 100 and 116.5 m). The data for the verification were filtered according to the following criteria:

- wind direction between 150° and 180° or between 230° and 300°.
- Temperature above 2°C to avoid ice formation on the cup anemometers.
- Wind speed above 3m/s, for good quality cup anemometer measurements.
- Lidar wind speed availability of 100% at all heights.
- No rain, for best quality lidar measurements.

The verification consists in performing, at each height, a linear regression between the simultaneous measurements from the cup anemometer and the lidar at the same height. Lidar measurements are usually validated when the regression slope is close to unity and a value of R^2 above 0.99. Although no systematic procedure is yet defined, such a verification is strongly recommended. The regressions obtained at the 5 heights ar shown in Figure 11.1.

11.2.1 Calibration coefficient at verification heights

Different methods can be used to calibrate a lidar. One method, already discussed in chapters 7 and 8, consists of shifting the speed profile so the wind speed at hub height measured by the lidar coincides with the cup anemometer measurement. However this method assumes a constant lidar bias (the same bias at all heights) which is not correct for most lidars.

Another option for the lidar calibration is the use of the regression slope obtained during the lidar verification at each height as a calibration factor. This method accounts for lidar error variability with height. A calibration factor, m_k, was obtained in this way for each one of the 5 heights used in the lidar verification. In the rest of the chapter, the number of heights where the lidar was calibrated directly with a cup anemometer was named N_c ($N_c = 5$).

11.2.2 Calibration coefficient at any height

The speed profile measurements during the power curve measurement was independent of the lidar verification. The power curve measurement using an equivalent wind speed can required the measurement of the wind speed at heights different from those of the cup anemometers on the met. mast used for the lidar calibration. The cup anemometer heights are fixed whereas the measurement heights for the equivalent speed depend on

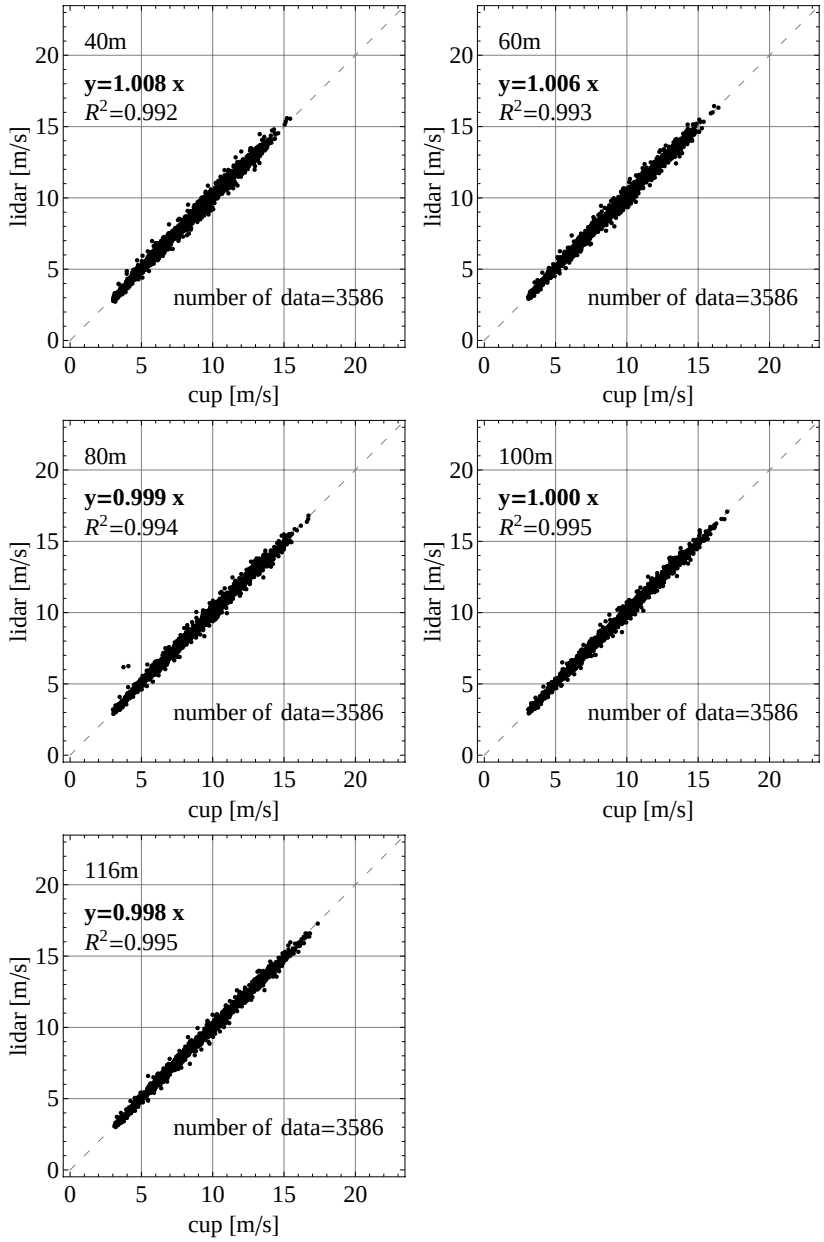

Figure 11.1: *Linear regressions between the lidar and cup anemometer measurements at 5 heights, obtained during the lidar verification*

the turbine hub height and the rotor diameter. Therefore, a calibration coefficient needed to be defined for the heights where no regression slope could be measured.

For heights below the top of the mast (116.5 m here), the calibration coefficient was obtained by linear interpolation. For instance for the measurement height h_j, between the lidar verification heights h_k and h_{k+1}, the regression coefficient is obtained by:

$$m_j = \frac{h_{k+1} - h_j}{h_{k+1} - h_k} m_{k+1} + \frac{h_j - h_k}{h_{k+1} - h_k} m_k \tag{11.1}$$

The "calibrated lidar wind speed" at the j^{th} height is then:

$$v_j^{lidar,calib} = v_j^{lidar,meas} / m_j \tag{11.2}$$

where $v_j^{lidar,meas}$ is the 10 minute mean wind speed measured by the lidar (during the power curve measurement).

For heights above the top of the mast, the calibration coefficient was assumed constant with height and equal to the calibration coefficient measured at the top of the mast:

$$m_j = m_{N_c} \tag{11.3}$$

As such a calibration modified the lidar measurements, both the wind speed at hub height and the equivalent wind speed are affected. The power curves, scatter in the power curves and AEPs obtained with the cup anemometer and the lidar after calibration are shown in Figure 11.2. The calibration has not affected the main results regarding the equivalent wind speed methods: in plot (a), the equivalent wind speed power curve is slightly shifted to the left compared to the power curve obtained with lidar measurements at hub height; in plot (b), the scatter obtained with the equivalent wind speed is smaller than the others and in plot (c), the AEP obtained with the equivalent wind speed is slightly higher than that obtained with wind speed measurements at hub height.

Furthermore, Figure 11.2 also compares the results obtained with lidar wind speed measurements at hub height and those obtained with the cup anemometer measurements. Plot (b) shows that the scatter in the power curve obtained with lidar measurements has not been affected significantly by the calibration and is still comparable to the scatter obtained with the cup anemometer measurements. Plot (a) shows that there is still a slight difference between the mean power curve obtained with the lidar measurements at hub height and that obtained with the cup anemometer. This small difference in power curve results in a small difference in AEP[2] as shown in plot (c). This result is due to the fact that these two different power curves were used with the same wind speed distribution, i.e. average and distribution shape (similar to the discussion in section 10.1)

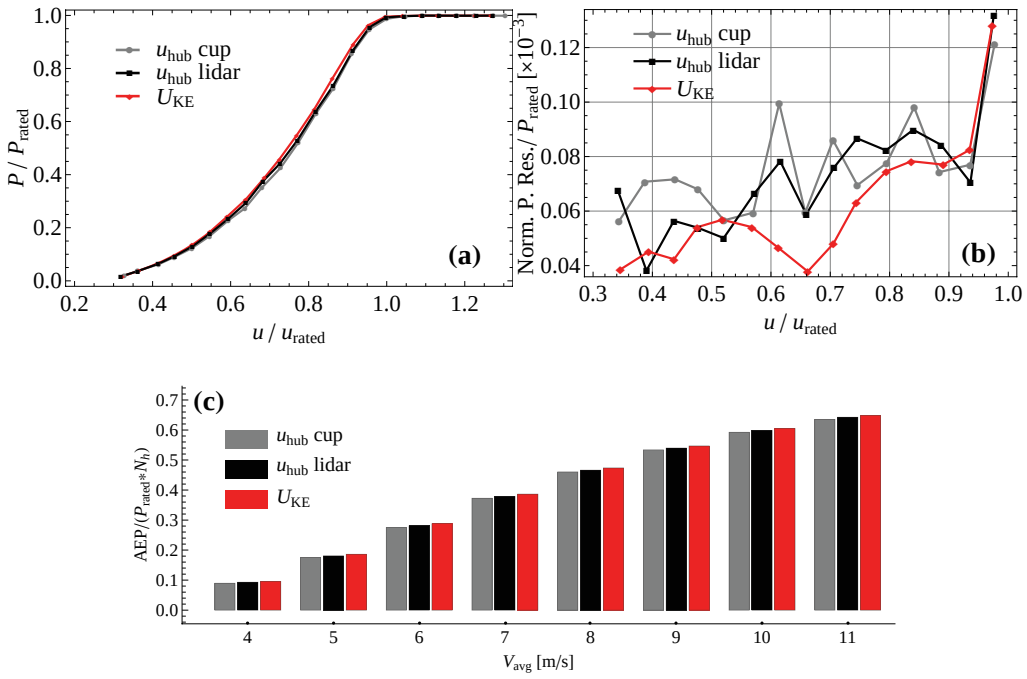

Figure 11.2: *Results obtained with the lidar after calibration compared to the cup anemometer results: (a): mean power curve, (b): scatter in the power curve, (c): AEP*

[2]AEP calculated as in the IEC 61400-12-1 standard using the Rayleigh distribution, see section 10.1

11.3 Definition of the uncertainty in measurements for a calibrated lidar

11.3.1 Uncertainty at verification heights

Since the final aim was to calculate the uncertainty in the power curve, the wind speed measurement uncertainty had to be calculated for each wind speed bin, as required in the IEC 61400-1-12 standard. The calibration described in the previous section was considered as a correction of the systematic error of the lidar measurements. Hence only the stochastic error needed to be accounted for in the uncertainty. The stochastic error of the lidar measurements was quantified with the standard deviation of the residuals in the regression between cup anemometer and lidar measurements, where each residual is defined by:

$$res_{i,l} = v_{i,l}^{lidar} - m.v_{i,l}^{cup} \tag{11.4}$$

where $v_{i,l}^{lidar}$ is the l^{th} lidar wind speed measurement in the i^{th} bin, $v_{i,l}^{cup}$ the l^{th} cup wind speed measurement in the i^{th} bin and m the regression slope - which depends on the height and is independent of the wind speed bin.

The uncertainty in lidar measurement was defined as the combination of the cup anemometer uncertainty with the standard deviation of the residuals. For each height, the data were binned according to the cup anemometer wind speed, and the uncertainty was defined for each wind speed bin as:

$$u_{lidar(k,i)}^2 = u_{cup(k,i)}^2 + u_{verif(k,i)}^2 \tag{11.5}$$

where $u_{lidar(k,i)}$ is the uncertainty of the wind speed measured by the lidar, $u_{cup(k,i)}$ the uncertainty of the wind speed measured by the cup anemometer (as defined in the IEC 61400-12-1 standard) and $u_{verif(k,i)}$the standard deviation of the residuals at the k^{th} height in the wind speed bin i at the k^{th} height.

11.3.2 Uncertainty at any height

In the same way as the calibration coefficient, the lidar uncertainty, at each height (j) and in each wind speed bin (i), was defined by linear interpolation for heights below the mast top height:

$$u_{lidar(j,i)}^2 = \frac{h_{k+1} - h_j}{h_{k+1} - h_k} u_{lidar(k+1,i)}^2 + \frac{h_j - h_k}{h_{k+1} - h_k} u_{lidar(k,i)}^2 \tag{11.6}$$

and was kept constant for heights above the top of the mast:

$$u_{lida(j,i)}^2 = u_{lidar(N_c,i)}^2 \tag{11.7}$$

According to this definition, the uncertainty in lidar speed measurements is necessarily higher than the uncertainty in cup anemometer measurements. This definition is suggested as a first approach, but it needs to be improved by including the calibration uncertainty (i.e. the uncertainty in the regression slope measurement) for example. Moreover, the assumption of a constant calibration factor and uncertainty above the top of the mast (where the coefficients are actually unknown) is rather poor.

11.4 Uncertainty in equivalent wind speed

The equivalent wind speed considered in this chapter is U_{KE} defined by eq. (5.9). For consistency and clarity, it is re-written with the notation adopted in this chapter:

$$V_{KE} = \left(\sum_{j=1}^{N} v_j^3 w_j \right)^{1/3} \tag{11.8}$$

where N is the number of measurement heights during power curve measurement, v_j is the measured wind speed at the j^{th} height and w_j the weight at this height defined as the ratio between the corresponding segment of the rotor swept area and the whole rotor swept area (A_j/A). The uncertainty in equivalent wind speed measurements was defined according to the formula for combined uncertainties when the inputs are correlated as defined in the Danish standard for measurement uncertainty expression (GUM, 1999):

$$u^2_{V_{KE},i} = \sum_{j=1}^{N}\sum_{g=1}^{N} w_j w_g \frac{v_{j,i} v_{g,i}}{V^2_{KE,i}} u_{v_j,i} u_{v_g,i} r(v_j, v_g) \tag{11.9}$$

where $u_{V_{KE},i}$ is the uncertainty in equivalent wind speed in the i^{th} bin, $u_{v_j,i}$ is the uncertainty in wind speed measurement at the j^{th} height in the i^{th} bin. As the equivalent wind speed was derived from speed profiles measured by the lidar, this speed uncertainty was evaluated according to eq. (11.6). $r(v_j, v_g)$ in eq. (11.9) is the correlation between the wind speed at the j^{th} height and the wind speed at the g^{th} height. The correlation coefficients were evaluated from one year of measurements of western winds at Høvsøre.

The final purpose of the uncertainty in equivalent wind speed was to be used in the calculation of the uncertainty in the power curve obtained with the equivalent wind speed method. The uncertainty in equivalent wind speed had therefore to be defined for each wind speed bin, where the bin was defined according to the equivalent wind speed: $v \leq V_{KE} < v + 0.5$. However, for the data contained in a wind speed bin obtained in this way, the average of the wind speeds at a given height is not necessarily between v and $v + 0.5$. The problem was then to defined what value should be taken for $v_{j,i}$ and $u_{v_{j,i}}$ in the evaluation of (11.9).

A simple solution would be to refer to the bin index (i) with no attention to the actual value of the mean speed at the j^{th} height. However, this, in a way, is the same as assuming that the wind speed profiles are almost constant with height (i.e. $v \leq v_{j,i} < v + 0.5\, \forall j \epsilon [1, N]$). Moreover, it raises a problem of a practical aspect as the wind speed distribution is not the same at all heights (because of the wind shear). Therefore, there is no data available in the high wind speed bins at low heights and no data available in the low wind speed bins at high heights. The equivalent wind speed uncertainty would only be calculated for a limited number of bins (not enough to meet IEC standard requirements).

Another solution, more in agreement with the equivalent wind speed method, was to use the actual value of the mean speed at the j^{th} height in the i^{th} bin, and use the uncertainty for the bin where this speed falls in. The wind speed bins that were then taken into account for the example of the wind speed bin number 11, defined by $7.75 \leq V_{KE} < 8.25$, are shown in Table 11.1. This did not make a big difference in the uncertainty value but it made the uncertainty calculations possible for all wind speed bins.

Measurement height number in wind speed profile	Wind speed bin to consider [m/s]	Corresponding bin number
9	$8.25 \leq v_{9,i} < 8.75$	12
8	$7.75 \leq v_{8,i} < 8.25$	11
7	$7.75 \leq v_{7,i} < 8.25$	11
6	$7.75 \leq v_{6,i} < 8.25$	11
5	$7.75 \leq v_{5,i} < 8.25$	11
4	$7.25 \leq v_{4,i} < 7.75$	10
3	$7.25 \leq v_{3,i} < 7.75$	10
2	$6.75 \leq v_{2,i} < 7.25$	9
1	$6.25 \leq v_{1,i} < 6.75$	8

Table 11.1: *Example of choice of bin to calculate equivalent wind speed uncertainty*

Once the uncertainty in equivalent wind speed measurement was obtained for each

bin, the uncertainty in the power curve as described in the IEC standard could be calculated with the equivalent wind speed instead of the cup wind speed at hub height.

11.5 Results

11.5.1 Power curve uncertainty

Figure 11.3 shows the combined uncertainty (see section 11.1) obtained for the cup anemometer at hub height, the lidar at hub height and the equivalent wind speed. The power curve uncertainty obtained with the lidar measurements at hub height is higher than that obtained with the cup anemometer measurements. The uncertainty obtained with the equivalent wind speed is, on average, similar to that obtained with lidar measurements at hub height.

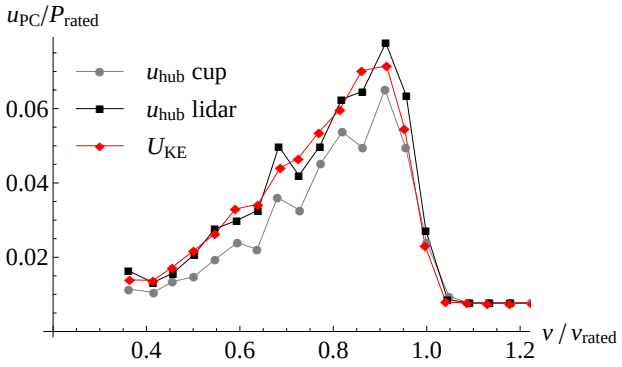

Figure 11.3: *Normalised combined uncertainty in power curve, per speed bin, obtained with the three kinds of wind speed: cup anemometer (at hub height), lidar measurement at hub height and equivalent wind speed*

Figure 11.4 shows the category A uncertainty in electric power obtained for each wind speed definition. The category A uncertainty in power obtained with the equivalent wind speed is the smallest on average. Indeed, the equivalent wind speed was shown to reduce the scatter in the power curve. As the scatter was defined as the mean residual error in each speed bin, it is related to the power standard deviation. Therefore the decrease of the scatter corresponds to a decreases of the category A uncertainty in power.

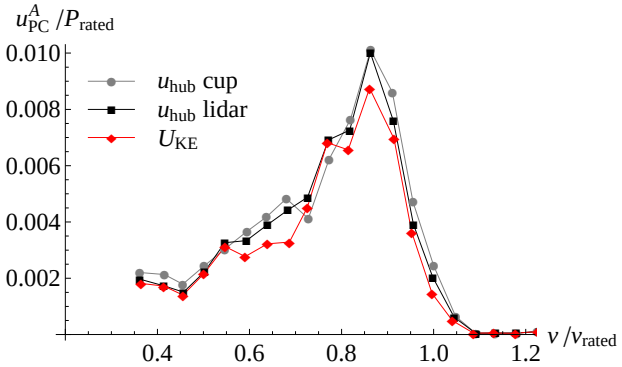

Figure 11.4: *Normalised category A uncertainty in power per wind peed bin obtained with the three kinds of wind speed*

Figure 11.5 (a) shows the category B uncertainty in wind speed obtained for each wind speed definition. This uncertainty results from the product of the wind speed measurement uncertainty (shown in Figure 11.5 (b)) with the related sensitivity factor (shown in Figure 11.5 (c)). The wind speed uncertainty of the lidar measurement at hub

height is larger than that from the cup anemometer, as expected from the definition of the lidar wind speed uncertainty (according to eq. (11.5)).

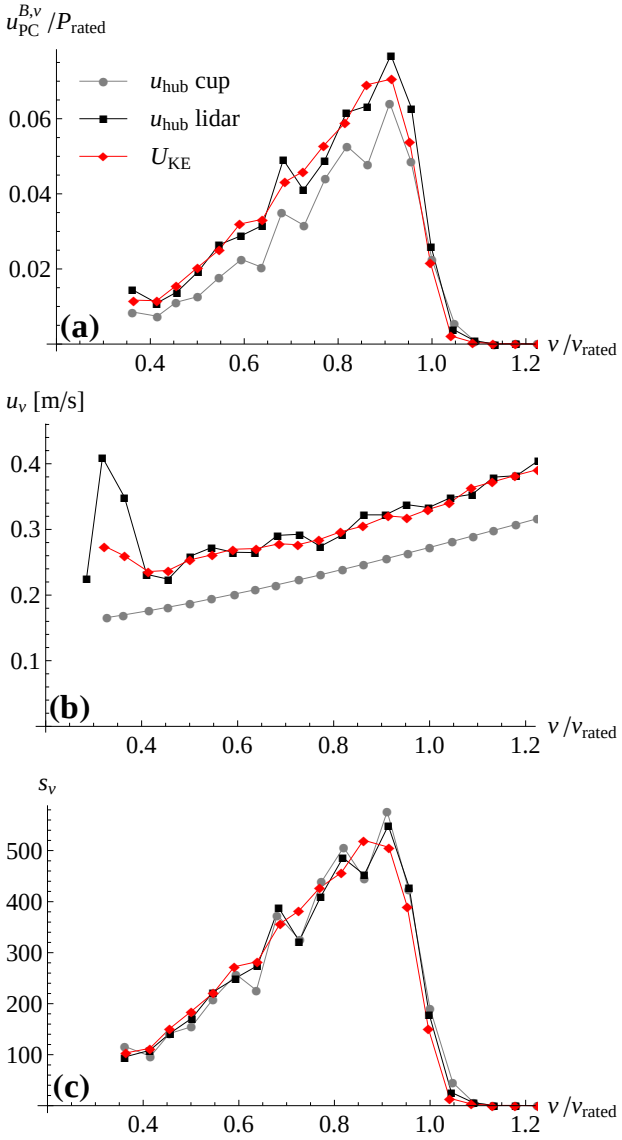

Figure 11.5: *(a): Normalised category B uncertainty in wind speed for the power curve; (b): wind speed uncertainty; (c): sensitivity factor for the wind speed uncertainty, per wind speed bin, obtained with the three kinds of wind speed*

If the equivalent wind speed was obtained with several cup anemometers, the uncertainty in equivalent wind speed could not exceed the highest cup anemometer uncertainty. Therefore, if the cup anemometer with the highest uncertainty is the one at hub height, or all cup anemometers have the same uncertainty, the uncertainty in equivalent wind speed would be smaller than the cup at hub height. However, if a cup anemometer having the highest uncertainty was different from the instrument at hub height, then the equivalent wind speed uncertainty could be larger than the uncertainty of the anemometer measurement at hub height.

It is similar for lidar measurements: if the maximum lidar uncertainty ($u_{v_{j,i}}$ in eq. (11.9)) is at another height than hub height, the equivalent wind speed uncertainty can be higher than the uncertainty in wind speed measurement at hub height. However, the lidar uncertainty depends both on the cup anemometer uncertainty and the standard deviation of the residuals. Here, the cup anemometer uncertainty at hub height has the

highest value among all the cup anemometers of the mast because it is boom mounted. The maximum standard deviation of the residuals is not at hub height. Therefore, the equivalent wind speed uncertainty can be higher than the uncertainty in wind speed at hub height. Consequently, there cannot be a systematic difference between the uncertainty in wind speed at hub height and the equivalent wind speed measurements as shown in Figure 11.5 (b).

The sensitivity factor is determined as the local slope of the mean power curve (IEC, 2005), it is different from one wind speed definition to another as the three power curves are different (see Figure 11.5 (c)). As the result of the combination of the wind speed uncertainty and the sensitivity factor, the part of the uncertainty in power curve due to the wind speed uncertainty is higher for the lidar measurements at hub height than for the cup anemometer measurement but is not systematically higher or smaller for the equivalent wind speed than for the lidar at hub height.

The consequence is that, in spite of the smaller category A uncertainty in power, the power curve combined uncertainty obtained with the equivalent wind speed method is similar to that obtained with the lidar measurements at hub height. Moreover, both of them are higher than the power curve combined uncertainty obtained with the cup anemometer measurements.

11.5.2 AEP uncertainty

According to the definition given by eq. (11.5), the lidar measurement uncertainty is necessarily larger than the cup anemometer measurement uncertainty. The consequence is that the uncertainty in the power curve is higher for lidar than for cup anemometer measurements, therefore the same conclusion is also true for the uncertainty in the AEP.

On the other hand, the uncertainty in AEP obtained with the equivalent wind speed is slightly smaller than that obtained with the lidar measurement at hub height in Figure 11.6. This is probably due to the weighting of the category A uncertainty which is different for the AEP uncertainty than for the power curve uncertainty.

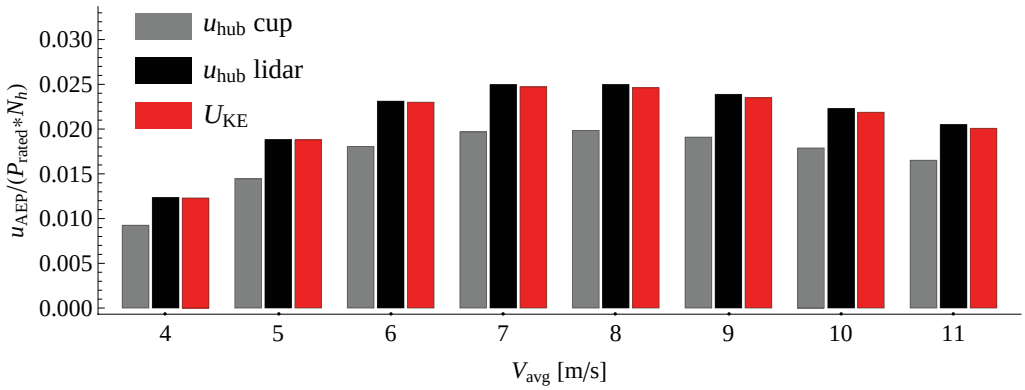

Figure 11.6: *AEP measurement uncertainty obtained with the three kinds of wind speed*

11.6 Summary and discussion

The use of the equivalent wind speed in the power performance measurements resulted in a reduction of the category A uncertainty in power. On the other hand, as the category B uncertainty in wind speed measurement obtained with a lidar varies with height, it can be higher for the equivalent wind speed than for the wind speed at hub height. Consequently, the equivalent wind speed method did not result in a systematic reduction of the power curve combined uncertainty. This uncertainty was in the same order of magnitude as the uncertainty obtained with the lidar measurement at hub height. The AEP uncertainty, on the other hand, was found to be slightly decreased with the equivalent wind speed.

However, such a direct comparison of the uncertainty obtained with the two methods could be discussed. Indeed, the power curve based on wind speed measurements at hub height does not account for the uncertainty due to climatic variations. According to the current IEC standard (IEC, 2005), this kind of uncertainty is included in the category A uncertainty in power. It is thus considered as a stochastic error in the measurements. The variability of the mean power curve due to the wind shear is not taken into account. Therefore, one could argue that an extra term should be added to the standard power curve uncertainty to account for the wind shear effect. Then the difference between the two methods for power curve measurements would be shifted in favor of the equivalent wind speed method.

Indeed, as explained in chapter 10, the equivalent wind speed power curve is less sensitive to the shear, therefore an extra term to account for the variability of the power curve due to shear is not needed (or if it is used, it should be smaller than for the standard power curve). Therefore the use of the equivalent wind speed results in two advantages for the AEP prediction: 1) the power curve is more repeatable and 2) the uncertainty in power curve measurement is similar to that obtained with wind speed measurements at hub height, which does not account for the uncertainty due to the wind shear.

Chapter 12

Discussion and further work

12.1 Equivalent wind speed method

The problem of the effect of shear on the power performance of wind turbines has been raised within the last years as the size of the wind turbines has considerably increased. The site dependence of the power curve has become an issue that cannot be ignored any longer. Indeed a wind turbine power curve is most of the time meant to be compared to another power curve or transferred from one site to another. Within this context, the latest version of the IEC standard for wind turbine power performance measurement (IEC, 2005) is currently under revision with, as one of the main tasks, the introduction of a method accounting for secondary parameters such as wind shear and turbulence. In the work described in this thesis, the definition of a wind speed equivalent to the wind speed profile in front of the turbine rotor was investigated as a method to account for the wind shear in the power performance measurement.

Such an equivalent wind speed can be defined in various ways. Mostly two definitions were investigated (U_{disk} and U_{KE}) but neither aerodynamic simulations nor measurements enabled us to define with precision which one could reduce the scatter the most. Nevertheless, the equivalent wind speed U_{KE}, defined according to a better kinetic energy flux approximation than the current one, has the advantage of showing directly the relation between the kinetic energy flux (input power to the turbine) and the power output. It therefore shows the true efficiency of the turbine to extract the power of the wind.

None of the equivalent wind speed definitions suggested here can result in a power curve completely independent of shear. The turbine response to shear does not only depend on the wind kinetic energy flux but also on the wind speed profile. Two different speed profiles with the same kinetic energy flux can result in two different power outputs. A power curve completely independent of the wind shear should account for the dynamics of the turbine which are specific to the turbine design and the operational settings. However, by including more accurate information about the wind profile, instead of assuming it to be constant, the power curve sensitivity to wind shear is significantly reduced. Therefore the error made by assuming the equivalent wind speed power curve to be independent of the site is much smaller than that made by assuming the standard power curve to be independent of the site.

Furthermore, as it was pointed out in the preliminary investigation with the aerodynamic simulations, the operational characteristics of a wind turbine in sheared inflow are not yet fully understood. One of the major issues is the spatial variation in induction over the rotor, as the shear influences the behavior of the wake behind the rotor. Simulations with models more advanced than the BEM model could help for a better understanding of such conditions, however, so far no agreement has been reached with those models either. Validation and improvements of the model need induction measurements in non uniform flow. This is technically challenging because it requires both measurements at the rotor and in the free wind (i.e. away from the turbine). Measurements at the ro-

tor can be acquired with a pitot tube. Away from the rotor, wind shear measurements require a mast mounted with several cup anemometers at various heights or a lidar.

Regarding the induction effect, the IEC 61400-12-1 standard requires wind speed measurements at hub height at 2 to 4 rotor diameters in front of the turbine in order to measure the free wind. The same rule was applied here to measure the wind speed profiles; the lidar was placed next to the mast, i.e. at about 2.5 rotor diameter from the turbine. However, the question of the correlation between the profile measured at this location with the profile at the turbine rotor should be addressed. The measurements analysed in this study were all taken in flat terrain, therefore it was fair to assume that the profiles measured upwind were the same as those at the rotor. However, as shown in (Stefanatos et al., 2008), this correlation of the profile between the measurement location and the turbine decreases in complex terrain, then limiting the use of the equivalent wind speed method as defined here to flat terrain.

One of the main weaknesses of the results presented in this thesis is probably that the most important results were obtained with one short data set. As the measurements were taken with a test turbine, only short periods with constant settings were available and the data set used did not reach the amount of data requires by the IEC standard. Moreover, these results may be specific to the Høvøsre site, which in spite of the flat terrain and the very few surrounding obstacles, was shown to present some peculiarities due to it proximity to the North Sea coast. To be fully validated, the equivalent wind speed method should be tested with other turbines at other sites, possessing different types of wind characteristics: speed shear, but also turbulence and direction shear.

This work was focused on the effect of speed shear, but the power performance can also be influenced by other wind characteristics, in particular the turbulence and the direction shear. The influence of turbulence was briefly investigated. The scatter due to turbulence did not mask the scatter due to shear and thus the use of an equivalent wind speed reduced the global scatter in the power curve. Accounting for the turbulence intensity in the equivalent wind speed cannot reduce the scatter near rated wind speed in the power curve and cannot normalise the power curve for turbulence intensity. On the other hand, the method suggested by Albers does normalise the power curve for any turbulence intensity. This method was successfully combined to the equivalent wind speed method to result in a power curve normalised for both the shear and the turbulence intensity. However, it must be noted that only low turbulence intensity was considered in this investigation, as the turbulence intensity rarely exceeds 12% on average at Høvsøre.

Furthermore the wind veer, i.e. variation of the direction with altitude, also influences the turbine power performance (Walter et al., 2009). Similarly to the wind shear, the wind veer modifies the angle of attack of the wind on the turbine blade, which then varies with the altitude. However, the variation is different from that due to wind speed shear as direction shear involves a wind component that is parallel to the rotor plan (Walter, 2007). The influence of wind veer has so far been the subject of only a few investigations mainly because of the lack of measurements. This is another benefit of lidar measurements. Indeed, a lidar measures the wind direction at several heights with a unique reference. Thus there is no offset between the measurements at different heights, contrary to measurements taken with several wind vanes. The analysis of the wind veer at Høvsøre (Cariou et al., 2010) showed that it is mainly clockwise with rather small amplitude (not exceeding 5° on average), which is expected to have a small influence on turbine power performance.

The use of an equivalent wind speed accounting for the speed shear in the power performance measurement can be a little confusing as the resulting power curve is not directly comparable to the standard power curve. Indeed, these two power curves have two different quantities in abscissa. A new power curve has been defined. For this reason, the most sensible way of estimating the AEP with the equivalent wind speed at hub height is to use the distribution of the equivalent wind speed. This means that the wind speed profile should be measured not only during the power curve measurement but also during the wind resource assessment.

As the equivalent wind speed should eventually result in a smaller uncertainty in AEP

estimation, the method is very attractive in theory. However, one could find it difficult to apply in practice since it requires measurements at several heights whereas only one is needed in the current standard power curve. The arrival of the lidar technology in the wind energy field appears as a good solution to this issue.

12.2 Lidar measurements

The mean power curve as well as the scatter in the power curve obtained with the lidar measurements at hub height were very similar to the cup anemometer measurements.Only when this condition is fulfilled can one expect a decrease in scatter with the equivalent wind speed based on speed profile measurements. The application of this method with a remote sensing instrument therefore requires a "good" instrument. For this reason the remote sensing instrument should be verified with a tall met. mast prior to the power curve measurement in order check that the deviation from the cup anemometers measurements is small enough to be used for this purpose. So far, the lidar was deemed to be suitable if the regression analysis of the lidar data plotted against the cup anemometer data resulted in a slope close to unity and a high value for R^2. However, a well defined procedure with more specific criteria for the selection of the instruments needs to be defined.

A step further in this direction is to actually make a calibration of the lidar, i.e. to define a coefficient to relate the lidar measurements to the reference cup anemometers measurements. Such a procedure has the advantage of transferring the traceability from the cup anemometers to the lidar, which is a requirement to get an accredited power curve based on lidar measurement.

Lidar measurement are different from cup measurements because of the volume averaging. However, since here we are interested in using a wind speed representative of the whole rotor swept area, the vertical averaging is not a problem, it may be an advantage.

On the other hand, the horizontal averaging may be an issue. As the laser beam is conically scanning, when the lidar is located at 2.5 rotor diameter of the wind turbine, some radial speeds are actually measured further away from the turbine and some others closer to the rotor. Therefore the measurement may be influenced by the induction and the distance which is optimum for the location of the cup anemometer might not be optimum for the lidar installation.

Hence, a direct comparison of the power performance measurement obtained with lidar measurements to cup anemometer measurements is not straightforward. It is also relevant to compare the uncertainty in power curve measurements obtained with the different instruments. In this investigation, the uncertainty in lidar wind speed measurements was defined relative to the uncertainty in cup anemometer measurements, resulting in a lidar uncertainty systematically higher than that of the cup anemometer. This may be unfair to the lidar and alternative calibration methods, avoiding the use of cup anemometers should be investigated.

Chapter 13

Conclusions

The use of an equivalent wind speed based on speed profile measurement in front of the turbine rotor was shown to be a good method to account for shear in the power performance measurement. This method decreases the scatter due to wind shear in the power curve, which results in a power curve that is less sensitive to the shear and hence more independent of the site and the season than the standard power curve. The method is attractive because of is simplicity of application once the speed profiles are known. Several equivalent wind speed definitions, i.e. various ways of averaging the speed profile over the rotor, resulted in a reduction of the scatter. However, the definition based on the approximation of the kinetic energy flux through the swept rotor area accounting for the speed profile has the advantage of having a physical interpretation, that is to show the efficiency of the turbine to extract the power from the wind.

The main difficulty in the practical application of the method is probably to obtain speed profiles that are accurate enough. Indeed, a simple extrapolation based on models such as the power law may be a good representation for only a few sites. For most sites (coastal areas, sites experiencing low level jets, complex terrain for example), measurements of the speed profile are necessary. In this investigation, the equivalent wind speed was derived from lidar measurements. A significant reduction of the scatter in the power curve was obtained with speed measurements at only 3 heights (one at hub height, one below and one above) whereas no improvement was obtained when the profile where extrapolated from measurements strictly below hub height. The measurement of the wind speed at at least one height above hub height therefore makes a significant difference. However, the total number of measurements necessary to obtain a significant improvement is probably relative to the site. It is therefore recommended to use as many measurement heights as possible. This investigation was realised with speed profiles derived from 9 measurements. Indeed a lidar has the advantage of measuring the wind speed and direction at up to 10 heights for the same cost as 3 heights.

In spite of being very relevant for the wind shear effects on the power performance measurement, the equivalent wind speed method was shown not to be suitable to reduce the power curve sensitivity to the turbulence. However, the equivalent wind speed accounting for the wind shear was successfully combined with another method for normalising the power curve for the turbulence intensity.

Such a power curve, normalised for wind shear and turbulence intensity, is more repeatable, which means that the difference between the power curve measured at two sites with different shear conditions is reduced. Therefore the power curve measured with the equivalent wind speed at a reference site can be transferred to another site resulting in a smaller error than by transferring the standard power curve. Furthermore, as the equivalent wind speed method reduces the scatter in the power curve, it decreases the uncertainty due to shear in the power curve measurement, which is not considered in the standard power curve uncertainty. Consequently, the equivalent wind speed power curve should result in much better AEP estimation. However, a consistent and more accurate AEP calculated with such a power curve requires the measurement of the equivalent

speed (i.e. the speed profiles) during the resource assessment.

Bibliography

Wind turbine generator systems - part 12: Wind turbine power performance testing. Technical Report IEC 61400-12, 1998a.

Wind turbines - part 1: Design requirements. Technical Report IEC 61400-1 (Ed 2.0), 1998b.

GUM: Guide to the expression of uncertainty in measurement. Technical Report DS/ENV 13005, 1999.

Wind turbines - part 12-1: Power performance measurements of electricity producing wind turbines. Technical Report IEC 61400-12-1 (Ed 2.0), 2005.

A. Albers. Turbulence normalisation of wind turbine power curve data. In *Proceedings of the European Wind Energy Conference (EWEC) 2010*, Warsaw, Poland, 2010.

A. Albers, T. Jakobi, R. Rohden, and J. Stoltenjohannes. Influence of meteorological variables on measured wind turbine power curve. In *Proceedings of the European Wind Energy Conference (EWEC) 2007*, Milan, Italy, 2007.

I. Antoniou, S.M. Pedersen, and P.B. Enevoldsen. Wind shear and uncertainties in power curve measurement and wind resources. In *Proceedings of WindPower 2007*, Chicago, Il., USA, 2009.

K. Bak. Research in aeroelasticity EFP. Technical Report Risø-R-1611, 2006.

R.M. Banta, R.K. Newsom, J.M. Lundquist, Y.L. Pichugina, R.L. Coulter, and L. Mahrt. Nocturnal low-level jet characteristics over Kansas during CASES-99. *Boundary-Layer Meteorology*, 105:221–252, 2002.

H. Bergström, P.-E. Johansson, and A.-S. Smedman. A study of wind speed modification and internal boundary layer heights in a coastal region. *Boundary-Layer Meteorology*, 42:313–335, 1988.

J.A. Businger, J.C. Wyngaard, Y. Izumi, and E.F. Bradley. Flux-profile relationships in the atmospheric surface layer. *Journal of Atmospheric Science*, 28:181–188, 1971.

N. Cariou, R. Wagner, and J. Gottschall. Analysis of the vertical gradient of direction and wind speed from met mast data at høvsøre. Technical Report Risø-R-1733(EN), 2010.

M. Courtney, R. Wagner, and P. Lindelöw. Testing and comparing of lidars for profile and turbulence measurements in wind energy. *Earth and Environmental Sciences: Conf. Series*, 2008.

A.G. Davenport. Rational for determining design wind velocities. *Proceedings of the American society of civil engineers, Journal of the structural division*, 86:39–68, 1960.

D.S.L. Dolan and P.W. Lehn. Simulation model of wind turbine 3p torque oscillations due to wind shear and tower shadow. *IEEE transactions on energy conversion*, 21(3), 2006.

C. Dyrbye and S.O. Hansen. *Wind Loads on Structure*. John Wiley and Sons, LTD, 1996.

P.J. Eecen, F.Mouzakis, and A.Cuerva. Accuwind: Work package 3 final report. Technical Report ECN-C–06-047, 2006.

D.L. Elliott and J.B. Cadogan. Effects of wind shear and turbulence on wind turbine power curves. In *Proceedings of the European Community Wind Energy Conference and Exhibition*, 1990.

P. Enevoldsen, H.E. Jørgensen, T.F Pedersen, and P.H Madsen. Wind flow aberrations at near coastal sites of importance for performance verification measurements. In *Proceedings of the European Wind Energy Conference (EWEC) 2006*, 2006.

S. Frandsen, I. Antoniou, J.C. Hansen, L. Kristensn, H.A. Madsen, B. Chaviaropoulos, D. Douvikas, J.A. Dahlberg, A. Derrick, P.Dunbabin, R. Hubter, R. Ruffle, D. Kanellopoulos, and G. Kapsalis. Redefinition power curve for more accurate performance assessment of wind farms. *Wind Energy*, 3:81–111, 2000.

J. Gottschall and J. Peinke. How to improve the estimate of power curves for wind turbines. *Enviro. Res. Lett.*, 3(015005), 2008.

U. Högström. Non-dimensional wind and temperature profiles in the atmospheric surface layer: a re-evaluation. *Boundary-Layer Meteorology*, 42:55–78, 1971.

R. Hunter, T.F. Pedersen, P. Dunbabin, A. Antoniou, S. Frandsen, H. Klug, A. Albers, and W.K. Lee. Task1: Measurement method to verify wind turbine performance characteristics. Technical Report Risø-R-1209(EN), 2001.

J. Jonkman, S. Butterfiled, W. Musial, and G. Scott. Definition of a 5 MW reference wind turbine for offshore system. Technical Report Development technical report NREL/TP-500-38060, February 2009.

H.E. Jørgensen, T. Mikkelsen, S.-E. Gryning, S. Larsen, P. Astrup, and P.E. Sørensen. Measurements from Høvsøre met. mast. Technical Report Risø-R-1592(EN), 2008.

K. Kaiser, H. Hohlen, and W. Langreder. Turbulence correction for power curves. In *Proceedings of the European Wind Energy Conference (EWEC) 2003*, 2003.

T.J. Larsen. HAWC2, the user's manual. Technical Report Risø-R-1597(ver.3-1), 2007.

T.J. Larsen. HAWC2Aero, the user's manual. Technical Report Risø-R-1631(ver.1-0), 2008.

T.J. Larsen and A.M. Hansen. Influence of blade pitch loads by large blade deflections and pitch actuator dynamics using the new aeroelastic code HAWC2. In *Proceedings of the European Wind Energy Conference (EWEC) 2006*, 2006.

P. Lindelöw. *Fiber Based Coherent Lidars for Remote Wind Sensing*. PhD thesis, 2007.

P. Lindelöw, M. Courtney, R. Parmentier, and J.P. Cariou. Wind shear proportional errors in the horizontal wind speed sensed by focused, range gated lidars. *Earth and Environmental Sciences: Conf. Series*, 2008.

P. Lindelöw-Marsden, N.G. Mortensen, and M.S. Courtney. Are lidar good enough for resource assessments? - accuracy of AEP predictions in flat terrain generated from measurements by conically scanning lidars. In *Proceedings of the European Wind Energy Conference (EWEC) 2009*, 2009.

H.A. Madsen. Short comings in state of the art engineering aerodynamic and aeroelastic models by comparison to advanced models. Technical Report Risø-I-2522(EN), 2008. Upwind deliverable WP2.2.

H.A. Madsen, R. Mikkelsen, S. Øye, C. Bak, and J. Johansen. A detailed investigation of the blade element momentum (BEM) model based on analytical and numerical results and proposal for modifications of the BEM model. *Journal of Physics: Conference Series*, 75(012016), 2007.

H.A. Madsen, V. Riziotis, F. Zahle, T.J. Larsen, E. Politis, M.O.L. Hansen, H. Snel, and F. Grasso. BEM modeling of inflow with shear in comparison with advanced model results. In *Proceedings of TORQUE 2010*, volume 1, Heraklion, Crete, Greece, 2010.

J. Mann. Wind field simulation. *Probabilistic Engineering Mechanics*, 13:269–282, 1998.

T. Mikkelsen. On mean wind and turbulence profile measurements from ground-based wind lidars: limitations in time and space resolution with continuous wave and pulsed lidar systems. In *Proceedings of the European Wind Energy Conference (EWEC) 2009*, Marseille, France, 2009.

A.S. Monin and A.M. Obukhov. Basic laws of turbulent mixing in the surface layer of the atmosphere. *Tr. Akad. Nauk SSSR Geophiz. Inst.*, 24(151):163–187, 1954.

E. Montes, A. Arnedo, R. Cordón, and R. Zubiaur. Influence of wind shear and seasonality on the power curve and annual energy production of wind turbines. In *Proceedings of the European Wind Energy Conference (EWEC) 2009*, 2009.

M. Motta, R.J. Barthelmie, and P. Vølund. The influence of non-logarithmic wind speed profiles on potential power output at Danish offshore sites. *Wind Energy*, 8:219–236, 2005.

J.N. Nissen. *On the application of a numerical model to simulate the coastal boundary layer.* PhD thesis, 2008.

I.A. Perez, M.A. Garcia, M.L. Sanchez, and B. de Torre. Analysis and parametrisation of wind profiles in the low atmosphere. *Solar Energy*, 78:809–821, 2005.

N. Sezer-Uzol and O. Uzol. Effect of steady and transient wind shear on the wake structure and performance of a horizontal axis wind turbine rotor. In *Proceedings of 47th AIAA Aerospace Sciences Meeting*, 2009.

N. Stefanatos, D. Zigras, D. Foussekis, F. Kokkalidis, P. Papadopoulos, and E. Binopoulos. Revising reference wind speed definition for power performance measurements of multi-MW wind turbines. In *Proceedings of the European Wind Energy Conference (EWEC) 2008*, 2008.

R.B. Stull. *An introduction to boundary layer meteorology.* Kluwer Academic Publishers, 1988.

J. Sumner and M. Masson. Influence of atmospheric stability on wind turbine power performance curves. *Journal of Solar Energy Engineering*, 128:531–538, 2006.

K.E. Swalwell, C. Chad, S. Schwartz, A. Wright, H. Oje, and A. Anders. Diurnal wind characteristics and WTG loading. In *Proceedings of the European Wind Energy Conference (EWEC) 2008*, Bruxelles, Belgium, 2008.

H.W. Tielmann. Strong wind observations in the atmospheric surface layer. *Journal of Wind Engineering and Industrial Aerodynamics*, 96:41–77, 2008.

G.P. VandenBerg. Wind turbine power and sound in relation to atmospheric stability. *Wind Energy*, 11:151–169, 2008.

D. VanLuvanee, V. Marquis, C. Henderson, M. Young, and A. Byrne. Effects of atmospheric conditions on wind turbine power performance and review of proposed correction techniques. In *Proceedings of WindPower 2009*, Chicago, Il., USA, 2009.

R. Wagner, T. Mikkelsen, and M. Courtney. Investigation of turbulence measurements with a continuous wave, conically scanning LiDAR. Technical Report Risø-R-1682(EN), 2009.

K. Walter. *Wind power systems in the stable nocturnal boundary layer*. PhD thesis, 2007.

K. Walter, C.C. Weiss, A.H.P. Swift, J. Chapman, and N.D. Kelley. Speed and direction shear in the stable nocturnal boundary layer. *Journal of Solar Energy Engineering*, 131(011013), 2009.

F. Zahle and N.N. Sørensen. Rotor aerodynamics in atmospheric shear flow. In *Proceedings of the European Wind Energy Conference (EWEC) 2008*, Bruxelles, Belgium, 2008.

Appendix: Meteorological mast at Høvsøre

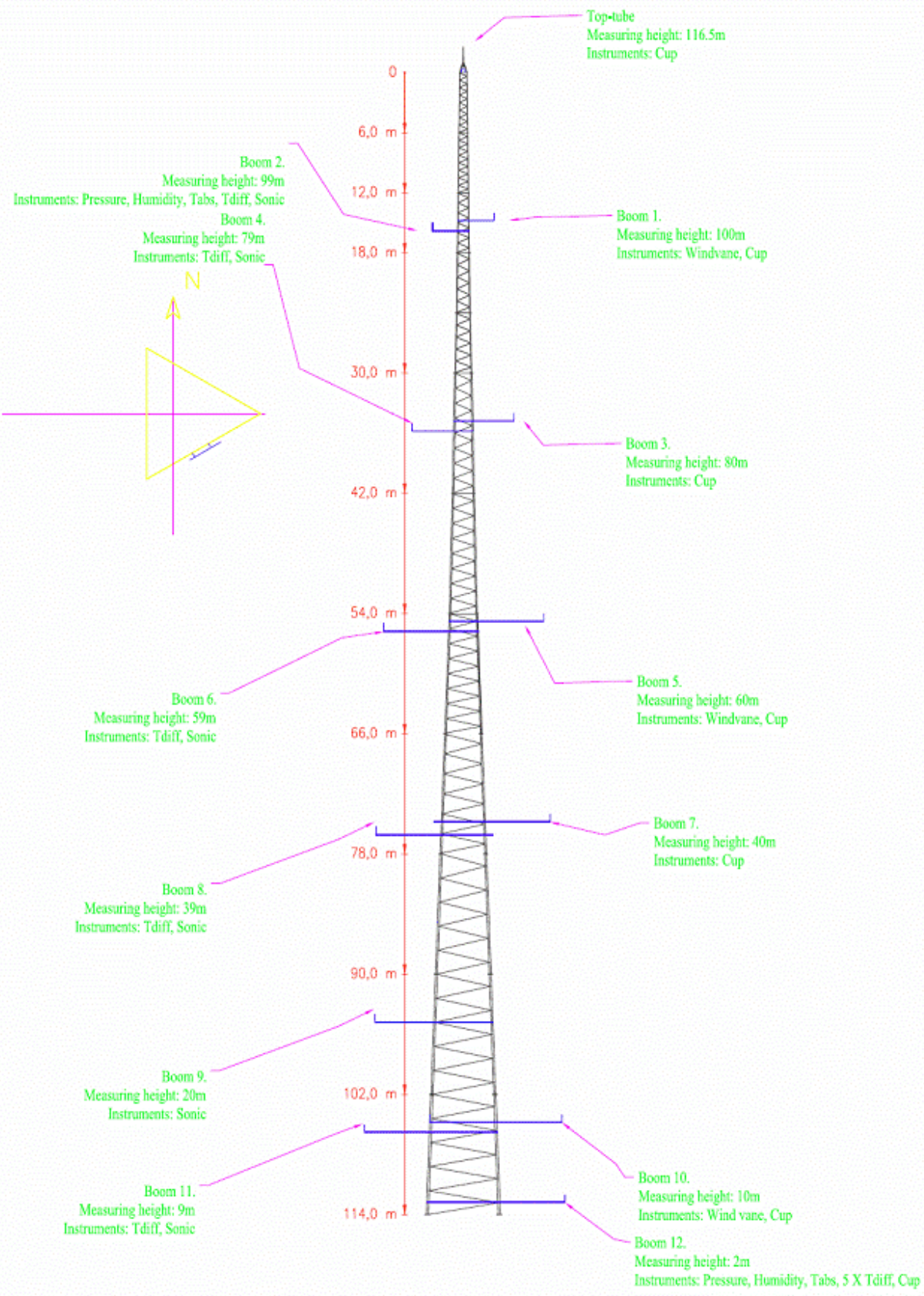
Top-tube
Measuring height: 116.5m
Instruments: Cup
0
6,0 m
12,0 m
18,0 m
30,0 m
42,0 m
54,0 m
66,0 m
78,0 m
90,0 m
102,0 m
114,0 m
Boom 2.
Measuring height: 99m
Instruments: Pressure, Humidity, Tabs, Tdiff, Sonic
Boom 4.
Measuring height: 79m
Instruments: Tdiff, Sonic
N
Boom 1.
Measuring height: 100m
Instruments: Windvane, Cup
Boom 3.
Measuring height: 80m
Instruments: Cup
Boom 6.
Measuring height: 59m
Instruments: Tdiff, Sonic
Boom 5.
Measuring height: 60m
Instruments: Windvane, Cup
Boom 8.
Measuring height: 39m
Instruments: Tdiff, Sonic
Boom 7.
Measuring height: 40m
Instruments: Cup
Boom 9.
Measuring height: 20m
Instruments: Sonic
Boom 11.
Measuring height: 9m
Instruments: Tdiff, Sonic
Boom 10.
Measuring height: 10m
Instruments: Wind vane, Cup
Boom 12.
Measuring height: 2m
Instruments: Pressure, Humidity, Tabs, 5 X Tdiff, Cup

Paper I: The Influence of the Wind Speed Profile on Wind Turbine Performance Measurements

Authors: **Rozenn Wagner**, Ioannis Antoniou, Søren M. Pedersen, Michael S. Courtney and Hans E. Jørgensen
Wind Energy (2009) **12**:348-362

Paper II: Accounting for the Speed Shear on Wind Turbine Performance Measurements

Authors: **Rozenn Wagner**, Michael S. Courtney, Julia Gottschall and Petter Lindelöw-Marsden
Submitted to Wind Energy

Risø DTU is the National Laboratory for Sustainable Energy. Our research focuses on development of energy technologies and systems with minimal effect on climate, and contributes to innovation, education and policy. Risø has large experimental facilities and interdisciplinary research environments, and includes the national centre for nuclear technologies.

Risø DTU
National Laboratory for Sustainable Energy
Technical University of Denmark

Frederiksborgvej 399
PO Box 49
DK-4000 Roskilde
Denmark
Phone +45 4677 4677
Fax +45 4677 5688

www.risoe.dtu.dk